Scholars' Mine

Fall 2012

Direct shear testing of fractured rocks from Missouri used to evaluate potential fault reactivation induced by carbon dioxide sequestration

Ishan Kumar

DIRECT SHEAR TESTING OF FRACTURED ROCKS FROM MISSOURI USED TO

EVALUATE POTENTIAL FAULT REACTIVATION INDUCED BY CARBON

DIOXIDE SEQUESTRATION

by

ISHAN KUMAR

A THESIS

Presented to the Faculty of the Graduate School of the

MISSOURI UNIVERSITY OF SCIENCE AND TECHNOLOGY

In Partial Fulfillment of the Requirements for the Degree

MASTER OF SCIENCE IN PETROLEUM ENGINEERING

2012

Approved by

Dr. Runar Nygaard
Dr. Andreas Eckert
Dr. Baojun Bai

ABSTRACT

Geological storage projects of CO_2 are designed to maintain secure storage for thousands of years. Carbon Capture and Storage has been identified as one of the methods which is used to reduce global emission of CO_2 and achieve lower concentration of CO_2 in the atmosphere by capturing the CO_2 from the flue gases and storing it in underground formations. Potential leakage of injected CO_2 from the reservoir to the surface is caused by the reactivation of pre-existing faults and fractures which is caused by the change in the state of stresses and the pore pressure. To avoid damage to the reservoir seals, ensure fault stability and validate maximum sustainable pore pressure, a geomechanical characterization which refers to the assessment of the in-situ stress, elastic properties and rock strength of the rock helps to determine the seal integrity of the caprock and the storage capacity of the reservoir during and after injection of CO_2 in underground formations.

In this study a direct shear apparatus was assembled in order to determine the direct and residual shear strengths of the rock. Mohr-Coulomb failure criteria, slip tendency parameters and joint roughness coefficient were used to determine the chances of the reactivation of pre-existing faults and fractures in the caprock and the reservoir rock. It was seen from the study that if in-situ stress regime were considered none of the faults or fractures is getting reactivated. This study also helped to develop a sustainable pore pressure window and the maximum sustainable pore pressure is calculated for the reactivation of faults. If the injection pressure of CO_2 is kept between the sustainable pore pressure window there will be no reactivation of faults and the leakage of CO_2 from the reservoir to the surface can be avoided.

ACKNOWLEDGMENTS

TABLE OF CONTENTS

Page

LIST OF ILLUSTRATION

LIST OF TABLES

1. INTRODUCTION

1.1. RATIONALE AND BACKGROUND

Current research indicates that there is a relation between climate change and burning of fossil fuels by human beings which releases greenhouse gases such as carbon dioxide (CO_2). National oceanic and atmospheric administration also studied that atmospheric concentration of CO_2 has risen from pre-industrial levels of 280 ppm to 396.78 ppm (Tans, 2012) in 2012 primarily as a consequence of the burning of fossil fuels for the energy production (Bachu, 2003). CO_2 emissions from coal-fired power plants contribute to over 30% of CO_2 emissions alone in United States and is expected to increase for the next 20 years with the increasing need for reliable sources of base load power (Litynski et al., 2009). Thus the electric power generation plants and industries are main sources for CO_2 emissions. Table1.1 shows the breakdown of the sources of CO_2 emissions due to fossil fuel usage in the United Stated and their percentage contribution to the total emissions. Figure 1-1 shows the carbon sequestration future advanced sequestration technologies until 2050.

Table 1.1. Percentage contribution for CO_2 emission from combustion of fossil fuels in United States (Folger, 2009)

Sources	Total Percentage
Electricity Generation	42%
Transportation	33%
Industrial	15%
Residential	6%
Commercial	4%
Total	100%

During the past 15 years, several different approaches were developed to capture and store CO_2 underground in order to stabilize CO_2 concentration in the atmosphere. Carbon capture and storage in geological formations can make a significant contribution to reduction of CO_2 in the atmosphere. Carbon capture and Storage (CCS) involves the technology to collect and concentrate the CO_2 produced from electric generation plants, industries and other energy related sources, transport it to a suitable storage location and then store it for a long duration. Figure 1.1 developed by the U.S. department of energy shows the typical projected implementation timeline for advanced sequestration technologies. It can be seen from the figure that the main emphasis till 2020 is on demonstration projects and commercial implementation occurs after that (Davis, 2004). Pumping of CO_2 into the ground is not a new process, it has been in use in the oil and gas industry for the past 30 years for the Enhanced Oil Recovery (EOR). Enhanced oil recovery was proposed as a form of CCS. In EOR, CO_2 is injected in the petroleum reservoirs in order to extract hydrocarbons (oil) and in the process some CO_2 is retained in the reservoir after all the extraction has been done (Vendrig et al., 2007). However it has to be noted that the primary purpose of EOR is to recover the remaining oil from the reservoirs and not CO_2 sequestration.
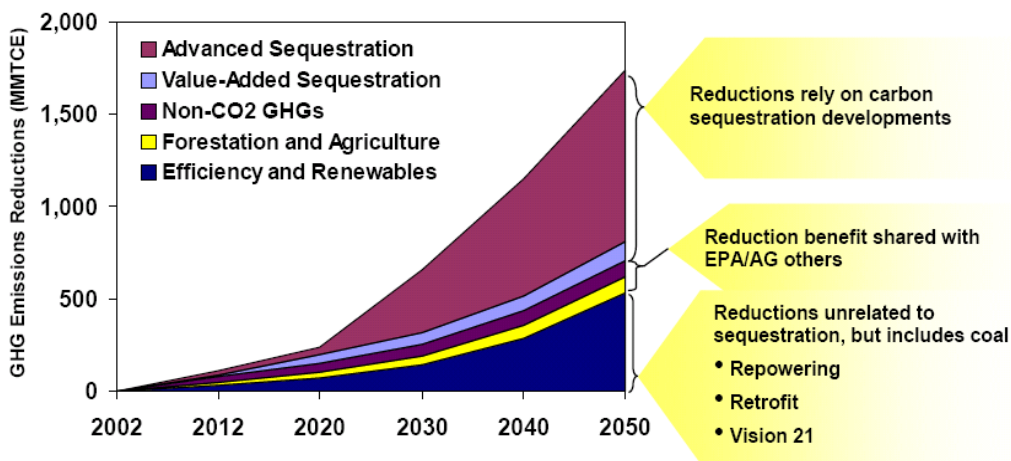
Figure 1-1. Carbon sequestration program plan developed until 2050 (Davis, 2004)

To reduce greenhouse gas emissions in the state of Missouri the Lamotte sandstone formation deposited in Missouri has been identified as a potential reservoir for the sequestration of CO_2 (Boongird et al., 2006). However the pore pressure inside a geological formation changes whenever a fluid is injected into the reservoir causing changes in the in-situ stress regime which in turn may lead to the reactivation of the pre-existing fractures creating a leakage pathway for the injected CO_2 to leak to the surface. In order to make sure that the long term storage is feasible and safe a comprehensive geomechanical assessment of the rock formations has to be performed to determine the potential leakage pathways. Such a geomechanical assessment often denoted as a mechanical earth model consists of the following steps (Lee et al., 2009):

- Determining Mechanical Stratigraphy

- Pore Pressure during and after injection of CO_2

- Overburden stress

- Orientation of Stress

- Minimum horizontal stress

- Maximum horizontal stress

- Elastic parameters

- Rock strength parameters

- Failure mechanism

1.2. THESIS OBJECTIVE

The objective of this thesis is to set up a direct shear apparatus and use "Direct Shear" testing to obtain the shear strength of the potential joints in the Lamotte sandstone formation and the overburden formations. This test is necessary in order to determine the possibility of any fault reactivation at the sequestration site in Missouri to aid in the identification of possible leakage pathways of CO_2 to the surface.

1.3. THESIS OUTLINE

The thesis consists of 7 sections and 4 appendices. Section 1 is the introduction, Section 2 is the literature review and basic theories, Section 3 is the sample preparation and site geology, cSection 4 is the laboratory setup and procedures, Section 5 shows the results, Section 6 deals with the analysis and discussion of the results and Section 7 provides the conclusions. There are 4 Appendices, Appendix A gives the details of the characterization details for each sample, Appendix B gives the results of the direct shear test, Appendix C gives all the plots obtained from the test, and Appendix D gives the images of the lab apparatus and the sample preparation.

2. LITERATURE REVIEW

2.1. OVERVIEW OF CO_2 CAPTURE AND SEQUESTRATION

The aim of CO_2 Capture and Sequestration also known as CCS is to reduce the quantity of CO_2 emitted to the atmosphere, by separating produced CO_2 from industrial and other energy related sources and storing it within geological formations. CO_2 sequestration has been a field of study since the early 1990's and became main stream after UNFCCC (United Nations Framework Convention on Climate Change) announced its goal of achieving stabilization on anthropogenic greenhouse gas emissions. Every advanced country is making efforts to reduce greenhouse gas emissions into the atmosphere and Kyoto Protocol was a landmark treaty signed by a number of countries geared towards achieving this ideal. The Kyoto Protocol was adopted in Kyoto in Japan in 1997 and targets were established for each developed country towards reducing carbon dioxide emissions. The agreement binds together 37 industrialized nations including the European community to reduce their average emission to 5 percent below their emission levels over the period from 2008 to 2012 (Onishi, 2002). The reduction in the amount of CO_2 emission can only be met by energy efficiency improvement and switching from high-carbon fossil fuels such as coal, towards less carbon-intensive energy sources, such as natural gases (Anderson et al., 2004). The fuel switching and other energy efficiency improvements can only take care of the reduction of CO_2 at the source, but still there is a limit of applying these changes without incurring some financial burden. Even with these changes there is always some production of CO_2. Carbon sequestration should be used in such a way that so that the carbon dioxide is captured and sequestered so as to reduce emissions further.

2.2. CO_2 CAPTURE AND SEQUESTRATION PROCESS DESCRIPTION

This process mainly involves three main steps (Benson, 2004):

a) CO_2 capture and separation

b) Compression and Transportation

c) Sequestration in Geological Formations

2.2.1. CO$_2$ Capture and Separation. The first step in the process of geological sequestration is the capturing of CO$_2$ and reproducing it in a concentrated form. Carbon dioxide is produced in electric power plants in the form of flue gas. The CO$_2$ is separated from the flue stream before injecting it underground. CO$_2$ has been captured from industrial process streams for 80 years (Metz et al., 2005), although most of the CO$_2$ is vented out to the atmosphere because there is no incentive or requirement to store it. There are three different approaches to capture CO$_2$ which are discussed below:

a) Post-Combustion Capture: Capturing of CO$_2$ from flue gas, which is produced by combustion of fossil fuels and biomass in air, is referred to as post-combustion capture. The flue gas from industries or other power generation plants is passed through equipment which separates most of the CO$_2$. The separated CO$_2$ is then transferred to the storage reservoir and the remaining CO$_2$ is discharged to the atmosphere.

b) Oxy-fuel Combustion Capture: In this process pure oxygen is used instead of air, resulting in a flue gas that is mainly CO$_2$ and H$_2$O which are easily separable and after which CO$_2$ can be captured, transported and stored. This process is still in the pilot stage because the temperature at which the CO$_2$ is burnt are far too high (about 3,500^o C) for typical power plants. The exhaust gas is cleaned of the additional pollutants like SO$_2$ and NOx which are then recycled back to the reaction unit to reduce the temperature.

c) Pre-Combustion capture: In this process the CO$_2$ is separated from the fuel by combining fuel with air/steam to produce hydrogen and carbon dioxide which is stored separately. The most commonly used technology utilizes steam reforming, in which steam is employed to extract hydrogen from natural gas. In the absence of a requirement or economic incentives, pre-combustion technologies have not been used for some power systems, such as natural gas combined-cycle power plants.

2.2.2. Compression and Transportation. CO_2 has to be compressed into super critical state before it is transported to the sequestration sites, wherein the density resembles a liquid but it expands to fill the space like a gas. Transport is the stage which links source and storage sites. CO2 is transferred in three states gas, liquid and solid. Commercial-scale transport uses tanks, pipelines and ships for gaseous and liquid carbon dioxide (Metz et al., 2005). Gas is transported at a temperature which is close to the atmospheric temperature which occupies a very large volume of storage, when the gas is compressed it occupies less volume of storage site. CO2 behaves differently when subjected to different temperature and pressure. There are two main methods for transporting CO2 to the storage sites which are discussed below:

1) Pipeline transport. Pipelines are the dominant ways of transporting CO_2 to the storage sites. Pipelines have been in use since a very long time in the United States for Enhanced Oil recovery (EOR) in the oil and gas industry. Currently more than 3,900 miles of pipeline transport CO_2 in the United States. The CO_2 is transported in a supercritical phase, the critical point at which the CO_2 exists in the supercritical phase is 1,070 psi. CO_2 is generally transported a temperature and pressure between 55 $^{\circ}$F and 110 $^{\circ}$F and 1,250 psi and 2,200 psi respectively (Forbes et al., 2008). The parameters which are to be taken into account while transporting CO_2 are purity and moisture content in CO_2. The presence of water molecules is very dangerous for the pipeline transport as CO_2 reacts with water to form carbonic acid which is corrosive which in turn corrodes the pipeline and could lead to leakage issues.

2) Ship Transport. The transportation of CO_2 by ship is mainly used by food and brewery industries. The process of ship transportation of CO_2 has a number of similarities as transportation of liquefied petroleum gas (LPG) by ship. The latest liquefied natural gas (LNG) carriers reach more than 200,000 m^3 capacity which is equivalent to 230 kt of liquid CO_2 (Metz et al., 2005). The ship transport cannot ensure the continuous supply of CO_2, there has to be a storage facility in which CO_2 can be stored before it is transferred to the sequestration site.

2.2.3. CO_2 Phase Behavior. The CO_2 is compressed before it is transferred to the sequestration sites through pipelines. The phase behavior of CO_2 changes with temperature, pressure and depth. This is one of the most important parameters to assess before sequestration of carbon dioxide. CO_2 is a thermodynamically very stable gas and is heavier than air with the density of 1.872 kg/m^3 at normal atmospheric conditions. CO_2 attains supercritical state at a temperature greater than 31.1^{o}C and pressure greater than 7.378 MPa. At this temperature and pressure CO_2 expands from 150 to 800 kg/m3 due to which it fills all the available volume and the liquid density of CO_2 with the increase in temperature and pressure. The higher the density of CO_2, lesser is the volume of required to fill up or sequester CO_2 in the available space as a separate phase (Bachu, 2000). Figure 2-1 shows the phase behavior of CO_2 with the change in temperature and pressure.
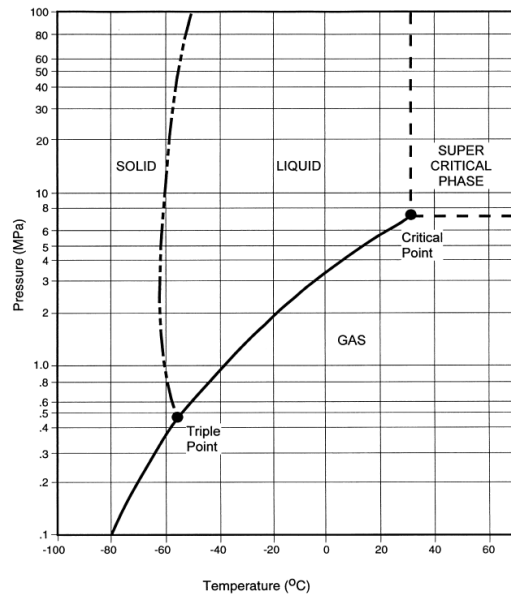
Figure 2-1. Carbon dioxide phase diagram (Bachu, 2000)

2.2.4. Sequestration in Geological Formations. There are several choices when selecting a geological formations for CO_2 storage. The initial choices are made based on the number of factors which includes the relative siting of major sources of CO_2 and secure storage sites and the availability of existing infrastructure (Espie, 2005). Underground storage of CO_2 is a phenomenon in which CO_2 is stored and trapped underground. Geological formations which are suitable for CO_2 storage occur in sedimentary basins where thick accumulations of sediments have been deposited over geological time periods of millions of years. Typically sedimentary basins consist of alternating layers of coarse sandstone and fine textured sediments like shale or clay. The sandstone serve as the storage reservoir with high permeability allowing CO_2 to be injected and the shale or clay layers serve as the seal which prevents CO_2 to migrate upwards. The pore spaces in grains or minerals are mainly filled with fluids like water, oil and gas. These spaces are distinguished by the presence of alternation layers of rocks with different textures. The same space where oil and gas are found is also utilized for CO_2 storage. CO_2 is basically injected at great depths. At greater depths CO_2 is more liquid than gas resulting in a more efficient use of the geological storage. The technology used for storing CO_2 in deep underground formations has already been in use in the oil and gas industry for Enhanced oil Recovery (EOR) (Benson, 2006). There are three types of geological formations which are considered for CO_2 sequestration: 1) Depleted oil and gas reservoirs 2) Deep saline reservoirs 3) Un-mineable coal seams as shown in Figure 2-2.
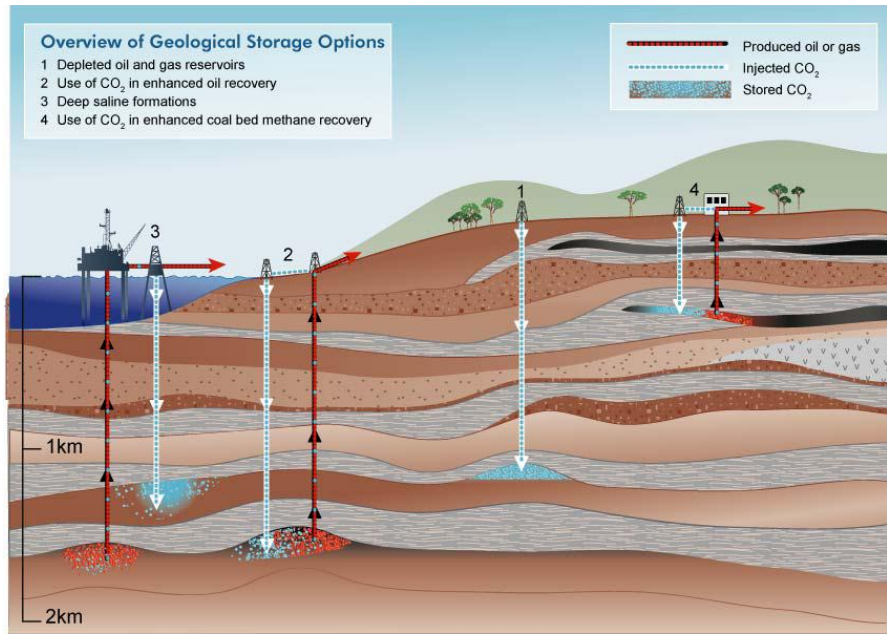
Figure 2-2.Several storage options for CO_2 in deep geological formations (Benson, 2006)

1) Depleted Oil and Gas Reservoirs: Storage of CO_2 in depleted oil and gas reservoirs is the best near term option of carbon dioxide sequestration. It is basically of two types:

   a) Oil Reservoirs: In the Enhanced oil recovery process the CO_2 is injected underground which dissolves into the oil and increases its volume which reduces the viscosity, and also increases the saturation and relative permeability of the oil. The density of CO_2 is less than oil and more than water, some of these properties make CO_2 ideal fluid for enhanced oil recovery. The pressure at which the CO_2 displaces the oil plays a vital role in the oil recovery and the CO_2 recovered is usually separated and re-injected into the reservoir to minimize the operating cost. In this process more than 50% and up to 67% of oil is recovered (Aladasani et al., 2012.). This cycle is repeated until maximum oil recovery is attained and the remainder is trapped in the oil reservoir by various means, such as irreducible saturation and dissolution in reservoir oil that is not produced and in pore space that is not connected to the flow path for the producing wells (Metz et al., 2005).

b) Gas reservoirs. The storage of CO_2 in gas fields requires a very large volume of storage space. The depleted gas field is utilized for CO_2 sequestration after the entire hydrocarbon has been produced. The properties of CO_2 is such that the density of CO_2 is greater than the hydrocarbon gases whereas the viscosity of CO_2 is less that the hydrocarbon gases. These properties allow CO_2 to displace hydrocarbon gases and increase ultimate recovery in EOR.

2) Deep saline reservoirs: Brine filled reservoirs have largest potential storage volume worldwide. Storage in brine field formations involves immiscible gravity dominated displacement by supercritical CO_2 with only 10% or even less dissolving into brine phase (Metz et al., 2005). However after a while CO_2 spreads on top of the formation and the surface area between CO_2 and brine increases which results in mixing of CO_2 with brine phase. The resulted mixture of CO_2 and brine is heavier than the unsaturated brine and settles at the bottom and is in a secure state.

3) Un-mineable coal seams. Coal beds which are not thick and deep enough or when the structural integrity of the coal is inadequate for mining are referred to as un-mineable coal seams. Even if coal cannot be mined, the coal beds are very permeable and have the capacity to trap gases such as methane. Methane is physically bound with coal bed. CO_2 has a higher capacity to bind with the coal bed than methane. Methane is recovered from coal beds after CO_2 is injected which displaces methane gas to the surface. This process is called Coal Bed Methane production. After the required methane has been recovered, the CO_2 is re-injected stored in the coal seams.

2.3. CO_2 STORAGE MECHANISMS IN GEOLOGICAL SEQUESTRATION

The effectiveness of geological CO_2 storage depends on the ability of the geological sinks and trapping mechanisms to confine the injected CO_2 for thousands of years. The most effective seals are those wherein the CO_2 is rendered immobile, sealed by a low permeable formation, or adsorbed by coal beds, or converted into solid minerals. The most important parameter which contributes to the presence of a barrier is the

permeability characteristics of the rock layers overlying or adjacent to the geological sinks (Nelson et al., 2005). Injected CO_2 can be trapped in the geological sinks by different types of mechanism. More than one type of trapping mechanism can also be present in a single geological sink. The geological sequestration of CO_2 can occur by physical or chemical trapping mechanism. There are at least four important trapping mechanisms for sealing CO_2 in geological formation 1) Physical trapping 2) solubility trapping 3) mineral trapping 4) Residual trapping (White et al., 2003). Figure 2.3 shows operating time frames of different trapping mechanisms.
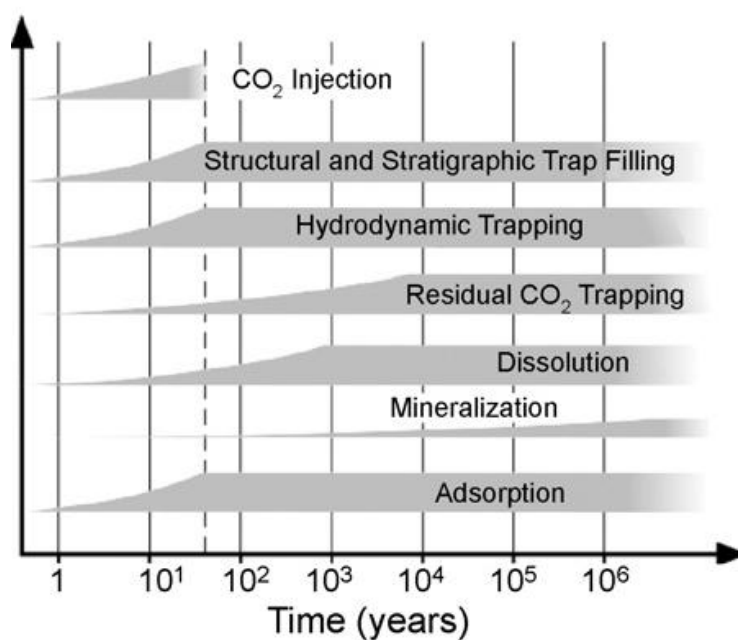
Figure 2-3. Operating time frame (Bachu et al., 2007)

2.3.1. Solubility Trapping. A geological sink is usually filled with formation water and is sealed or capped by a low permeability rock which stops leakage of CO_2 to the surface. In this type of trapping, CO_2 dissolves or reacts with formation water to form carbonic acid. Solubility trapping occurs in EOR during CO_2 flooding wherein CO_2

dissolves into the oil in the reservoir. The CO_2 after dissolving in the crude oil becomes heavy and settles down in the geological sink (Shaw et al., 2002).

2.3.2. Physical Trapping. Physical trapping basically is of two types structural and Stratigraphic traps. Structural traps are closed, physically bound traps and structures, which are mainly filled with saline water, oil or gas. Structure traps may have fractures or faults which are sometimes useful for CO_2 trapping in some cases and sometimes they serve as the pathway for the migration of CO_2 to the surface. Stratigraphic traps are formed from the changes in the rock formations by variation in the setting where rocks were initially deposited. Both of these traps are suitable for CO_2 trapping. It is to be noted that if the formation is always over pressured which can lead to the fracturing of caprock or reactivation of pre-existing faults (Streit et al., 2005).

2.3.3. Hydrodynamic Trapping. Hydrodynamic trapping is not based on just one single trapping mechanism but is a combination specific physical or chemical trapping mechanisms. In this type of trapping CO_2 occupies the pore space of the geological sinks. Hydrodynamic trapping can occur even if the pore space is initially 100% filled with water. When the CO_2 is injected into the formation, it displaces water from the pore space because CO_2 is less dense than water and migrates upward till it reaches an impermeable caprock which seals CO_2 in a local stratigraphic or structural trap. CO_2 dissolution occurs as soon as CO_2 contacts the formation water. Mineral precipitation can also occur initially but dissolution has to occur first. The storage capacity depends on the in situ conditions, rock mineralogy, and the volume of water that reacts with the injected CO_2. After the injection is stopped, the residual gas trapping occurs in which the plumes of the CO_2 migrate towards the impermeable formation. As this CO_2 dissolves overtime after it comes in contact with the formation water. It is to be noted where the distance from the deep injection site to the end of the overlying impermeable site is hundreds of miles than it takes millions of years for CO_2 to reach from geological sink to the surface.

2.3.4. Adsorption Trapping. In physical adsorption of CO_2, the CO_2 molecules are rendered immobile when they are trapped at near liquid like surfaces of coal organic matter, kerogen or minerals. The most common geological sinks where adsorption

trapping occurs are coal seams and shales. The hydrostatic pressure cause by the formation water controls the CO_2 adsorption process (Nelson et al., 2005).

2.3.5. Mineral Trapping. Mineral trapping is very much dependent on the temperature and pressure, rock matrix and composition of formation water. In this type of trapping dissolved CO_2 undergoes chemical reactions with minerals like Ca, Mg, and Fe which results in formation of solid carbonate mineral phase. These reactions depend on the contact surface between the mineral grains and the formation water containing dissolved CO_2, and also on the rate of fluid flow through pore spaces (Gunter et al., 2004). The chemical reactions that generate solid carbonate mineral phase are reversible and the rate of reaction is also very slow. Geological sinks which are low in carbonates and are rich in glauconite, illite, anorthite, chlorite or smectite minerals are most favorable sites for mineral trapping (Nelson et al., 2005). It is to be noted that mineral trapping is most secure permanent form of geological CO_2 sequestration.

2.3.6. Residual-Gas Trapping. The Residual gas trapping process is linked to the hydrodynamic trapping mechanism. This trapping mechanism is based on the irreducible gas saturation after the water which was expelled by the injected CO_2 moves back to the pore space. When the CO_2 is injected through the injection wells, it tends to create a vertical and lateral flow path as it moves away from the injection well and move towards the top of aquifer due to the buoyancy forces. CO_2 start to displace the water at the leading edge of the plume and water displace CO_2 at the trailing edge after the injection has stopped. A trail of immobile CO_2 is left behind the plumes as it migrates upwards. Residual trapping occurs only after the injection has stopped. It is to be noted that residual trapping does not occur in the structural and stratigraphic traps where water drainage occurs when CO_2 is injected. Residual gas trapping plays an important role overtime after injection of CO_2 becomes less or gets stopped as a decreasing amount of CO_2 will remain in a free, mobile phase over time which can be seen in Figure 2-4 (Bachu et al., 2007).
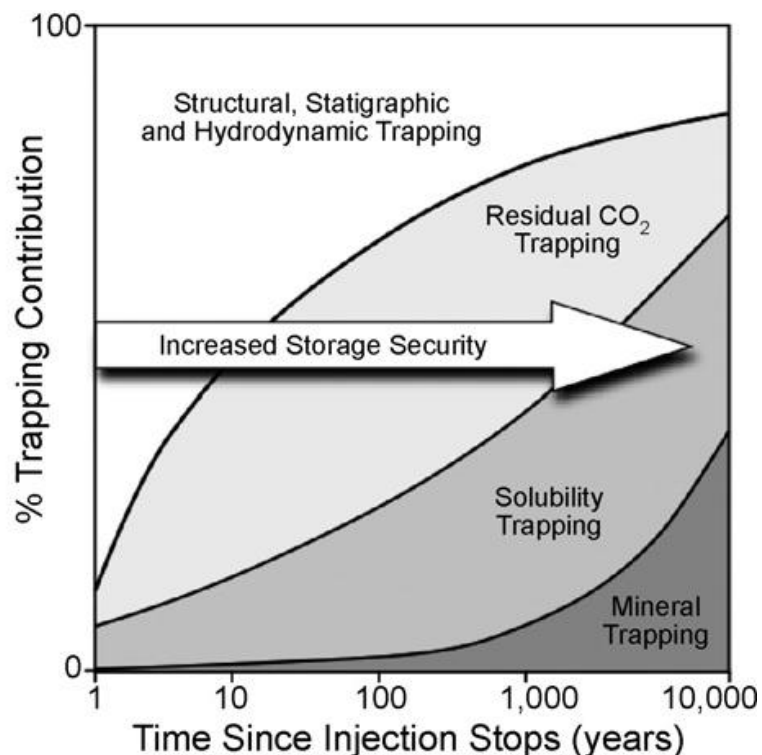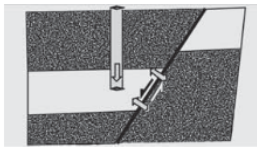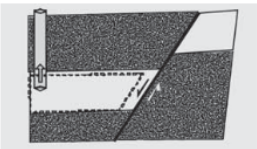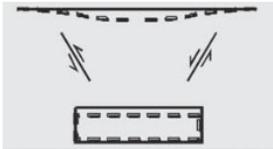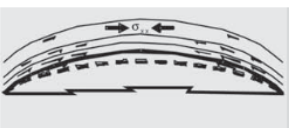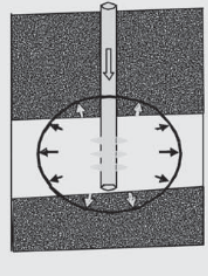
Figure 2-4. Storage capacity of different trapping mechanism (Bachu et al., 2007)

2.4. GEOLOGICAL FAILURE MECHANISMS AND RISK ANALYSIS FOR SITE SELECTION

Geological storage of CO_2 is designed to maintain and secure storage for thousands of years. But in some cases there is a possibility of leakage of CO_2 to the surface. The caprock provides a low permeability sealing above the geological sink which prevents upward migration of CO_2 to the surface. The reactivation of pre-existing faults and fractures occurs due to seismic activities which may cause leakage of CO_2 to the surface. All these factors are to be taken into account before the sequestration as they can contribute to a complex leakage scenario. The critical geomechanics and methods of assessment and mitigation are shown in Table 2.1. Each risk factor in the table is described by mechanisms involved and methods to assess and mitigate the risks associated with it.

Table 2.1. Geomechanics risk mechanism for loss of bounding seal integrity (Hawkes et al., 2005)

S.No.	Risk Factor		Mechanism	Mthod of Assessment and Mitigation
1	Reactivation of faults within or bounding reservoir: a)Pressure change in the fault plane		Local pressure increases near a fault during injection reduces effective normal stress-Reducing the shear strength of the fault	1.Geomechanical analyses to determine maximum safe pressure. 2. Inject into reservoir "sweet spots" to avoid locally high pressures. 3. Preferential selection of injection wells that are distant from faults.
	b) Pressure changes that are prevasive throughout the reservoir		1. In-situ stress magintudes changes. 2. During the depleted reservoir pressure risk of fault activation is increases.	1. Geomechanical analyses is done to determine slip at minimum reservoir pressure 2. Previous data should be monitored for any indication of seismicity.
2	Reactivation of faults in the caprock		1. Overbuden subsidence is caused by the reservoir compaction which in turn is due to the depleted pressure. 2. Shear stress develops in the caprock	1. Geomechanical analyses is done to determine if the shear stresses at minimum reservoir pressure were capable of reactivating faults. 2. Previous data should be monitored for any indication of seismicity.
3	Induced Shear Failure		1. Expansion or contraction of reservoir during injection results in the shear stresses at the reservoir-caprock bouondary. 2. large compressive horizontal compressive stresses are developed in the anticline reservoirs	Geomechanical analyses is done to determines the maximum safe change in pressure.
4	Out of zone hydrulic fractures: a) Before injection of CO2		1. Hydrualic is caused by the fracture treatment or high pressure squeezez. 2. Waterflood can also cause hydraulic fracture. 3. Fracturing of caprock is possible during cementing or workovers	Histroy should be montiored to find out any containment loss. 2. Cementing and workover should be monitored.
	b) Duriing CO2 injection		1. Injection above fracturing pressure causes fracture in the reservoirs. If stress contrast is low, fracture can grow into the caprock.	1. Fracturing is not done. 2. A safe upper pressure limit is identified and a safety margin should be maintained below it.
5	Leakage outside of casing due to poor cement emplacement in yielded and enlarged boreholes		1. Stress at at adjacent well can cause rock yielding, detachment and enlargement. 2. Cement emplacement may be poor in severly enlarged or rugose hole sections. 3. Zones of high near well may exist if induced shear fractures and microcracks are not penetrated by cement.	1. Near by wells are drilled with a mud type and mud density sufficient to mitigate severe yielding and enlragement. 2. High rick wells are continously monitored.

2.4.1. Faults and Fractures. Faults and Fractures may be present in many geological formations. They control the movement of fluids from place to place and must be assessed in a site specific basis. In some cases faults and fracture provide a way for CO_2 to migrate from greater depths to shallower depths. In other cases they create a seal to trap oil and gas in geological sinks. These seals have contained oil and gas for millions of years. The role of faults and fractures is assessed by studying regional geology, hydrology and geochemistry. From the information from all these studies it can be predicted whether these features will favor the fluid flow or they will act as a barrier. Well testing can be done on fluids which are withdrawn from the formation with the continuous monitoring of pressure (Benson, 2006).

2.4.2. Fault Reactivation. Fault reactivation is one of the most important factor for safe storage of CO_2 in geological sinks. Faults are natural geological discontinuities in the upper crust. Natural resource extraction like mining, oil wells can change the state of stresses and consequences of that can cause the reactivation of pre-existing faults and fractures. Fault activation is basically activation of pre-existing faults which may occur whenever the shear stress acting on the fracture plain exceeds the Mohr-Coulomb failure criteria which is represented by the equation 1 where τ_s is the shear stress, φ is the friction angle, c is the cohesion and σ_n is the normal stress. The practical application of this equation is that whenever the left side exceeds the right side the fault will slip which will create the possible leakage pathways for CO_2. Whenever a gas is extracted, the reservoir tends to contract with normal stress generally decreasing. Slippage mainly occurs in the vertical faults because of the stiffness of the surrounding porous medium opposes the vertical deformation. However gas injection causes expansion of the reservoir with increasing normal stress. The reactivation of faults is less in injection than extraction. But slippage on the border faults may still occur during the initial phase of injection. The importance of reactivation of faults for the sequestration is related to the possible generation leakage pathways for CO_2 (Ferronato et al., 2010).

$$|\tau_s| \geq c + \sigma_n tan\varphi \tag{1}$$

According to Anderson's scheme fault can also be classified as normal or extensional, strike-slip and reverse or thrust faults as a function of minimum horizontal stress, maximum horizontal stress and the vertical stress as shown in Figure 2.5.
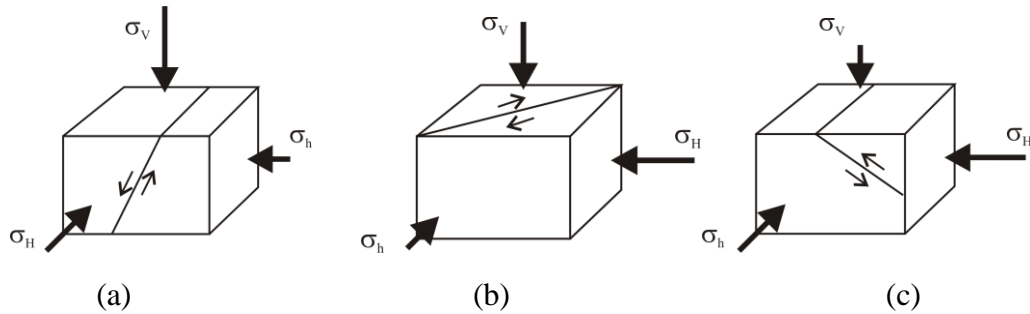
Figure 2-5. Anderson's classification of faults a) Normal fault b) Strike-slip fault c) Reverse fault (Nacht et al., 2010)

Fault reactivation is controlled by shear stress (τ) and the normal stress components (σ_n) on the fault plane which can be expressed for a normal faulting regime in a two-dimensional case as:

$$\tau = \frac{(\sigma_v' - \sigma_h')}{2} sin2\delta \tag{2}$$

$$\sigma_n = \frac{(\sigma_v' + \sigma_h')}{2} + \frac{(\sigma_v' - \sigma_h')}{2} cos2\delta \tag{3}$$

$$\sigma_v' = \sigma_v - \alpha p \tag{4}$$

$$\sigma_h' = \sigma_h - \alpha p \tag{5a}$$

$$\sigma_h' = \left(\frac{v}{1-v}\right)(\sigma_v) + \alpha p(1 - \frac{v}{1-v}) \tag{5b}$$

In the above equations δ is the fault's dip angle, σ_v' and σ_h' are the effective vertical and minimum horizontal stresses, σ_v and σ_h are the total vertical and minimum horizontal stresses. Fault strength is obtained by the Mohr-Coulomb criterion:

$$\tau_{slip} = c + \mu(\sigma_n - \alpha p) \tag{6}$$

$$\sigma_n' = \sigma_n - \alpha p \tag{7}$$

$$\mu = tan\varphi \tag{8}$$

Where τ_{slip} is critical shear stress for slip to occur, c is the cohesion, equation (8) shows the fault's friction coefficient for a given fault's friction angle where φ is the angle of friction, α is the Biot's coefficient and p is the pore pressure. A parameter was generated to measure the likelihood of reactivation of a given fault which is shown below:

$$ST = \frac{\tau}{\tau_{slip}} \tag{9}$$

Slip tendency parameter ranges from $0 \leq ST \leq 1$. The higher the slip tendency factor greater will be the chances of fault reactivation. Fault becomes hydraulically conductive whenever shear stress violates the Mohr-Coulomb failure criteria. The fault's cohesion is usually lower than 1 MPa and is commonly taken as zero. If equation (9) is applied for a cohesion less faults with $\mu=0.6$, normal faults with dip angle $\delta\sim60^{\circ}$ are obtained which are more prone to reactivation.

The pore pressure also has a vital role to play in fault reactivation. Pore pressure to prevent the fault reactivation is dependent on the stress and the fluid paths of the reservoir. The vertical stress is same as the overburden and the crust is not vertically restrained, so the vertical stress components are less affected by the pore pressure. On the other hand, the reservoir is constrained in the horizontal direction so the minimum horizontal stress is largely affected by the pore pressure. Figure 2.6 and 2.7 illustrates two different scenarios, depletion and injection. During depletion, minimum horizontal stress decreases and thus the differential stress increases, as a result fault can reactivate even if the effective stress are increasing as shown in Figure 2-6. However during injection the minimum horizontal stress increases and thus reduces the differential stress which can be seen in Figure 2-7 (Nacht et al., 2010).
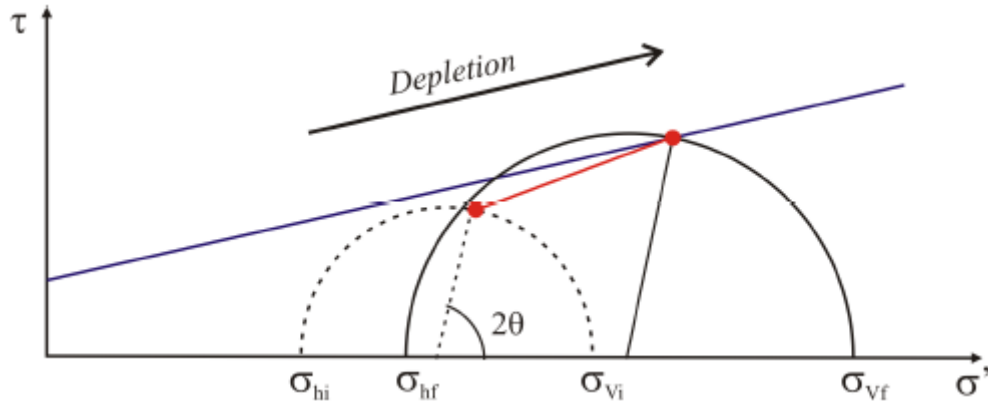
Figure 2-6. Reactivated fault during depletion (Nacht et al., 2010)
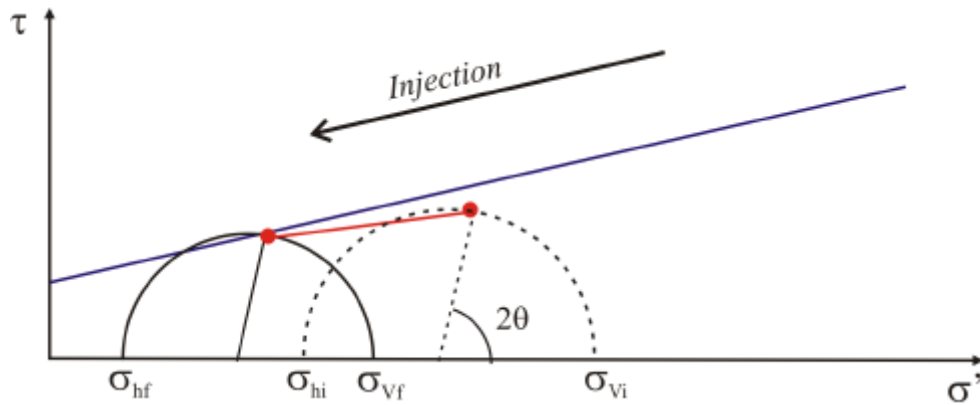
Figure 2-7. Reactivated fault during injection (Nacht et al., 2010)

There are number of mechanisms that can result in the reactivation of existing fault, either during injection or production. Some of these mechanisms are discussed below (Hawkes et al., 2005):

For faults within or bounding the reservoir, the chances of fault reactivation increases when the injection pressure penetrates the fault plane. It can be seen from equation (4) that if the pore pressure is increased, the slip tendency of the fault will also increase when all the other parameters remain unchanged. So geomechanical analyses

should be conducted to identify the maximum injection pressure to avoid fault reactivation.

For faults within or bounding the reservoir, the changes in the magnitude of stress will be induced when the change in pore pressure is pervasive throughout the reservoir. The magnitude of these stress changes is generally proportional to the magnitude of the pressure change but this change is affected by many properties of the reservoir like thickness, shape, orientation of the faults etc. Minimum pressure is experienced during depletion and maximum pressure is expected during injection.

Pore pressure changes may cause expansion and contraction of the reservoir. If the expansion of the reservoir is large enough than it can induce the displacement of the overburden above the reservoir and if there is any high angle fault in the overburden than there is a risk that the induced shear stresses can reactivate them. In some cases the risk mechanism is more related to the reservoir depletion rather than the injection. Geomechanical analyses to assess reservoir stability of CO_2 storage is mainly focused on the risk associated at maximum reservoir pressure.

Shear stresses are induced due to the pressure or temperature changes in the reservoir due to the fluid injection or production which causes the reservoir to expand or contract. When the fluid is injected from the surface, there is temperature induced shear stresses which when coupled with the pressure changes poses a high risk to the caprock integrity. Following are some of the factors that pose high risk to caprock integrity (Hawkes et al., 2005):

- High reservoir compressibility
- Stiff caprock
- Large pressure changes
- Low strength caprock
- Shallow depths
- Anticlinal reservoirs

These factors may create leakage pathways for the migration of CO_2 from geological sinks to the surface. The increase or decrease in pore pressure also affects the efficiency of these factors.

Injection of fluids at high injection pressures and low temperature causes hydraulic fractures. Undesired creation of hydraulic fractures may be risky and to avoid that a suitable pressure should be selected for fluid injection. The occurrence of hydraulic fractures inside the reservoir is desired as it improves storage efficiency. The near wellbore pressures which are associated with high rate injection can be mitigated by the preferential selection of high permeability reservoirs and usage of horizontal wells for CO_2 storage.

Whenever a borehole is drilled inside a formation there is a change in the state of stress around the borehole. Borehole is stable when the strength of the rock is more than the induced stresses. The rocks surrounding the borehole tends to fracture when the induced stresses are more than the strength of the rock and yielding will occur which in turn will cause the detachment of the yielded rock from the borehole. These wells sometimes may also have poor cement emplacement which may create a leakage pathway for the CO_2 to the surface. Following are some of the factors which affect borehole stability:

- Formation pressure
- Near well pore pressure change
- Rock strength
- In situ stresses

Buckling failure can be a result of the poor cement job and reservoir compaction which can apply high axial load on the casing strings within the reservoir. All the parameters if monitored or assessed properly then there are less chance of casing deformation and failure.

Roughness is a measurement of the inherent surface movement, interlocking and undulations relative to its mean plane. Shear strength is dependent on the roughness especially in dislocated and interlocking fractures. Barton proposed a joint roughness

coefficient (JRC) to describe the joint roughness ranging from a scale of 0 to 20. Typical roughness profiles are shown in Figure 2-8. Join wall compressive strength (JCS) is also a very important component of shear strength and deformation in case of direct rock to rock contact and unfilled joints. Slight dislocation of the joints caused by the shear displacements causes small asperity in the contact areas of rock which approaches the compressive strength of the rock wall material which may produce asperity damage. Basic angle of friction and residual angle of friction represents minimum shear resistance.
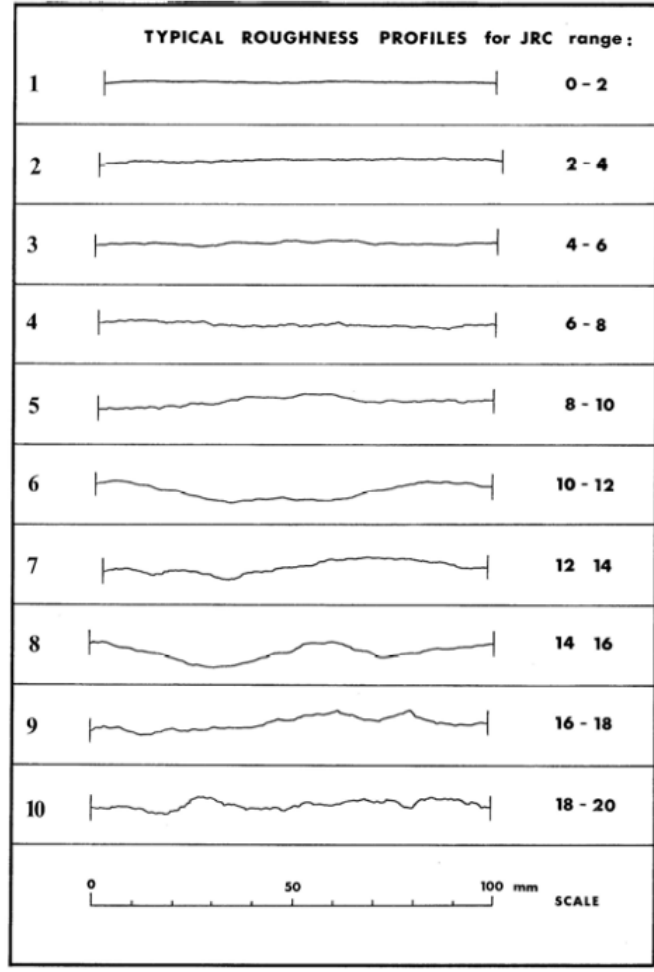

Figure 2-8. Typical roughness profile of joints (Barton, 2008)

2.5. ROCK MECHANICS: PROPERTIES

Rock mechanics is the applied and theoretical science of the mechanical behavior of the rocks and rocks masses. It is mainly concerned with the response of rock and rock masses to external forces. The state of stress of the formation changes when CO_2 is injected into the subsurface formation. Pore pressure also changes when CO_2 is injected underground which may cause reactivation of previous faults and fractures or create new ones which may create a leakage pathway for the CO_2 to the surface. In order to predict and anticipate the response of the rock to the injection it is necessary to do laboratory experiment and study geomechanics of the formation.

Rock Mechanics properties are calculated on the basis of following four elastic constants:-

- Poisson's ratio(ν)
- Young's Modulus(E)
- Bulk Modulus(K)
- Shear Modulus(μ)

When the material is compressed in one direction, the material tends to expand in the other two directions perpendicular to the direction of compression. This phenomenon is called poisson's effect.

Poisson's ratio is also defined as the ratio of radial or transverse to the longitudinal axial strain experienced by the rock. It is represented by equation (10).

$$\nu = \frac{\varepsilon_{radial}}{\varepsilon_{longitudinal}} \tag{10}$$

Young's Modulus is the measure of stiffness of an elastic material and is quantity used to characterize materials. It is also defined as the ratio of uniaxial stress to the uniaxial strain in the range of stress in which Hooke's law holds. It is represented by equation (11).

$$\sigma = \varepsilon E \tag{11}$$

Where σ is the axial stress and ε is the axial strain and E is the young's modulus.

The bulk modulus measures the substance's resistance to uniform compression. It is represented by equation (12).

$$K = \frac{\sigma}{\Delta v / v} \tag{12}$$

Where K is the bulk modulus, σ is stress, Δv is the change in volume, v is the volume.

Shear modulus is a measure of the resistance to shear deformation. It is also defined as the ratio of the shear stress (σ_{shear}) to the shear strain (ε_{shear}) when a shear force is applied to the object. Shear modulus is represented by (13).

$$\mu = \frac{\sigma_{shear}}{\varepsilon_{shear}} \tag{13}$$

2.6. STRESS

Stress is a measure of the internal forces acting within a deformable body. It is the measure of average force per unit area of a surface within the body on which internal forces act.

2.6.1. Forces and Stresses. Forces have vector nature and are basically composed of normal and the shear components. Normal force acts perpendicular to the plane of the surface and shear force acts parallel to the plane of the surface. The stress is the measure of the internal forces acting within a deformed body. The state of stress is generally defined by the traction vectors passing through that point. The traction generally varies with the orientation of the surface on which it acts and is most conveniently represented with the aid of an entity known as the stress tensor. The stress tensor is found by using

co-ordinate transformation on the traction vectors corresponding to three mutually perpendicular planes. This relation is known as Cauchy's second law:

$$T_i = \sigma_{ij} n_j \qquad (14)$$

Where σ_{ij} is the stress tensor which is expressed as follows:

$$\sigma_{ij} = \begin{bmatrix} \sigma_{xx} & \sigma_{xy} & \sigma_{xz} \\ \sigma_{yx} & \sigma_{yy} & \sigma_{yz} \\ \sigma_{zx} & \sigma_{zy} & \sigma_{zz} \end{bmatrix} \qquad (15)$$

2.6.2. Principal Stresses. For a particular coordinate system, all shear stresses will vanish. The stress field is completely defined by the three normal stresses which are known as Principal stresses. The three principal stresses are normal to each other, but not necessarily equal in magnitude. For a stress field having just the principal stresses than the stress tensor would be expressed as:

$$\sigma_{ij} = \begin{bmatrix} \sigma_{xx} & 0 & 0 \\ 0 & \sigma_{yy} & 0 \\ 0 & 0 & \sigma_{zz} \end{bmatrix} \qquad (16)$$

2.6.3. Stress Derivatives. Stress derivatives are explained below:

Differential Stress: It is the difference between the maximum principal stress and the minimum principal stress. It is expressed as follows:

$$\sigma_d = \sigma_1 - \sigma_3 \qquad (17)$$

Mean Stress: It is the average of all the principal stresses and is expressed as follows:

$$\sigma_m = \frac{(\sigma_1 + \sigma_2 + \sigma_3)}{3} \qquad (18)$$

Deviatoric Stress: It is expressed as:

$$\sigma_{ij} = \begin{bmatrix} \sigma_{xx} - \sigma_m & \tau_{xy} & \tau_{xz} \\ \tau_{xy} & \sigma_{yy} - \sigma_m & \tau_{yz} \\ \tau_{xz} & \tau_{yz} & \sigma_{zz} - \sigma_m \end{bmatrix} \qquad (19)$$

2.6.4. Mohr Circle. The graphical representation of the state of stress at a point is represented by Mohr Circle. The Mohr Circle is used to represent shear stress and normal stress on all planes in all possible orientations. Mohr circle was developed as a technique which could be easily remembered and can determine new stress components graphically. The equation of stress is derived from the equation of plane stresses. If geological sign convention is considered than compressive stress is positive and tensile stress is negative.

Normal and shear stresses on a point P are $\sigma_n(P)$ and $\tau(P)$:

$$\sigma_n(P) = \frac{1}{2}(\sigma_1 - \sigma_3) + \frac{1}{2}(\sigma_1 - \sigma_3)cos2\theta \qquad (20)$$

$$\tau = \frac{1}{2}(\sigma_1 - \sigma_3)sin2\theta \qquad (21)$$

Where σ_1 is the maximum principal stress, σ_3 is the minimum principal stress and 2θ is the angle between the magnitude of shear stress and normal stress with σ_1 measured in anti-clockwise direction.

Equation (20) and (21) can be rearranged to form equation of a circle:

$$\{\sigma_n - 1/2(\sigma_1 + \sigma_3)\}^2 + \tau^2 = \{1/2(\sigma_1 - \sigma_3)\}^2 \qquad (22)$$

Equation (18) has the form:

$$(x - a)^2 + y^2 = r^2 \qquad (23)$$

Which is the equation of the circle with the radius centered on the x-axis at a distance from origin.

Now: Radius:

$$r = 1/2\ (\sigma_1 - \sigma_3) \tag{24}$$

Distance:

$$a = 1/2\ (\sigma_1 + \sigma_3) \tag{25}$$

Differential stress represents the diameter of the circle and mean stress represents the center of the circle. Figure 2-9 shows the Mohr diagram for the stress at a point.
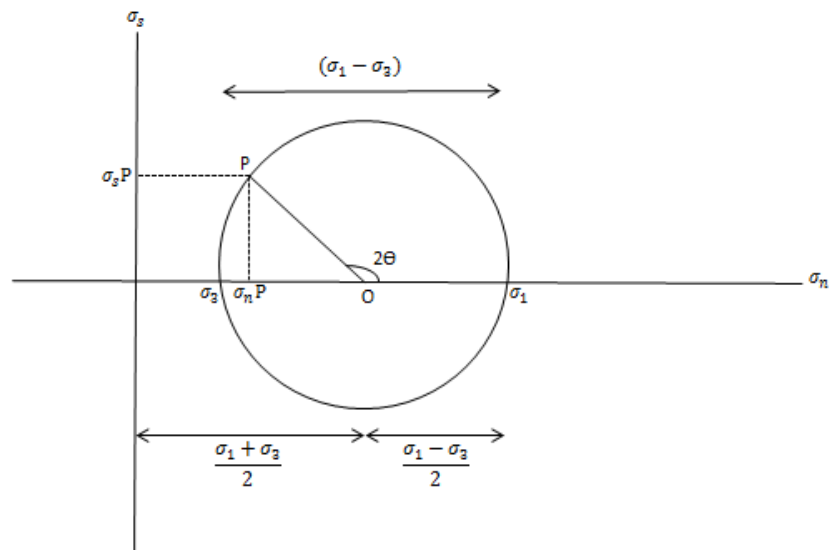
Figure 2-9. Mohr diagram for stress

2.7. FAILURE CRITERIA

Whenever the rock is over stressed i.e. above critical stresses, the rock is subject to failure. Rock failure is a function of anisotropy, geometry and most importantly in-situ stress regime. Whenever there is a disturbance in the in-situ stress regime the rock tends towards failure. The direct shear strength is determined and rocks were tested for failure by direct shear testing method.

Mohr-Coulomb failure criteria: This is one of the most important failure criteria used for the analysis of rock failure. It is basically a linear relation between normal stress, coefficient of friction and shear stress resisted by the cohesion of the material which is represented by equation (26).

$$\tau = S_0 + \mu\tan\varphi \tag{26}$$

Where τ is the Shear stress, S_0 is the Cohesion, μ is the Coefficient of friction and φ is the Angle of frition.

The Mohr-envelope is generated by plotting a curve which joins the points of failure of the rock. There is no available method for the calculation of cohesion (S_0=0) and angle of friction if there are pre-existing faults. Mohr circle is drawn at in-situ and effective stresses condition and if the potential change in stresses causes the mohr circle to cross the Mohr Envelope that it results in the reactivation of faults. Figure 2-10 shows the development of the mohr circle and the failure envelope at zero cohesion. Any pre-existing fracture whose orientation lie in the shaded region will slip. Increase in pore pressure will shift the mohr circle towards the failure envelope.
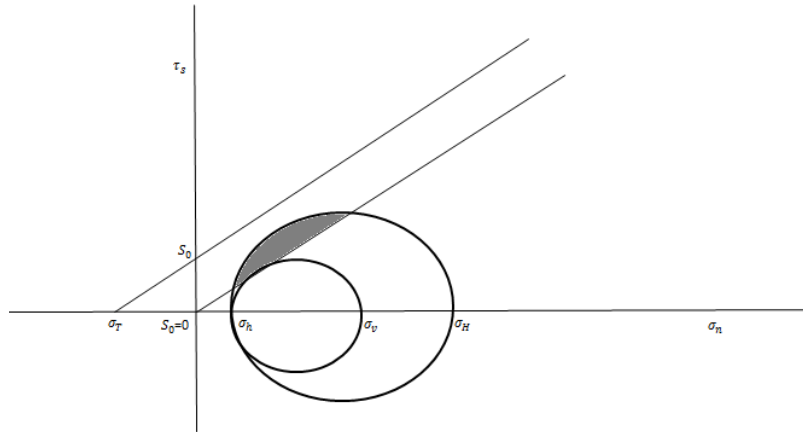
Figure 2-10. Mohr circle representing fault reactivation

3. GEOLOGY, SELECTION AND PREPARATION OF ROCK SAMPLES

3.1. GENERAL GEOLOGIC BACKGROUND

The rock used for mechanical testing in this research was cored from the outcrops of formations found in the region under consideration for CO_2 sequestration. The formation selected as a possible reservoir for CO_2 storage was the Lamotte sandstone. Due to the extensive permeability and anticipated porosity, the Lamotte sandstone will constitute a major storage area for the injection of CO_2. The upper cambrian Lamotte Sandstone rests on the Precambrian basement and is overlaid successively by the upper Cambrian Bonn Terre Dolomite, Davis shaly dolomite and Derby-Doerun dolomitic shale formations. All of these formations form part of the Ozark uplift. The Ozark dome is an asymmetrical uplift with the apex located at South East of Missouri State in an area called as St Francois mountains. Figure 3.1 shows the detailed stratigraphy of the cambrian Lamotte and the overlying formations (Boongird et al., 2006).
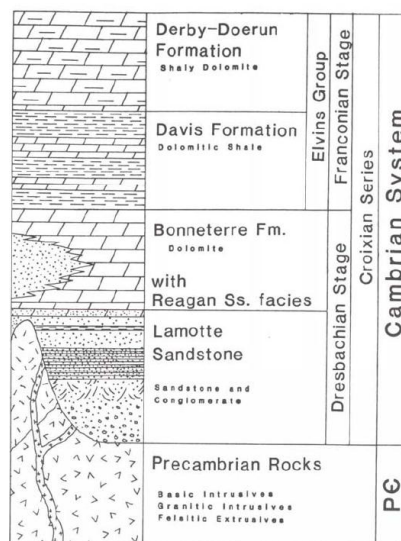

Figure 3-1. Stratigraphy of site of interest (Boongird et al., 2006)

3.1.1. Lamotte Sandstone.   The Lamotte sandstone is the upper cambrian and lowermost paleozoic sedimentary formation in the state of Missouri. The Lamotte rests on unconformably on a variety of precambrian lithologies, mostly igneous and metamorphic rocks. The Lamottte is overlaid by the Bonne Terre formation. The cambrian age was between 544 to 505 million years ago and was characterized by a shallow continental sea overlying Missouri which existed nearer to the equator. The boundary between the Lamotte and the overlying Bonne Terre formation is usually characterized as the region where lithology changes from slightly dolomitic sandstone to a sandy dolomite (Boongird et al., 2006).

3.1.2. Bonne Terre Dolomite. Immediately above the Lamotte formation lies the Bonne Terre formation. The Bonne Terre formation is a complex lithic unit with three layers (lower, middle and upper) strata in the unit and constitutes the main host of lead which is the major resource in the state of Missouri. Lyle in 1973 had conducted a detailed facies and petrography report and names four facies, four reef, reef complex, back reef and offshore reef (Boongird et al., 2006).

3.1.3. Elvin's Group.   The dual formation of Davis shaly dolomite and Derby-Doerun dolomitic shale is known as Elvin's Group formations. These formations are expected to form the cap rock due to their limited porosity and permeability and thus expected to hold CO_2 in place after injection. The Davis is characterized by high shale content and having a conformable contact, wherever identifiable, with the overlying Derby-Doerun formation (Boongird et al., 2006).

3.2. SAMPLE GEOLOGY & SELECTION

The samples were created from the outcrops of the formations which were representative of the actual site geology. Sourcing refers to the breaking of the rock from the rock outcropping to be used as a source for creating rock samples. The source rocks were obtained using the coordinates shown in Table 3-1. The points which were considered during selection of the source rock are shown below:

- Orientation of the rock with respect to the magnetic north before breaking the rock
- Rock should be subjected to least weathering
- Bedding faults and Fractures
- Source rock is selected based on the visual inspection

Table 3.1. Sampling details

Formation	Lithology	Depth	GPS Co-ordinates
Bonne Terre	Shaly Dolomite	Outcrop	N37°49'735" W90°40'48"
Davis	Shaly Dolomite	Outcrop	N37°51'8251" W90°33'7614"
Derby-Doerun	Shaly Dolomite	Outcrop	N37°49'8881" W90°31'6696"
Lamotte	Sandstone	Outcrop	N37°49'735" W90°34'789"

3.3. SAMPLE PREPARATION FOR DIRECT SHEAR TEST

The samples had to be prepared by cutting the source rock using the rock saw in the department. The dimension of the rock sample is based upon the experiments to be performed. The experiment conducted was direct shear test.

3.3.1. Sample Dimension. Cubical test specimen of dimension 4" in length, 4" in width and 5" in height were used for the test. Rock boulders were carefully cut into cubical shape using the rock saw. Fractures were created in the rock samples very carefully using a chisel and a hammer by hitting the cubical rock sample at the center. Rock sample after creating the fracture is shown in Figure 3-2.
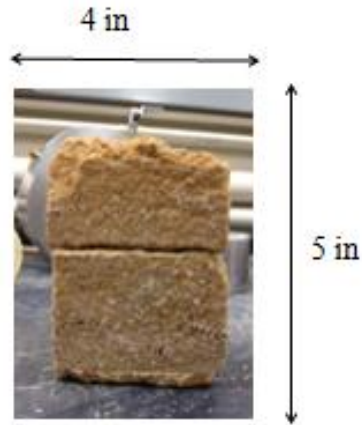
Figure 3-2. Rock sample after creating the fracture

3.3.2. Cementing of the Rock Sample.   Quick drying cement was used for the cementing of sample inside the shear ring. A 1:3 water-cement ratio was used for the cementing purpose. Following steps were taken in the process:

- One half of the rock sample is placed inside the bottom shear ring and is positioned at the desired location using modeling clay
- Cement slurry is poured from the sides of the rock sample in the bottom shear ring to within a few millimeters from the top which can be seen from Figure 3-3.

Figure 3-3. Cementing of the rock sample

- Cement slurry is allowed to set for 4-5 hours

- Two halves of the spacer rings were placed on the top of the bottom shear ring

- Gap is filled using the molding clay so that the cement slurry does not go inside the fracture which can be seen in Figure 3-4

Figure 3-4. Rock sample inside the shear ring

- Upper ring is fully tightened by the holding screws after it is placed on the spacer ring

- Another batch of cement slurry was poured on the top of the molding clay filling the upper specimen within a few millimeters from the top

- Cement is allowed to cure to gain its full strength

- Spacer bars are removed after the cement is fully cured and the rock sample is ready for the testing which can be seen Figure 3-5

Figure 3-5. Shear ring wihtout spacer

4. LABORATORY EXPERIMENTAL SETUP & PROCEDURE

This section describes the laboratory setup to conduct the direct shear test and laboratory procedure used to determine the rock mechanical properties of rock samples. The direct shear apparatus is used to determine the peak and residual shear strength of a test material as a function of stress normal to the shear plane.

4.1. DIRECT SHEAR TESTING SYSTEM

The GCTS direct shear apparatus is able to test a wide range of rock mechanics specimen to determine the shear strength of the fractures in the rocks. The system works on the application of normal load and horizontal shear load. The normal and shear deformations are monitored using either linear variable differential transducers (LVDTs) or dial gauges. The shear load, shear deformation, normal load and the normal deformation are monitored by the GCTS CATS software which includes inputs from them. At the end of the experiment shear stress vs time graph is generated from which peak and residual shear strength are determined, Shear strength is measured by the apparatus is in KPa (Kilopascals). Two air/oil booster pumps are used to set the normal load and shear displacement rate. Figure 4-1 illustrates the schematic diagram of direct shear apparatus.

Figure 4-1 shows different components of direct shear apparatus. Normal load is applied from the Normal actuator, shear load is applied from the shear actuator. Hydraulic/air pressure of 30:1 is used to apply normal and shear load on the rock sample. Normal pneumatic oil is used in the hydraulic pump which is supplied to the shear and normal actuator through strong rubber cables as shown in Figure 4-1. Control panel is also shown in the figure from which all the parameters are controlled.
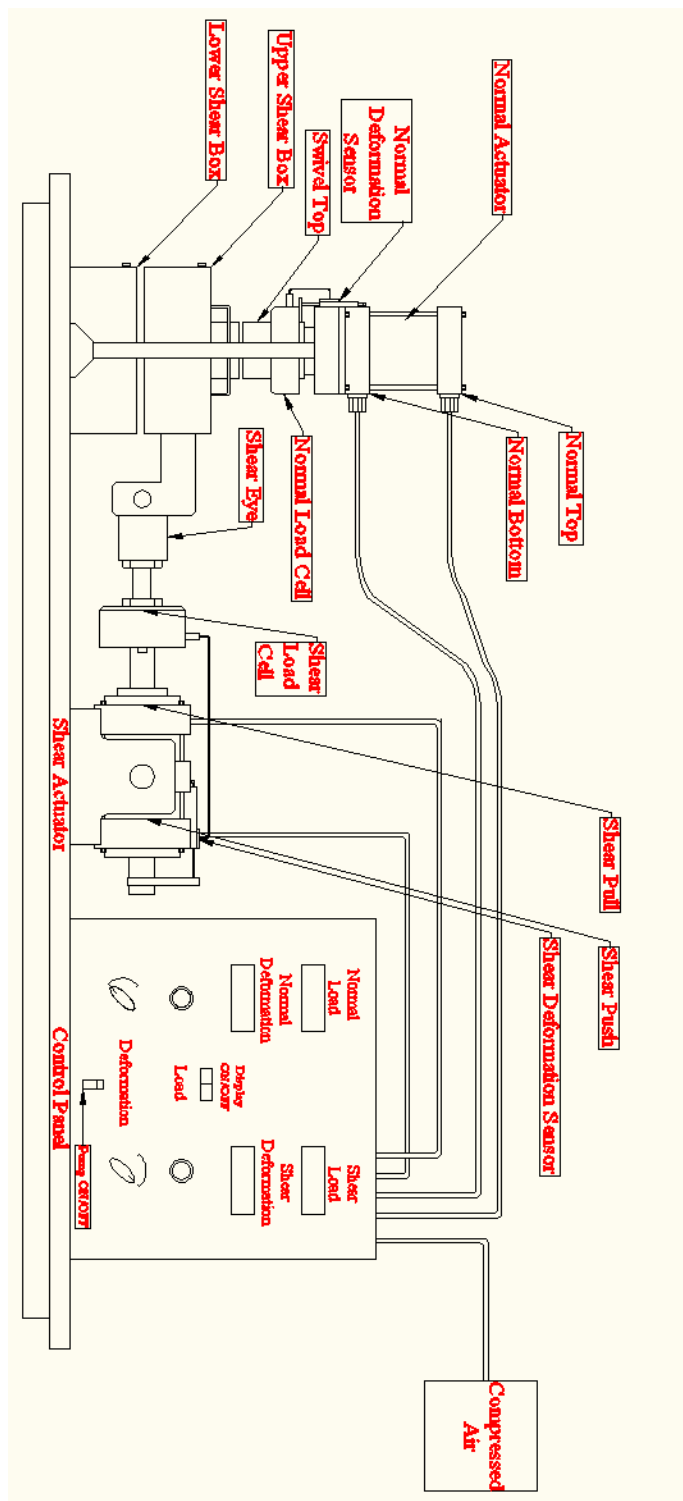
Figure 4-1. Direct shear apparatus

4.2. DIRECT SHEAR APPARATUS COMPONENTS

The system was composed of the following components:

- Normal loading mechanism
- Shear loading mechanism
- Normal and shear load detection
- Normal and shear deformation detection
- Pump system
- Direct shear sample mounting

4.2.1. Normal Load Mechanism. The normal load is evenly distributed over the plane to be tested and is applied using a hydraulic mechanical system. The normal load is applied through a normal load actuator and the normal load actuator stroke must be greater than the dilation expected during the experiment.

4.2.2. Shear Loading Mechanism. The shear load is also applied using a hydraulic system. The shear load is applied through a shear actuator which is mounted on the apparatus to apply horizontal load. The load is distributed evenly along one half face of the test sample with the resultant force acting in the direction of shearing. There are also low friction devices built in the apparatus so as to make sure that the resistance to shear displacement is less than the shear force applied.

4.2.3. Normal and Shear Load Detection. The normal load is monitored using normal load cell mounted between the normal load actuator and the top of the shear box. The shear load is monitored using a shear load cell mounted between the shear load actuator and side of the shear box. The load accuracy is $\pm$ 2% of the maximum force reached in the test.

4.2.4. Normal and Shear Deformation Detection. The normal deformation is measured using a normal load sensor which is a linear variable differential transducer (LVDT) attached at the top of the normal load cell and the swivel pipe. The shear load is measures using a shear load sensor which is also a linear variable differential transducer (LVDT) attached to the top of the shear actuator.

4.2.5. Pump System. Two air/oil booster pumps operate at 100 psi and this compressed air allows the user to easily set the normal load and alter the shear deformation rate. The shear pump includes a 4-way valve to easily reverse the loading direction. The values of the normal load and shear deformation are digitally displayed, and all the controlling knobs are set on a easy to use front panel of a metal cabinet.

4.2.6. Direct Shear Sample Mounting. Test sample for direct shear test were 4 inches in length, 4 inches in width and about 5 inches in height. The samples are prepared using a rock saw. The rock sample is cemented using quick dry cement inside two shear rings of 6 inch diameter each which are capable of holding 150 mm dia/150 mm high rock sample. The shear ring is then placed inside the shear box for the experiment. The shear box is then subjected to the constant normal load and horizontal load with an increment of 0.05mm/second. Figure 4-2 show the schematic diagram of the shear ring with the spacer after samples has been prepared.

Figure 4-2. Shear ring with the spacer

4.2.7. Data Acquisition & Measurement System Components. The direct shear system features electronic sensors and digital displays which are set in front of the panel of the metal cabinet to monitor the loads and the deformations. A standard A/D automatic data acquisition with USB interface is included in the system which automatically logs and refines test data. The USB interface connects the control panel with the computer. All the data is recorded within a CATS software. The GCTS Direct Shear Test mode program within the CATS software is an easy to use program which allows user to directly setup and conduct the direct shear tests. The program allows for real-time determination and control of various test inputs, such as corrected area of the specimen, normal stress and shear stress. The software also enables the conductance of the tests in multiple stages like consolidation, universal stage or shear loading. The consolidation stage is used to perform the normal consolidation, universal stage is used to define different test sequence and finally shear loading is used for the optimization of the shear loading. Electric sensors are attached to the system from which program measures normal load, shear load, normal deformation and shear deformation. The test inputs defined for the direct shear test are shown in Table 4.1.

Table 4.1. Test inputs

S. no.	Input	Procedure
1	Shear Load	It is manually incremented at the rate of 0.05mm/sec
2	Normal load	It is calculated from the mechanical earth model equations
3	Area	Depends on the specimen

4.3. LAB EXPERIMENTAL PROCEDURE

The Direct Shear test is administered to find the shear strength of the rock. The system components of the direct shear apparatus are shown in Figure 4.1. The operation of the system is explained in Section 4.2. The step by step procedure to run the direct shear test on the lab set up is shown below:

1. Four rock samples at different depths are tested for shear strength and their dimensions are noted down in a excel file with the geological data. Photographs should be taken to keep up the record of the test progress.
2. Apparatus should be set up before the experiment.
3. Sample is to be properly cemented before the experiment and the spacer bars should be removed before the shear rings are placed inside the shear box.
4. Before the sample is placed inside the shear box the screw on the top of lower shear box should be unscrewed to create the passage for the air when the sample is inserted as shown in Figure 4-1.
5. Sample should be carefully inserted into the bottom shear box using some friction reducing fluid on the sides of the shear ring. If the sample doesn't go in easily a rubber hammer should be used to hit the sample very carefully from the top so that it does not break from the middle.
6. Once the sample is inside the lower shear box the screw is used to shut the passage of air.
7. The top shear box is to be lifted from the handle after unscrewing the screw at the top of upper shear box and is to be slowly lowered onto the top of shear ring.
8. Friction reducing fluids are used to reduce the friction between the shear ring and the shear box and a rubber hammer is used to hit the upper shear box from the top. The screw is again used to shut off the air.
9. Fracture is exposed at this time between both the shear rings.
10. Pumps, apparatus and the computer is switched on once the sample is in place.
11. Software is to be started and a new project is created. All the inputs were inserted in the new project for the desired sample.
12. The knobs on the front of the control panel should be checked shown in Figure 4-1 before each experiment.

13. Turn normal load knob fully counterclockwise and the shear load fully clockwise.

14. Turn normal direction control to down and shear direction control to pull.

15. Pump is turned on to start the experiment.

16. The swivel top was properly placed and aligned with the upper box.

17. The normal load is turned clockwise to increase the normal load to the desired value.

18. The normal load is maintained constant throughout the experiment.

19. After all the settings in the software are done the experiment is executed and the shear load knob is turned to the left to slowly maintain the increment of the shear load at the rate of 0.05mm/sec.

20. The shear loading is till the peak and residual shear strength of the rock sample is achieved.

21. The data from the test is collected and analyzed to get the shear stress v/s time graph from which peak and the residual shear strengths are obtained.

22. After the experiment the cemented rock inside the shear ring is taken out very carefully using a hammer and a chisel.

5. RESULTS

Geomechanical properties were determined by analyzing the results of the laboratory experiments on four different rock samples. Direct shear and residual shear strength were determined in the laboratory. The rock mechanical testing includes 4 tests on Davis, 3 tests on Derby-doe run, 1 test on Lamotte and 1 test on Bonne Terre. Many samples broke during the sample preparation phase and only 9 rock samples were tested. Failure envelopes were generated using the laboratory data and was compared with the available insitu data to predict the sustainable fluid pressure for underground CO_2 storage.

5.1. DIRECT SHEAR TEST RESULTS

5.1.1. Direct Shear Strength. Total of nine direct shear tests were carried out on four rock samples. Normal stress was calculated using equation (3). The samples were loaded till direct shear and residual shear strength was reached. The shear strain was calculated using equation:

$$Shear\ Strain = \frac{Deformation}{Original\ Length} \tag{27}$$

The sample characteristics are shown in appendix A. The lab worksheet showing the test summary is shown in appendix B. The direct shear strength are averaged and shown in Figure 5.1. Comparison of direct shear strength is shown in Figure 5-2. In the Direct Shear test it was found that Davis has the highest shear strength followed by Bonne Terre, Derby Doerun and then Lamotte. The Lamotte being a reservoir rock shears first, Davis, Derby-Doerun are the caprocks and the Bonne Terre serves as a partial seal over the reservoir have higher strength than the reservoir rock will ensure the partial seal integrity.
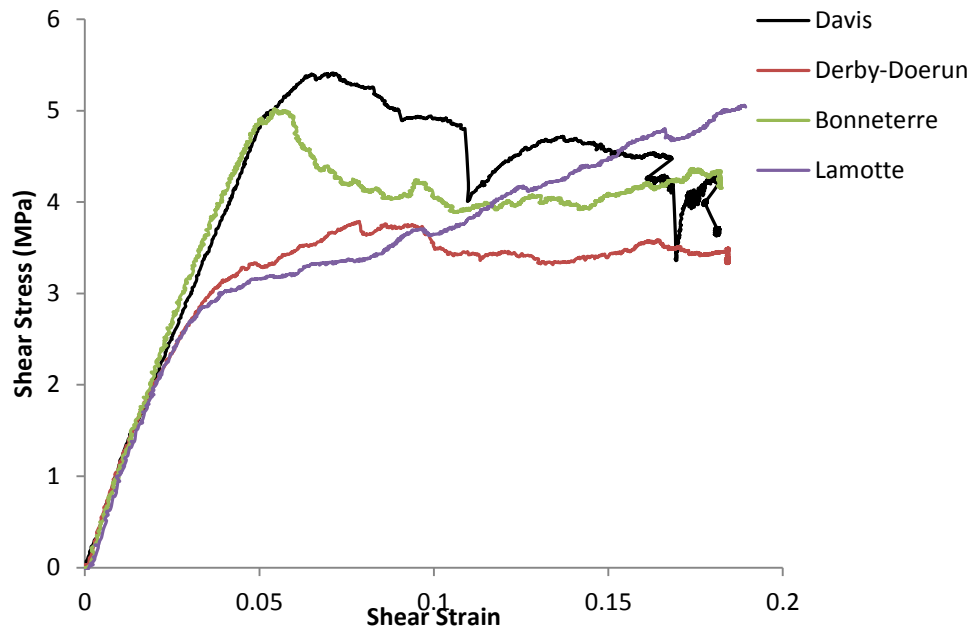
Figure 5-1. Averaged shear strength plot
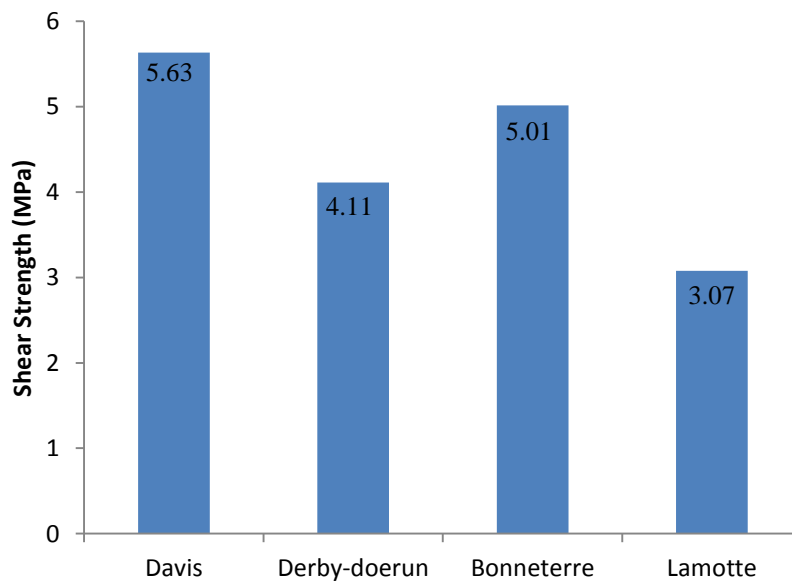
Figure 5-2. Comparison of direct shear strength

5.1.2. Failure Envelopes. The tests were carried out at constant normal load. The shear stress vs. normal stress for all four types of rocks are shown in Figure 5-3.
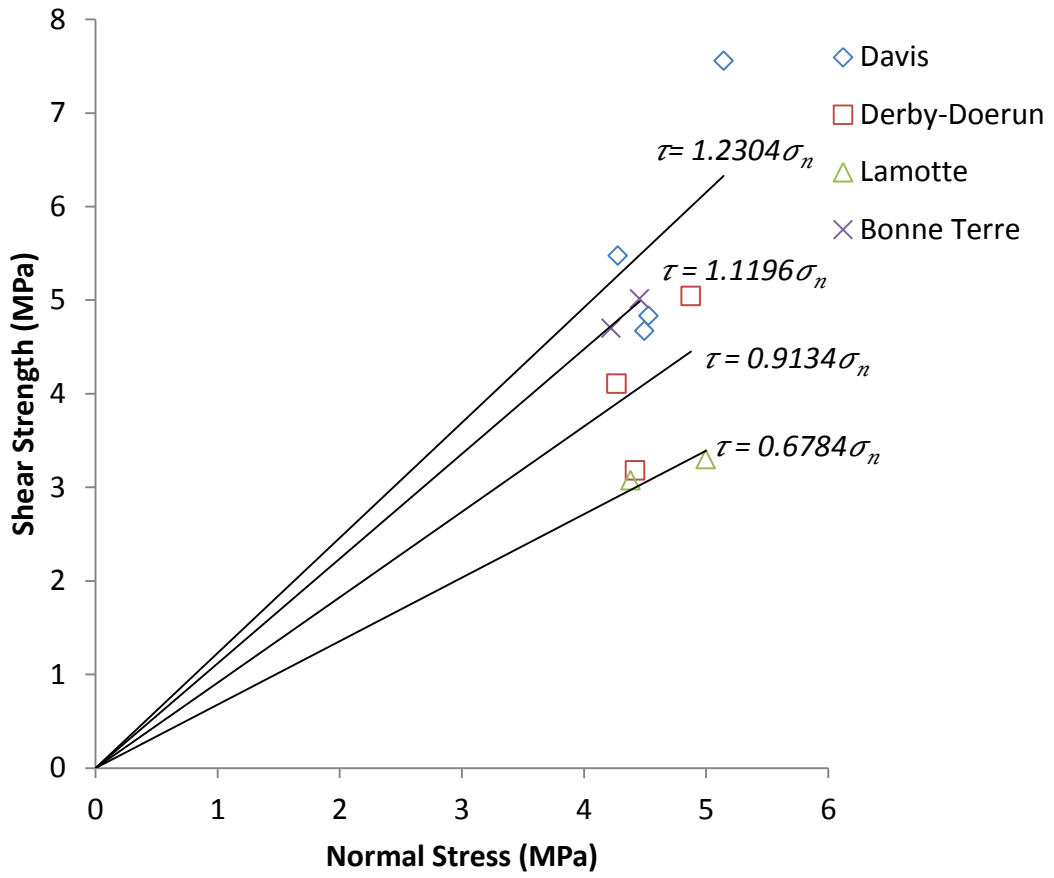
Figure 5-3. Failure envelope of Davis, Derby-Doerun, Lamotte and Bonne Terre are plotted. Equations for the linear Mohr Coulomb has been shown

Linear relationships between the shear and the normal stresses is obtained for all tests which are plotted in Appendix B. The basic friction angle is calculated from the slope of residual shear strength vs. normal stress plots. Table 5.1 shows the direct and residual shear strength properties. Table 5.2 shows rock deformation properties obtained from direct shear test.

Table 5.1. Results of direct shear test

S. No.	Rock formation	Test No.	Residual shear strength (MPa)	Peak shear strength (MPa)
1	Davis	1	4.57	5.47
2	Davis	2	5.01	7.55
3	Davis	3	4.34	4.83
4	Davis	4	3.82	4.67
5	Derby-Doerun	1	3.51	5.04
6	Derby-Doerun	2	3.1	3.18
7	Derby-Doerun	3	3.53	4.10
8	Lamotte	1	4.88	3.07
9	Bonne Terre	1	4.07	4.66

Table 5.2. Rock deformation properties

S. No.	Rock sample	Test No.	Shear modulus (GPa)	Poisson's ratio	Young's modulus (GPa)	Bulk modulus (GPa)
1	Davis	1	0.11	0.2	0.28	0.15
2	Davis	2	0.14	0.2	0.34	0.19
3	Davis	3	0.11	0.2	0.28	0.15
4	Davis	4	0.09	0.2	0.21	0.12
Average			**0.11**	**0.2**	**0.28**	**0.15**
5	Derby-DoeRun	1	0.11	0.2	0.27	0.15
6	Derby-DoeRun	2	0.11	0.2	0.27	0.15
7	Derby-DoeRun	3	0.10	0.2	0.25	0.14
Average			**0.11**	**0.2**	**0.26**	**0.14**
8	Lamotte	1	0.08	0.2	0.19	0.10
9	Bonne Terre	1	0.10	0.2	0.24	0.13

Shear modulus (G) is determined from the slope of actual shear strength vs shear strain plot. Young's modulus (E) and bulk modulus (K) is calculated from equations (28) and (29). Poisson's ratio was assumed to be 0.2 for the calculation of deformation properties.

$$E = 2G(1 + v) \tag{28}$$

$$K = \frac{E}{3(1-2v)} \tag{29}$$

5.1.3. Fault Reactivation and Comparison with the Intact Rock Data. The results of the direct shear tests were used to get the failure envelopes for the rock characterization. Mohr-Coulomb failure criteria and the concept of fault reactivation were used to generate the failure envelopes. Figures 5-4 to 5-7 shows the failure envelopes generated for all four types of rocks.
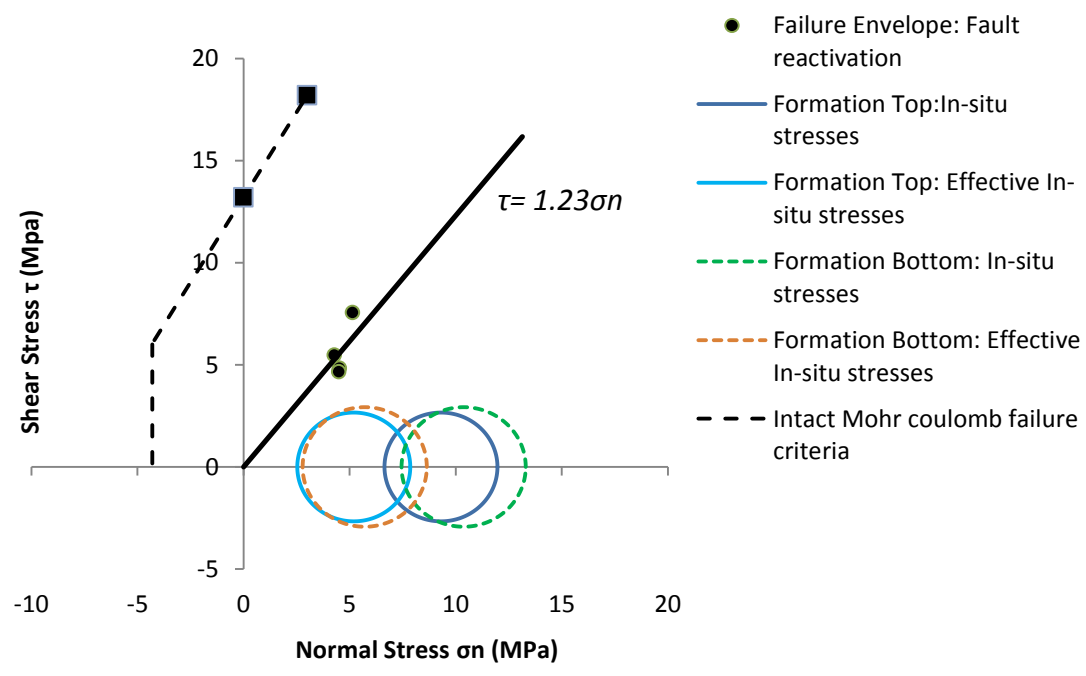
Figure 5-4. Failure envelopes of Davis Shaly Dolomite. Mohr circles have been plotted at in-situ and effective in-situ stresses. Equations for the linear Mohr-Coulomb are also shown
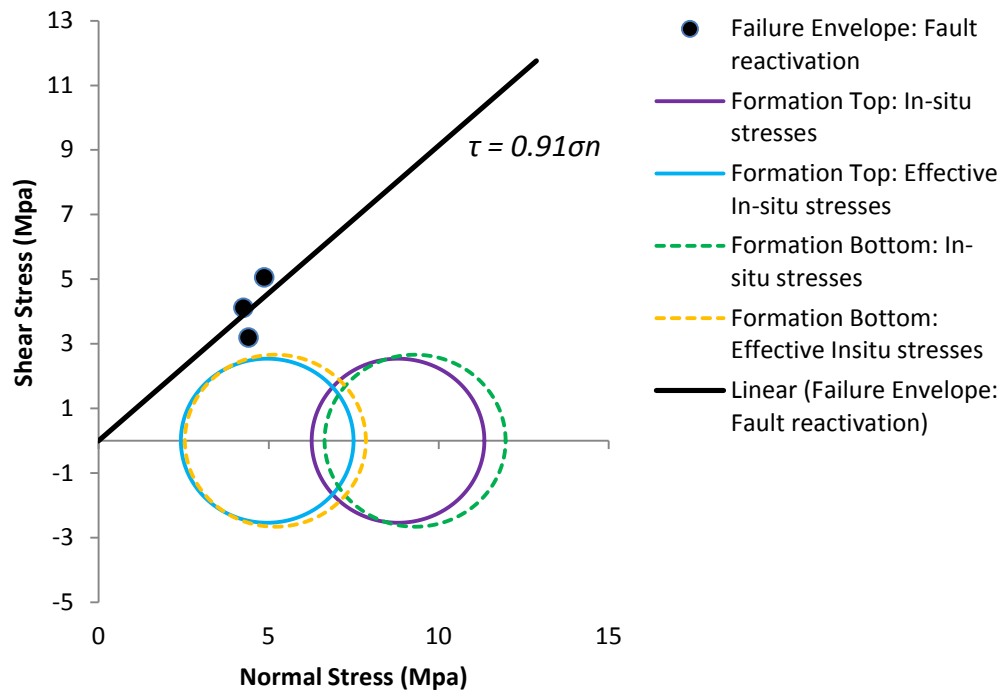
Figure 5-5. Failure envelopes of Derby-Doerun. Mohr circles have been plotted at in-situ and effective in-situ stresses. Equations for the linear Mohr-Coulomb are also shown
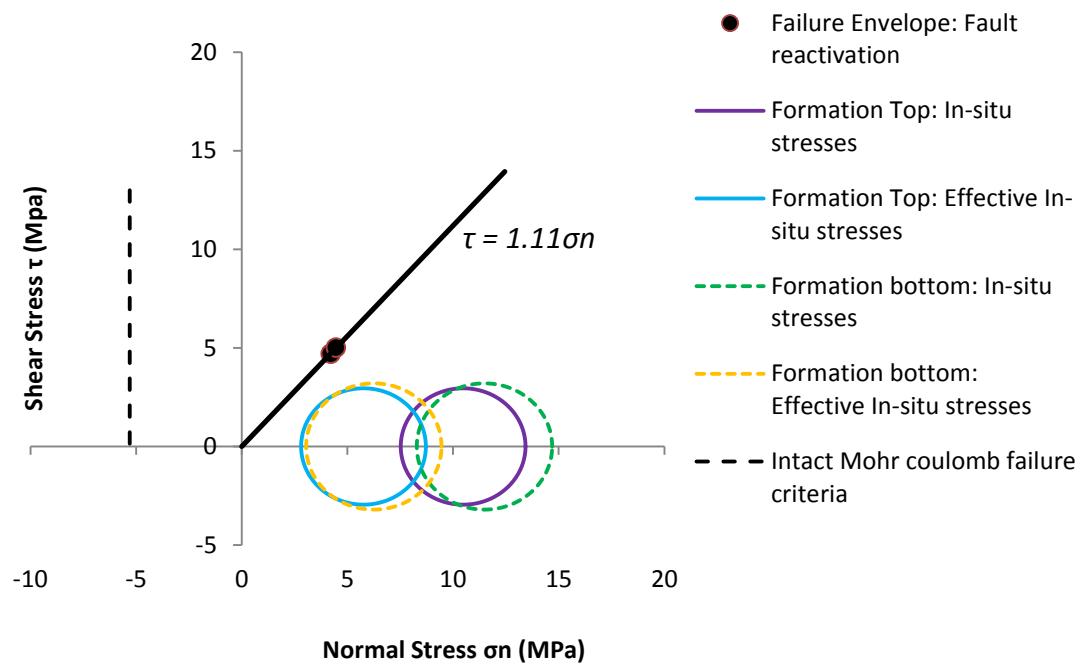
Figure 5-6. Failure envelopes of Bonne Terre Dolomite. Mohr circles have been plotted at in-situ and effective in-situ stresses. Equations for the linear Mohr-Coulomb are also shown
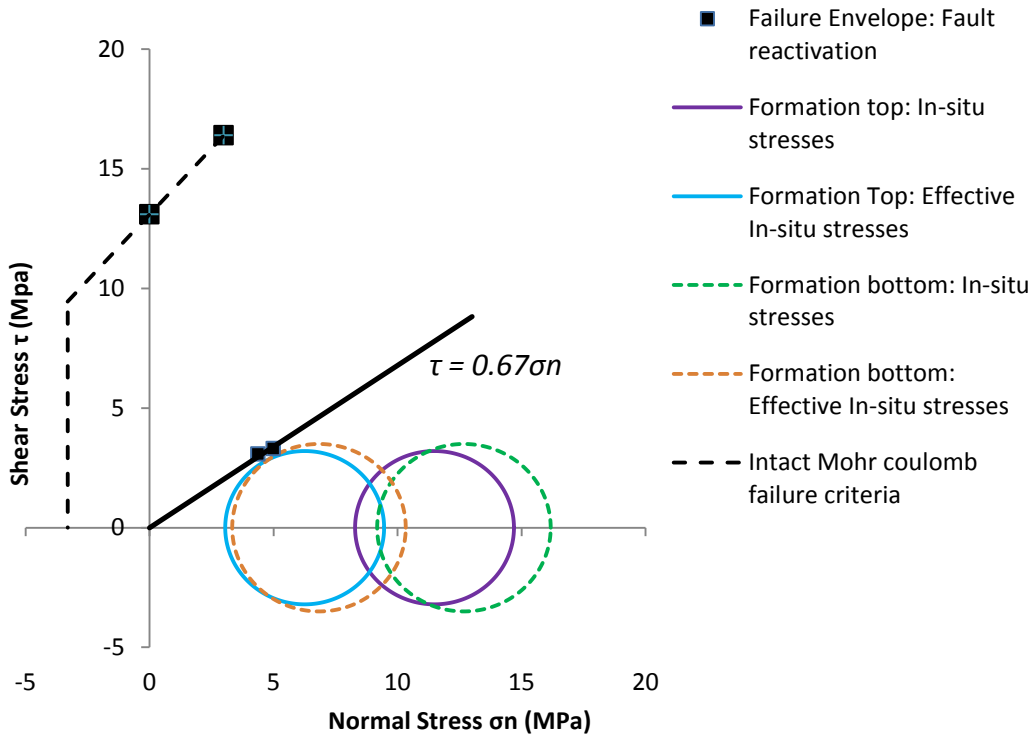
Figure 5-7. Failure envelopes of Lamotte sandstone. Mohr circles have been plotted at in-situ and effective in-situ stresses. Equations for the linear Mohr-Coulomb are also shown

5.1.4. Pore Pressure at Fault Reactivation.   The pore pressure for all the rock formations at which the pre-existing faults will get reactivated is plotted. Figures 5-8 to 5-15 shows the comparison of the Mohr circle at safe pore pressure and with pore pressure at fault reactivation at failure effective stresses and with the failure effective stresses with the stress path.
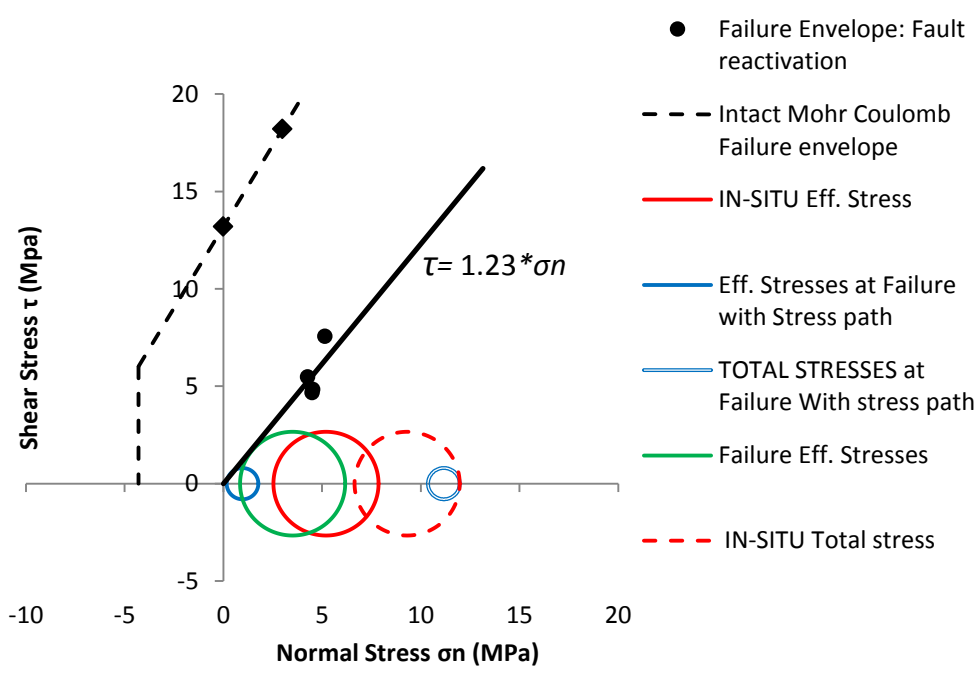
Figure 5-8. Comparison of Mohr circle for Davis for formation top at safe effective stress and with the Mohr circle at fault reactivation
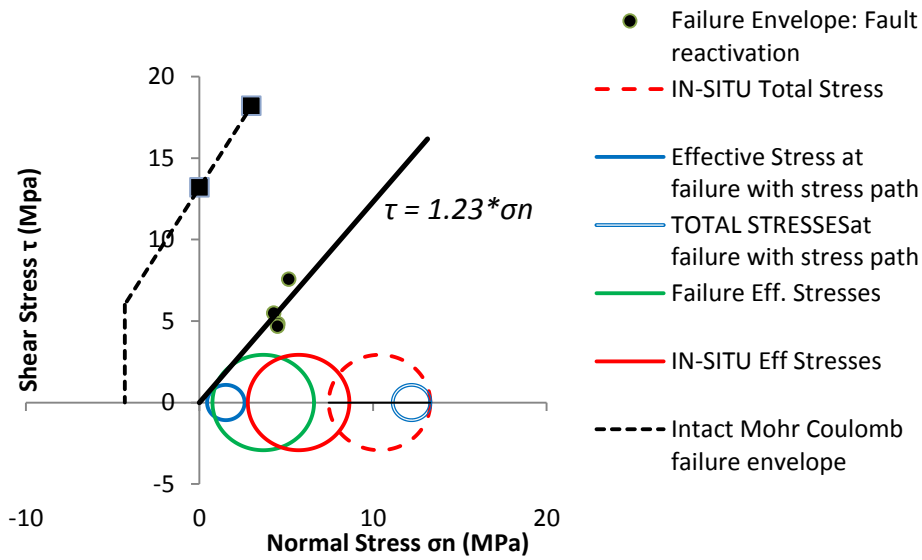
Figure 5-9. Comparison of Mohr circle for Davis for formation bottom at safe effective stress and with the Mohr circle at fault reactivation
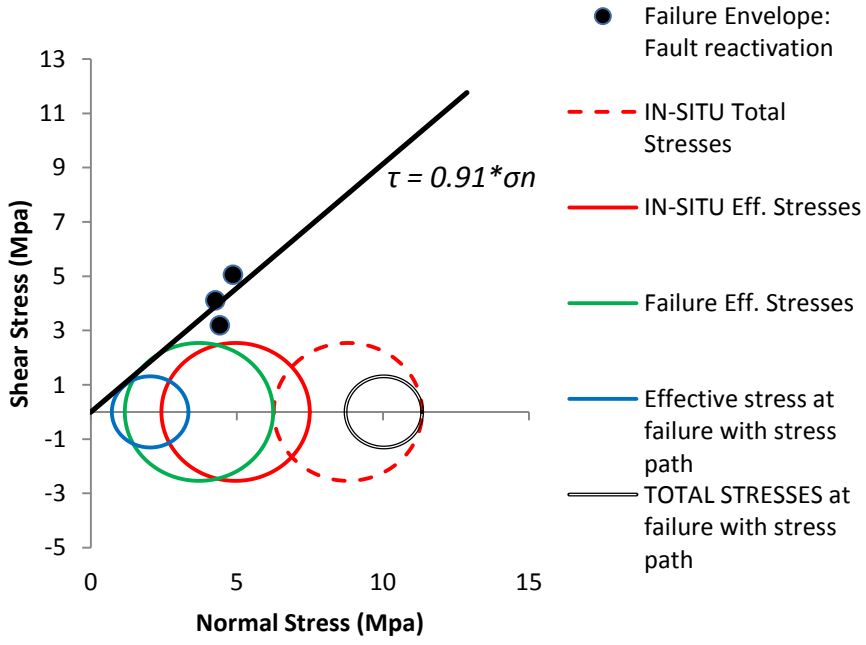
Figure 5-10. Comparison of Mohr circle for Derby-Doerun for formation top at safe effective stress and with the Mohr circle at fault reactivation
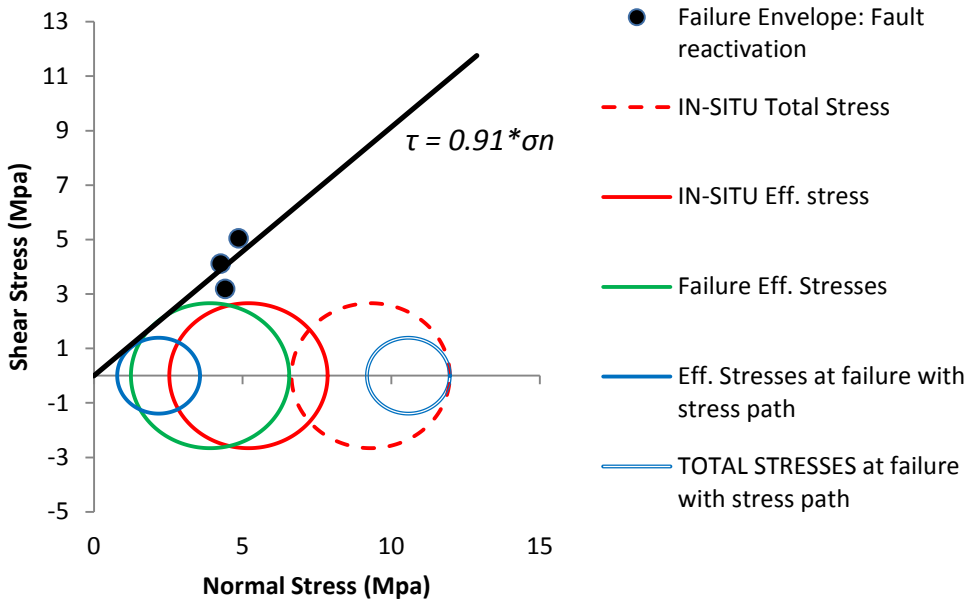
Figure 5-11. Comparison of Mohr circle for Derby-Doerun for formation bottom at safe effective stress and with the Mohr circle at fault reactivation
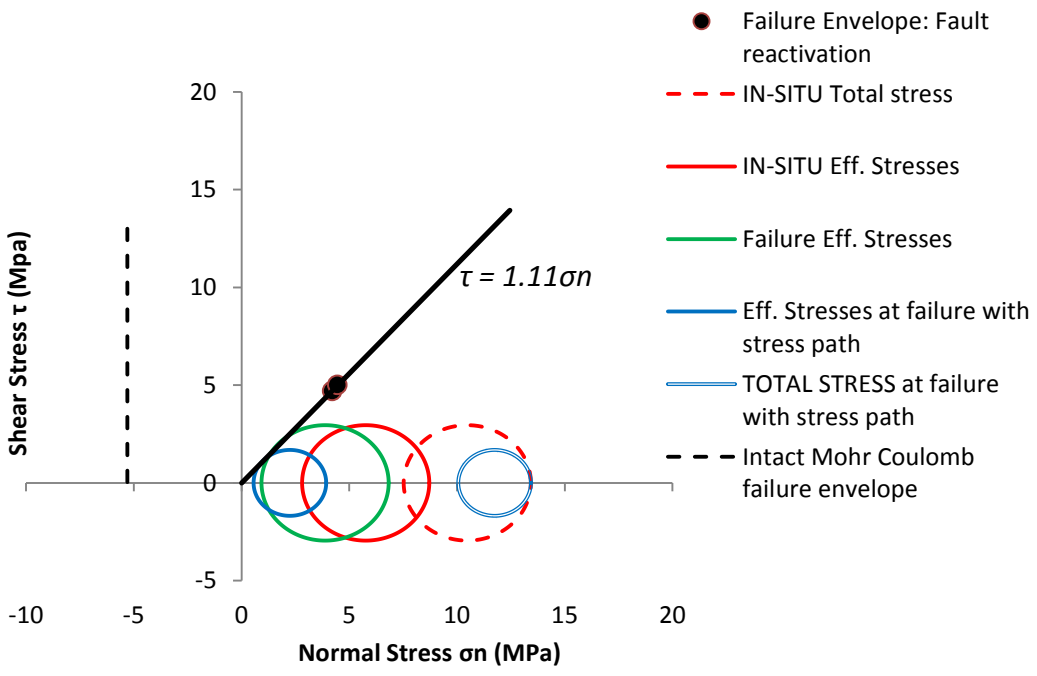
Figure 5-12. Comparison of Mohr circle for Bonne Terre for formation top at safe effective stress and with the Mohr circle at fault reactivation
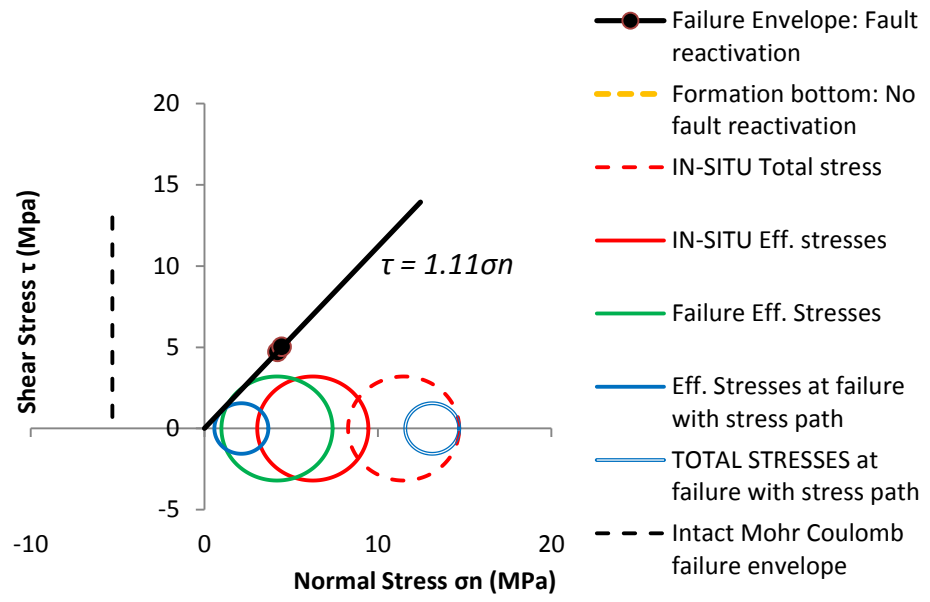
Figure 5-13. Comparison of Mohr circle for Bonne Terre for formation bottom at safe effective stress and with the Mohr circle at fault reactivation
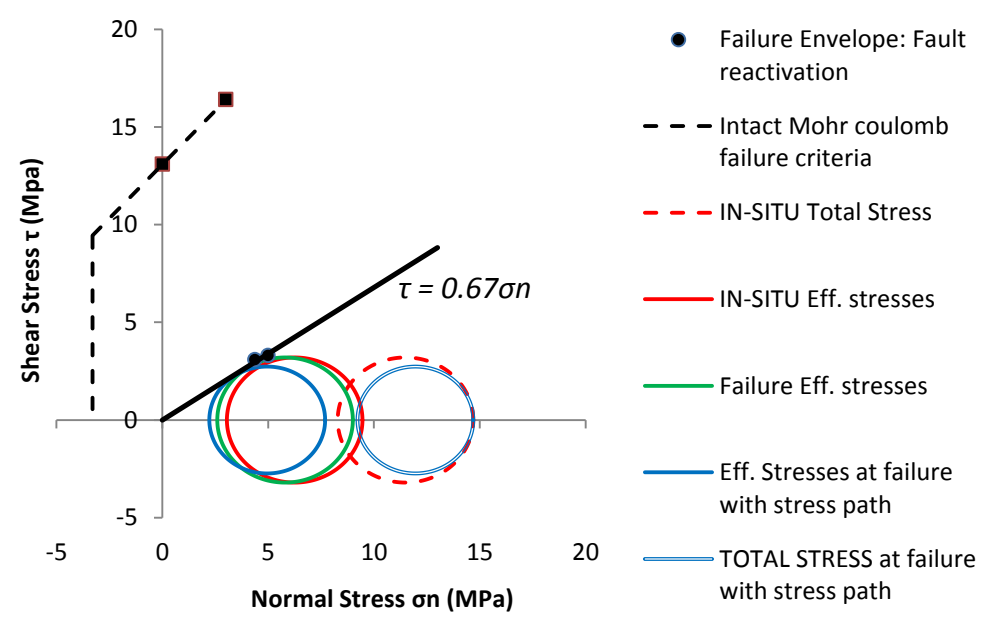
Figure 5-14. Comparison of Mohr circle for Lamotte for formation top at safe effective stress and with the Mohr circle at fault reactivation
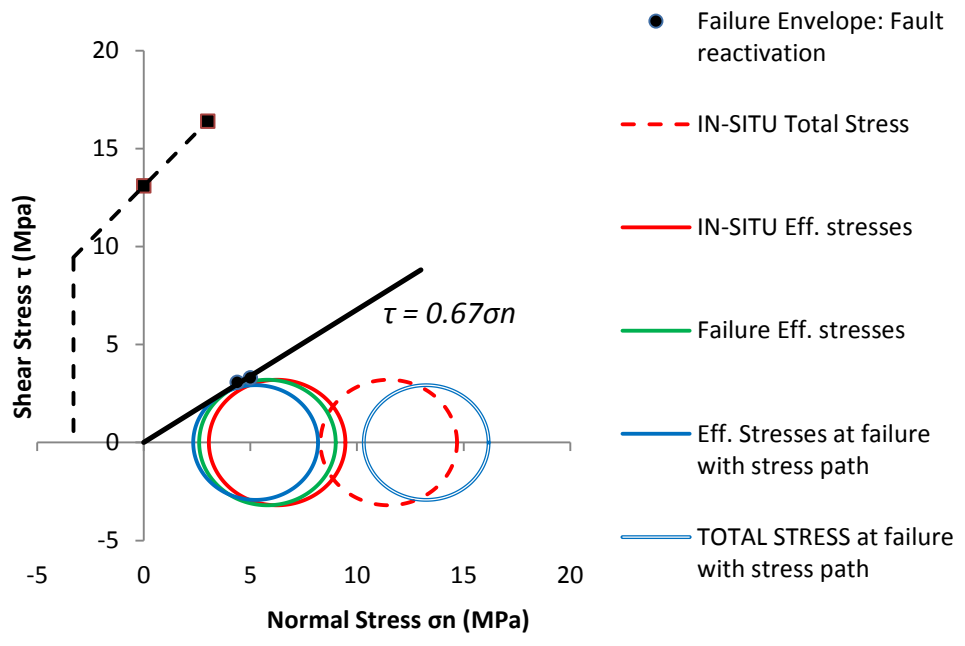
Figure 5-15. Comparison of Mohr circle for Lamotte for formation bottom at safe effective stress and with the Mohr circle at fault reactivation

The values of effective overburden stress and the effective minimum horizontal stress were taken from in-situ lab sonic tests (Akpan, 2012). The poisson's ratio for all rock formation for the calculation of pressure at failure effective stresses with stress path was calculated from triaxial tests (Govindrajan, 2012). Equation (2) and (3) were used for the calculation shear stress and the overburden stress. Equation (5a) and (5b) were used for the calculation of minimum horizontal stress for conventional model and for the stress coupling. Table 5.3 shows the increase in pore pressure (PP) for the effective stresses at failure. Table 5.4 shows increase in pore pressure for the effective stresses at failure with the stress path.

Table 5.3. Sustainable pore pressure window at failure effective stresses

S. No	Formation	Lithology	Formation top			Formation bottom		
			Safe PP at form-ation (Mpa)	PP at fault react-ivation (Mpa)	Inc-rease in PP (Mpa)	Safe PP at form-ation (Mpa)	PP at fault react-ivation (Mpa)	Inc-rease in PP (Mpa)
1	Davis	Shaly dolomite	4.1	5.8	1.7	4.7	6.7	2.0
2	Derby-Doerun	Dolomitic shale	3.8	5.1	1.3	4.1	5.4	1.3
3	Bonne Terre	Dolomite	4.7	6.6	1.9	5.2	7.3	2.1
4	Lamotte	Sandstone	5.23	5.69	0.46	5.8	6.4	0.6

.

Table 5.4. Sustainable pore pressure window at failure effective stresses with stress path

S. No.	Formation	Lithology	Formation top			Formation bottom		
			Safe PP at form-ation (Mpa)	PP at fault react-ivation (Mpa)	Inc-rease in PP (Mpa)	Safe PPat form-ation (Mpa)	PP at fault react-ivation (Mpa)	Inc-rease in PP (Mpa)
1	Davis	Shaly dolomite	4.1	10.2	6.1	4.7	10.7	6.0
2	Derby-Doerun	Dolomitic shale	3.8	8.0	4.2	4.1	8.4	4.3
3	Bonne Terre	Dolomite	4.7	9.5	4.8	5.2	11.0	5.8
4	Lamotte	Sandstone	5.23	7.0	1.77	5.8	8.0	2.2

5.1.5. Comparison of Actual and Predicted Shear Strength of rocks. Barton's criteria was used to calculate the predicted shear strength for the rock samples (Barton, 2008). The calculations used average values of the joint rough coefficient (JRC) obtained from Figure 2-9, the JCS is obtained from the triaxial tests and the basic friction angle was determined from the slope of residual shear strength vs. normal stress plot. Figure 5-16 to Figure 5-19 shows the comparison of the actual shear strength from direct shear test with the predicted shear strength. Equation (25) was used to calculate the predicted shear strength. Table 5.5 show the predicted shear strength for all the rock samples and all parameters used for the calculation in which σ_n is the peak normal stress, Φ_b is the basic friction angle.

$$\tau = \sigma_n \tan\left[\mathrm{JRC}\log(\mathrm{JCS}/\sigma_n) + \varphi_b \right] \tag{30}$$

Table 5.5. Predicted shear strength parameters

S. No	Rock form-ation	Test No.	(σn) (MPa)	Residual shear strength (MPa)	Peak shear strength (MPa)	JCS	Ave-rage JRC	Φb	Predicted shear strength
1	Davis	1	4.27	4.57	5.47	71.2	5	43.89	5.09
2	Davis	2	5.14	5.01	7.55	71.2	5	43.89	6.04
3	Davis	3	4.52	4.34	4.83	71.2	5	43.89	5.37
4	Davis	4	4.49	3.82	4.67	71.2	5	43.89	5.33
5	Derby-Doerun	1	4.87	3.51	5.04	65	7	36.74	4.81
6	Derby-Doerun	2	4.41	3.1	3.18	65	7	36.74	4.4
7	Derby-Doerun	3	4.26	3.53	4.1	65	7	36.74	4.27
8	Lamotte	1	4.38	4.88	3.07	59.05	3	44.64	4.87
9	Bonne Terre	1	4.45	4.07	5.01	168.36	5	42.52	5.38
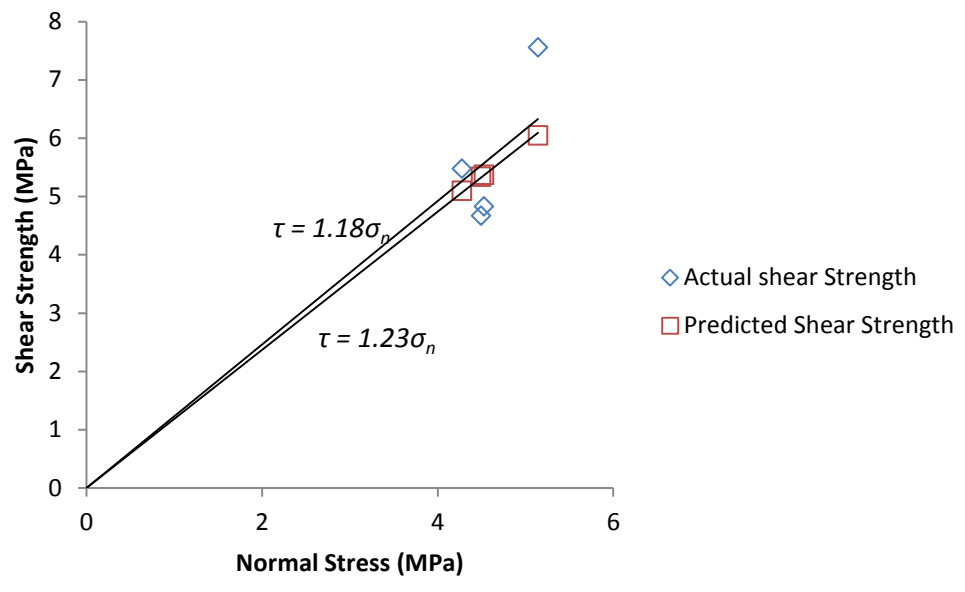
Figure 5-16. Comparison of actual and predicted shear strength for Davis
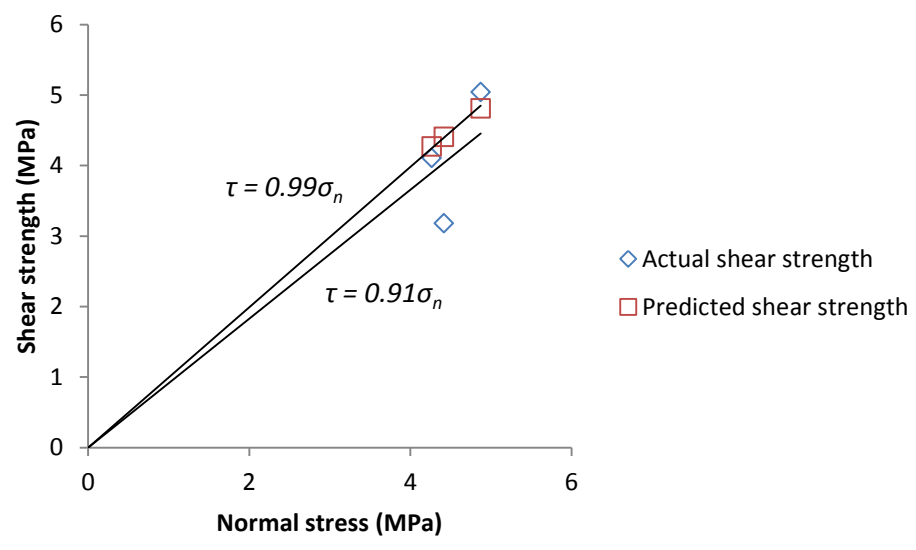
Figure 5-17. Comparison of actual and predicted shear strength for Derby-Doerun
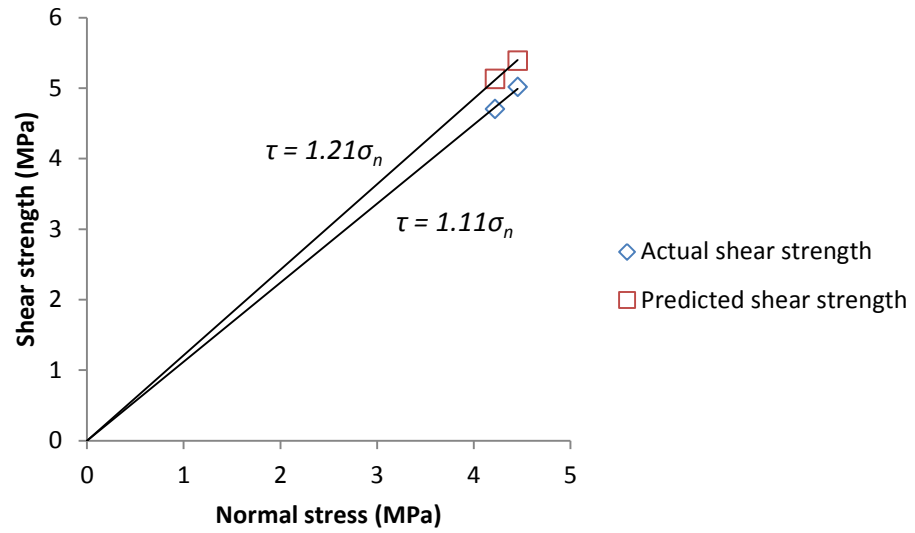
Figure 5-18. Comparison of actual and predicted shear strength for Bonne Terre
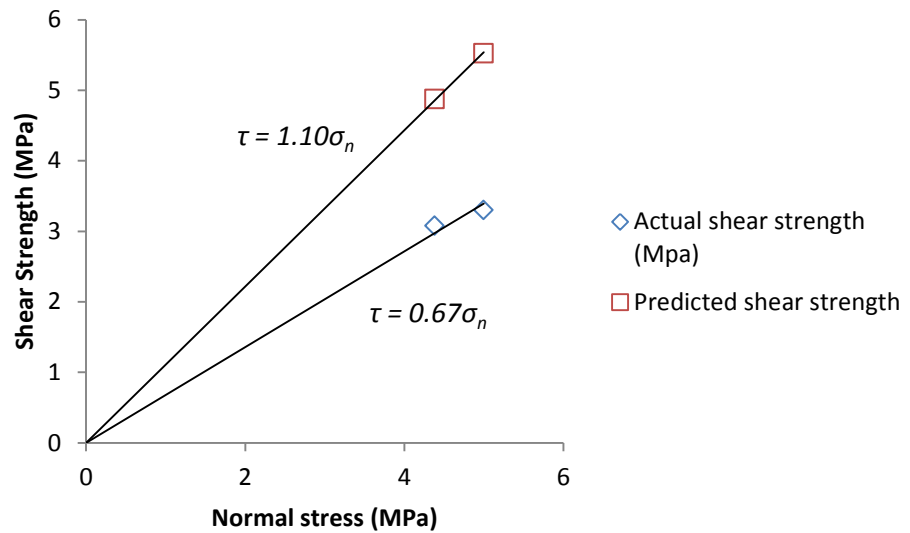
Figure 5-19. Comparison of actual and predicted shear strength for Lamotte

5.1.6. Slip Tendency Parameter. Slip tendency parameter was calculated for all four rocks at the top (FT) and bottom (FB) of their formation and shown in Table 5.6. The average values of the normal stresses for all four rocks were used for the calculations. τ_{slip} was calculated using equation (4) where cohesion is taken as zero and $\delta \sim 60^{\circ}$. Effective normal stress is calculated from equation (26) and coefficient of friction is calculated from equation (32). Shear stress and Normal stress were calculated using equation (2) and (3) where the value of effective overburden stress and effective minimum horizontal stress for each formation were obtained from the in-situ sonic lab test (Akpan,2012). Slip tendency parameter was calculated using equation (5).

$$\sigma_n{}' = (\sigma_n - \alpha p) \tag{31}$$

$$\mu = tan\varphi \tag{32}$$

In equation (31) $\sigma_n{}'$ is the effective normal stress, σ_n is the normal stress, α is the biot's coefficient which is assumed to be 1 for the calculation and p is the pore pressure. In equation (32) μ is the coefficient of friction and φ is the angle of friction.

Table 5.6. Slip tendency parameters for top and bottom of the formation

S.No.	Rock Formation	τ (FT)	τ_{slip} (FT)	**ST (FT)**	τ (FB)	τ_{slip} (FB)	**ST (FB)**
1	Davis	2.30	4.75	**0.48**	2.53	5.22	**0.48**
2	Derby-Doerun	2.19	3.35	**0.65**	2.30	3.52	**0.65**
3	Bonne Terre	2.55	4.79	**0.53**	2.77	5.20	**0.53**
4	Lamotte	2.77	3.18	**0.87**	3.03	3.45	**0.87**

6. DISCUSSION

The objective of this research is to seek a relationship between the direct shear strength of rocks and their physical and mechanical properties. The deformation properties obtained from the direct shear test were compared with values obtained from the triaxial tests and also with the values obtained from the in situ sonic velocity tests. The results obtained from the direct shear test were obtained to get the failure envelope and then analyzed for the fault reactivation. Actual shear strength of rough joints obtained from the direct shear test were compared with the predicted shear strength using Barton's criteria. Failure envelope of fractured rock were compared with the failure envelope of intact rock and statistical analysis was also done to check if the data obtained for all the rocks were significantly different from each other.

6.1. COMPARISON OF DEFORMATION PROPERTIES

The deformation properties include Young's modulus, Shear modulus, bulk modulus and poisson's ratio. The poisson's ratio of 0.2 was assumed to determine the deformation properties. Figures 6-1 to 6-3 shows deformation properties obtained from various tests. The values plotted are averaged obtained from the datasets. It can be seen that that the values of Young's modulus, bulk modulus and Shear modulus obtained from the Direct Shear test are insignificant. The values of the deformation properties for all four rocks obtained from triaxial and in-situ sonic tests are very high compared to the values obtained from Direct Shear test. The changes are mainly dominated by the state of stress and the overburden. In direct shear test the rock was already fractured due to which redistribution of stresses takes place which cause block movement, aperture changes on natural joints etc, which is why the values of deformation properties are expected to be insignificant. The triaxial and in-situ tests are used to calculate the deformation properties of the intact rock that is why the values obtained from these two tests for all four types of rocks are much higher.
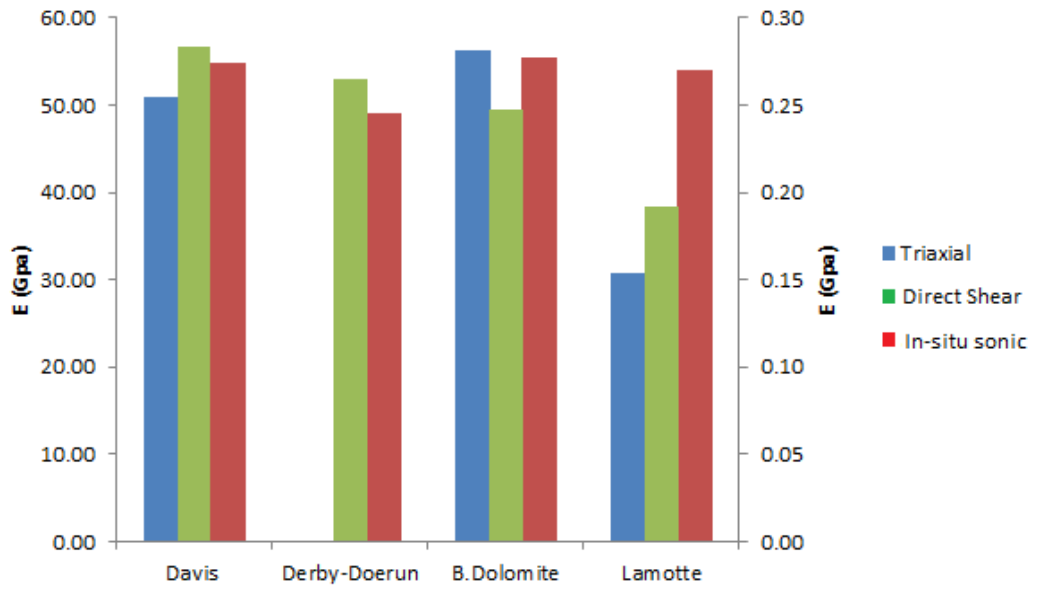
Figure 6-1. Comparison of averaged Young's modulus for four different rocks obtained from three lab testing methods
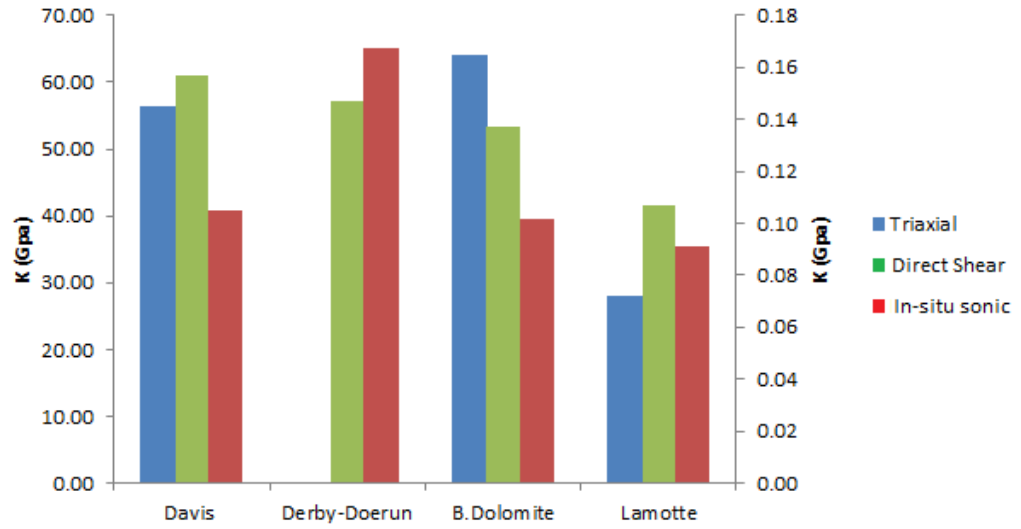
Figure 6-2. Comparison of averaged bulk modulus for four different rocks obtained from three lab testing methods
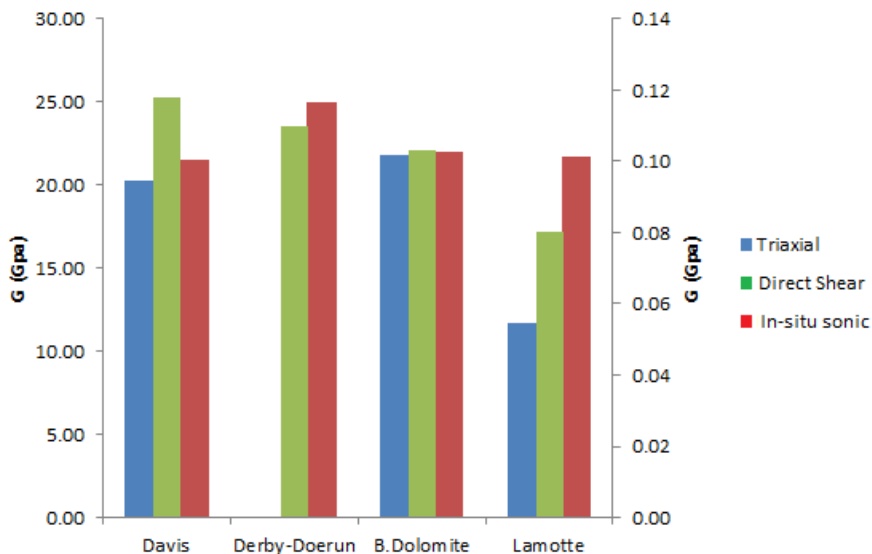
Figure 6-3. Comparison of averaged shear modulus for four different rocks obtained from three lab testing methods

6.2. COMPARISON OF DIRECT SHEAR STRENGTH

Averaged shear strength of Davis shaly dolomite, Derby-Doerun, Bonne Terre dolomite and Lamotte sandstone were plotted against shear strain in Figure 5-1.The comparison of the direct shear strength is shown in Figure 5-2. Results were determined using the direct shear apparatus applying a constant normal load for each rock type. It can be seen from the figure that Lamotte being the reservoir has the lowest direct shear strength. The Davis shaly dolomite has much higher direct shear strength followed by Bonne Terre dolomite and Derby-Doerun. The smoothness of the plots in Figure 5-1 represents the roughness of the fractures of the rock types. The fractures were created manually in the lab for the testing purpose and it was seen that fractures in the Lamotte sandstone were smoother than the caprock. There were less undulations in the fractures of Bonne Terre than Davis and Derby-Doerun. The residual shear strength for all four rock types is determined after the shear strength reaches its peak value and starts to decrease and finally becomes constant. The comparison of the residual shear strength for all the rock samples is shown in Table 5.1.

6.3. COMPARISON OF FAILURE SCENARIOS BETWEEN ROCKS AND ANALYSIS OF FAULT REACTIVATION

Failure envelopes of all four rock types were generated using Coulombs failure criteria and shear stress was plotted against normal stress. Figure 5-3 shows the comparison of failure envelopes for all four rock types. These failure envelopes were generated to study the fault stability associated with CO_2 sequestration. Analytical shear slip analysis is conducted using in-situ stress magnitudes and the pore pressure within the fault plane.

The possible activation of the pre-existing fault may occur whenever the shear stress acting on the fault plane exceeds the Mohr-Coulomb failure criteria which is shown in Figures 5-4 to 5-7. As no direct measurement of cohesion and friction angles are available, the friction angle of 60° is used as the fractures in the rock are natural fractures (Ferronato et al., 2010). The in-situ vertical, minimum horizontal stresses, and the pore pressure for the each rock formation at particular depths were calculated from porosity sonic logs (Akpan, 2012). Mohr circles based on in-situ and effective stresses for the top and bottom of the formation were generated and plotted under Mohr-Coulomb failure envelope obtained from direct shear tests and triaxial tests for all four types of rocks. Injection of CO_2 will increase the amount of pore pressure which in turn will lead to a reduction in stress causing the Mohr circle to shift closer to the failure envelope. The size of the Mohr circle increases with depth as more stress is induced on each formation as seen in Figures 5-4 to 5-7. There are more chances of fault reactivation in Lamotte sandstone as the Mohr circle is closest to the failure envelope which can be seen in Figure 5-7. If there are any pre-existing faults in the rock formations than the fault reactivation will occur before the tensile failure. A safe pore pressure window for the top and bottom of the formation was also generated and the pressure at which the fault will get reactivated after was calculated based on Figures 5-8 to 5-15. It can be seen from Table 5.3 that the if the pressure is kept between the sustainable pore pressure there will not be any reactivation of pre-existing fractures but if the pore pressure exceeds the sustainable pore pressure than there will be reactivation of faults which will cause the leakage of CO_2 to the surface. It can observed from the analyses that the pore pressure for Derby-Doerun at which the faults are getting reactivated at the top and bottom of the formation are 5.1

Mpa and 5.4 MPa and the pore pressure for Lamotte at which the fault are getting reactivated for top and bottom of the formation are 5.69 MPa and 6.4 MPa. This could be detrimental to the CO_2 sequestration process as the faults in the caprock are getting reactivated before the fault in the reservoir. However the pore pressure at which the faults are getting reactivated in Bonne Terre for top and bottom of the formation are 6.6 Mpa and 7.3 MPa and for Davis the values are 5.8 MPa and 6.7 MPa. As long as the pore pressure is kept under 6.5, the faults in Davis and Bonne Terre will not get reactivated and hence sequestration of CO_2 can still be achieved.

In case of stress coupling the value of minimum horizontal stress will increase and the value of overburden stress will decrease with the increase in pore pressure which will cause the reduction in the size of mohr circle as shown in Figures 5-8 to 5-15. Pore pressure of the effective stresses at failure with the stress path for all rock formations was also calculated based on Figures 5-8 to 5-15 which are shown in Table 5.4. It can be observed from the analyses that the pore pressure for Lamotte at which the faults are getting reactivated for top and bottom of the formation are 7 MPa and 8 MPa and the pore pressure for Derby-Doerun the values are are 8 MPa and 8.4 MPa. If the pore pressure during injection of CO_2 in the reservoir exceeds 8.4 MPa than the pre-existing faults in Lamotte and Derby-Doerun will get reactivated. However the pore pressure in Bonne Terre at which the faults are getting reactivated for top and bottom of the formation are 9.5 MPa and 11 MPa and for Davis the values are 10.2 MPa and 10.7 MPa. For the pore pressure/stress coupling if the pore pressure is kept under 10.4 MPa, the faults in Davis and Bonne Terre will not get reactivated which is necessary for CO_2 sequesatration.

6.4. COMPARISON BETWEEN THE ACTUAL SHEAR STRENGTH AND PREDICTED SHEAR STRENGTH

Barton's criteria was used to calculate the shear strength of joints. This method was primarily used to assess the capability of the criteria, the adequacy of the JCS determined by triaxial test and the sensitivity of the JRC and JCS on Barton's shear strength. The uniaxial compressive strengths of Davis shaly dolomite, Bonne Terre

dolomite and Lamotte sandstone rocks were determined from triaxial test and a value of uniaxial compressive strength for Derby-Doerun was assumed in between Davis and Bonne Terre (Govindarajan, 2012). An average value of JRC was taken from Figure 2-9 for each rock type based upon the discontinuities surface with standard profile. Basic friction angle was assumed as residual friction angle which was obtained from the failure envelope of residual shear strength for each rock type. Predicted shear strength was calculated based upon the roughness of the fracture in the rock. Figures 5-16 to figure 5-19 shows the comparison of the actual shear strength with the predicted shear strength for each rock type. It was seen from all the figures that the Barton's over predicts the shear strength of all four rocks. The shear strength calculated using Barton's criteria were higher than the actual shear strength for all four rock types. Table 5.4 shows all parameters which were used for the calculation of predicted shear strength for each rock type. The asperity of Davis and Derby-Doerun were much higher than Lamotte and Bonne Terre which was assumed based on visual inspection of the fracture which in turn differing from the actual shear strength by 60% for Lamotte, 87% for Bonne Terre, 98.8% for Davis and 87.8% for Derby-Doerun.. It was seen from the figures that the predicted shear strength of Davis and Derby-doe run are closer than Bonne Terre and Lamotte. Analysis of the predicted shear strength shows the dependency of the shear strength on asperity. Greater the asperity higher will be the shear strength and vice versa.

6.5. SLIP TENDENCY PARAMETER

Slip tendency parameter was calculated for all four rocks. The likelihood of reactivation of a fault is measured by the slip tendency parameter. It can be seen from table 5.5 that Lamotte has the highest slip tendency parameter followed by Derby-Doerun, Bonne Terre and Davis. The value of slip tandency parameter both top and formation bottom of the formation is same for all four roks. The values of slip tendency parameter are 0.87 for Lamotte, 0.53 for Bonne Terre, 0.65 for Derby-Doerun, and 0.48 for Davis. It can be seen that Lamotte being a reservoir has higher value for slip tendency parameter than the cap rocks because of more permeability and porosity. Fault reactivation is necessary in the reservoir during injection of CO_2. Davis and Derby-

Doerun are the caprocks having lower value of slip tendency parameter than Lamotte. The Bonne Terre provides a partial seal over reservoir have low value of slip tendency parameter.

7. CONCLUSIONS

The objective of this research was to determine and to analyze the shear strength of four different rock types situated at different depths. The laboratory test data was used to characterize the rock formation for CO_2 sequestration project. The direct shear and residual shear strength of the rock samples were determined as a part of the determination of the rock material characteristics. To achieve this objective a large shear box apparatus was assembled which was used for the testing of rock specimens. This thesis describes the design and construction of the apparatus, detailed sampling of the rock formations as well as the interpretation and application of shear testing on large rock specimen. The evaluated rock properties from direct shear tests were used as an input for the simulation of sequestration of CO_2. In-situ stress parameters from sonic porosity logs were used for the calculation of the normal load for each rock formation at different depths.

The deformation properties obtained from the direct shear test were compared with the values obtained from triaxial testing as well as in-situ sonic logs. It was found that the values of deformation properties obtained from direct shear test were much lower than the values obtained by triaxial tests and in-situ sonic logs. The reason for this that the direct shear test were conducted on fractured rock and triaxial tests and in-situ sonic logs were conducted on intact rocks.

A relationship of JRC with the shear strength was also established during this research. The shear strength obtained from the test was compared with the shear strength calculated using Barton's criteria. The values of the predicted shear strength from Barton's criteria were differing by 60% for lamotte, 87% for Bonne Terre, 98.8% for Davis and 87.8% for Derby-Doerun. It was also found that the shear strength increases proportionaly with roughness.

The shear strength of the rocks were 5.6332 MPa for Davis, 4.1105 MPa for Derby-Doerun, 5.0147 MPa for Bonne Terre and 3.0763 MPa for Lamotte. Mohr-Coulomb failure criteria was used to evaluate the fault reactivation scenarios for all four type of rocks. A sustainable pore pressure window was calculated based on in-situ stress

conditions and fault reactivation criteria. For the conventional model the pore pressure at which the fault reactivation at the formation bottom will occur were 5.8 MPa for Davis, 5.1 MPa for Derby-Doerun, 6.6 MPa for Bonne Terre and 5.69 MPa for Lamotte. If the pore pressure is kept between 5.69 MPa and 6.6 MPa than only the faults in Lamotte will reactivate which is desirable and yet within the safe limits for avoiding reactivation of faults in the caprocks. In case of stress coupling the pore pressure at which the fault reactivation at the formation bottom will occur were 8 MPa for Lamotte, 11 MPa for Bonne Terre, 8.4 MPa for Derby-Doerun and 10.7 for Davis. In this case if the pore pressure is kept between 8 MPa and 9 MPa than only the faults in the Lamotte will get reactivated which is desirable and is the safe limit for avoiding reactivation of pre-existing faults in Davis and Bonne Terre.

The slip tendency parameter of the rocks at the formation bottom were 0.87 for Lamotte, 0.53 for Bonne Terre, 0.65 for Derby-Doerun and 0.48 for Davis. It can be seen that the Lamotte has the lowest value of slip tendency parameter which favors fault reactivation. The faults in derby-Doerun will reactivate after Lamotte and faults in Davis and Bonne Terre will reactivate at last because they have lower value of slip tendency parameter.

APPENDIX A.

SAMPLE DETAILS

Table A-1 Direct shear sample details

S. No.	Rock formation	Sample length (in)	Sample width (in)	Rock sample Size (in^2)	Shear rate (mm/sec)
1	Davis	4	4	16	0.05
2	Davis	4	4	16	0.05
3	Davis	4	4	16	0.05
4	Davis	4	4	16	0.05
5	Derby-Doerun	4	4	16	0.05
6	Derby-Doerun	4	4	16	0.05
7	Derby-Doerun	4	4	16	0.05
8	Lamotte	4	4	16	0.05
9	Bonne Terre	4	4	16	0.05

APPENDIX B.

TESTS RESULTS SUMMARY

Table B-1 Direct shear strength results

S. No.	Rock formation	Test No.	Peak normal load (KN)	Peak normal Stress (MPa)	Peak normal deformation (mm)	Peak shear load (KN)	Peak shear strain	Peak shear strength (MPa)
1	Davis	1	41.35	4.27	3.56	52.93	0.05	5.47
2	Davis	2	49.85	5.14	17.67	73.24	0.05	7.55
3	Davis	3	49.8	4.529	9.88	53.13	0.05	4.83
4	Davis	4	49.8	4.49	7.93	51.76	0.06	4.67
5	Derby-Doerun	1	47.94	4.87	1.63	49.61	0.04	5.04
6	Derby-Doerun	2	45.85	4.41	11.1	33.01	0.12	3.18
7	Derby-Doerun	3	48.29	4.26	8.13	46.48	0.05	4.1
8	Lamotte	1	49.8	4.38	12.4	34.96	0.04	3.07
9	Bonne Terre	2	49.8	4.45	2.53	56.05	0.05	5.01

Table B-2 Residual Shear strength results

S. No.	Rock formation	Test No.	Residual shear load (KN)	Residual shear strength (MPa)	Deformation at residual shear strength (mm)	Residual shear strain	Max deformation (mm)
1	Davis	1	37.11	4.57	21.82	0.17	24.02
2	Davis	2	40.82	5.01	21.48	0.17	24.02
3	Davis	3	40.43	4.34	23.97	0.17	22.75
4	Davis	4	35.94	3.82	23.09	0.18	23.09
5	Derby-Doerun	1	27.93	3.51	23.34	0.18	23.29
6	Derby-Doerun	2	29.3	3.1	22.7	0.18	22.75
7	Derby-Doerun	3	33.4	3.53	22.7	0.18	22.75
8	Lamotte	1	46.29	4.88	22.46	0.17	24.02
9	Bonne Terre	1	40.04	4.07	19.18	0.14	24.02

Table B-3. Slip Tendency parameters for formation top

S. No	Rock formation	θ	μ=tan Φ	PP (FT)	σv (FT)	σh (FT)	τ (FT)	σn (FT)	σn' (FT)	τ slip (FT)	ST (FT)
1	Davis	60	1.23	4.11	11.9	6.64	2.30	7.97	3.86	4.75	0.48
2	Derby-Doerun	60	0.91	3.84	11.3	6.26	2.19	7.53	3.69	3.35	0.65
3	Bonne Terre	60	1.12	4.71	13.4	7.52	2.55	8.99	4.28	4.79	0.53
4	Lamotte	60	0.68	5.2	14.6	8.28	2.77	9.88	4.68	3.18	0.87

Table B-4. Slip Tendency parameters for formation bottom

S. No.	Rock Form-ation	θ	μ=tan Φ	PP (FB)	σv (FB)	σh (FB)	τ (FB)	σn (FB)	σn' (FB)	τ slip (FB)	ST (FB)
1	Davis	60	1.23	4.66	13.3	7.44	2.53	8.90	4.24	5.22	0.48
2	Derby-Doerun	60	0.91	4.1	11.9	6.64	2.30	7.97	3.87	3.52	0.65
3	Bonne Terre	60	1.12	5.23	14.6	8.28	2.77	9.88	4.65	5.20	0.53
4	Lamotte	60	0.68	5.84	16.1	9.17	3.03	10.9	5.08	3.45	0.87

APPENDIX C.

DIRECT SHEAR TEST PLOTS
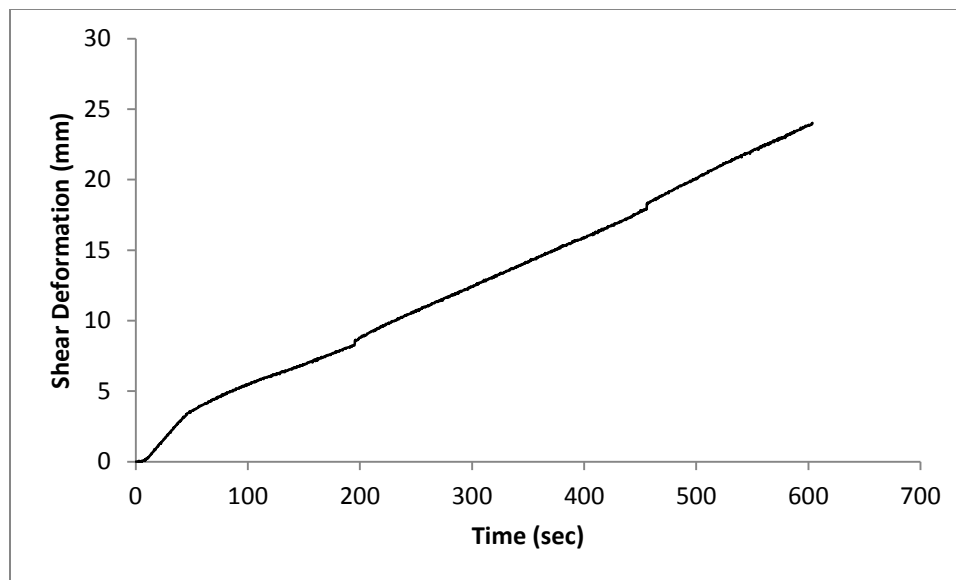
Figure C-1. Shear deformation vs time plot for first sample of davis
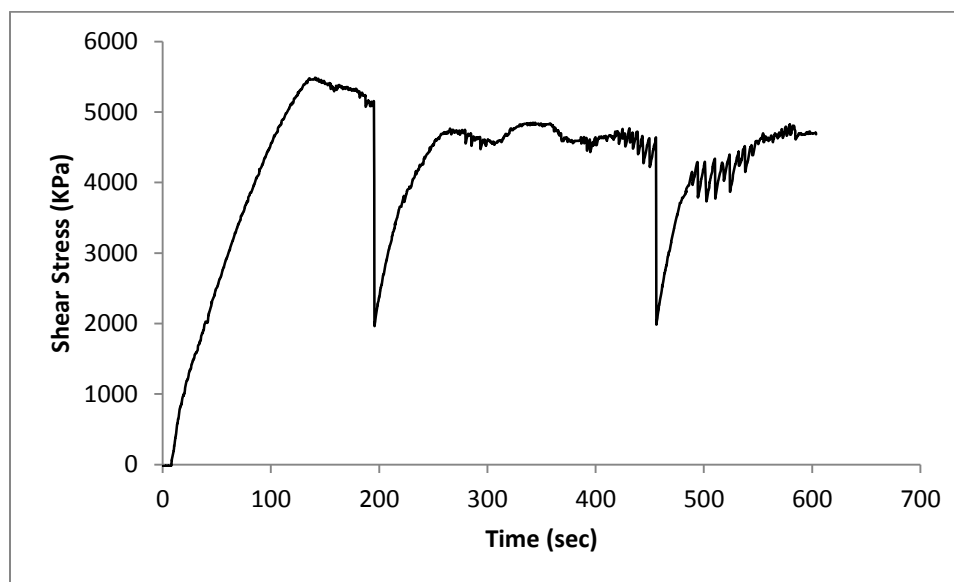
Figure C-2. Shear stress vs time plot for first sample of davis
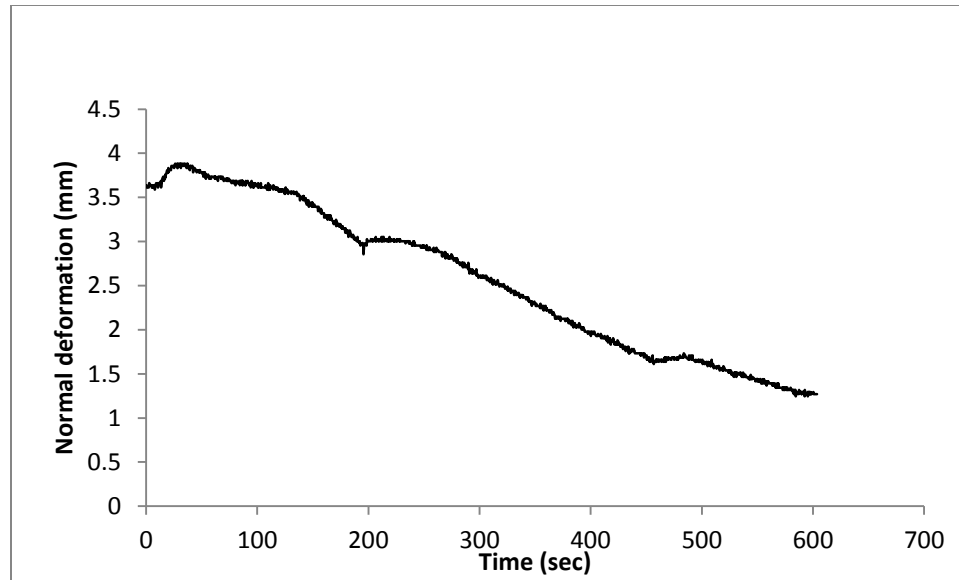
Figure C-3. Normal deformation vs time plot for first sample of davis
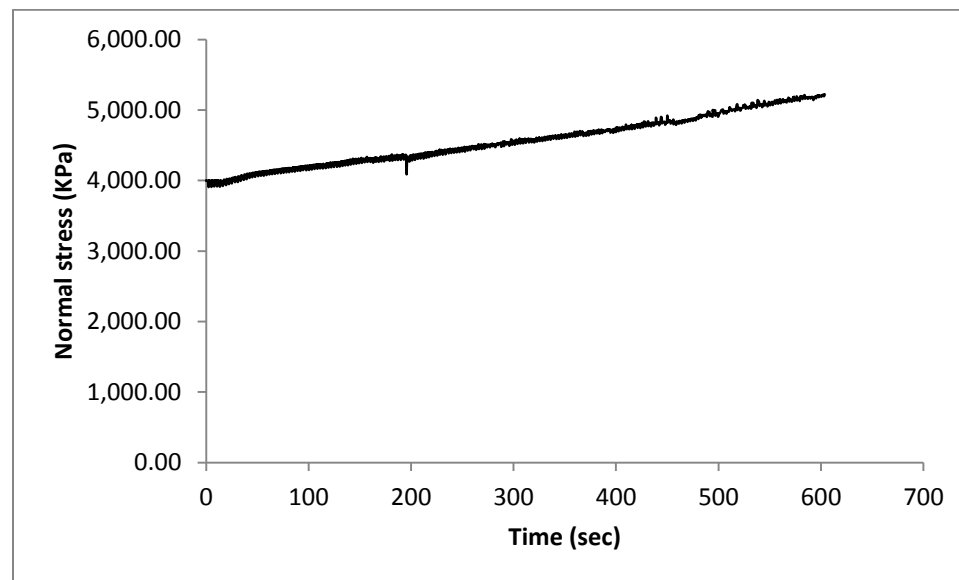
Figure C-4. Normal stress vs time plot for first sample of davis
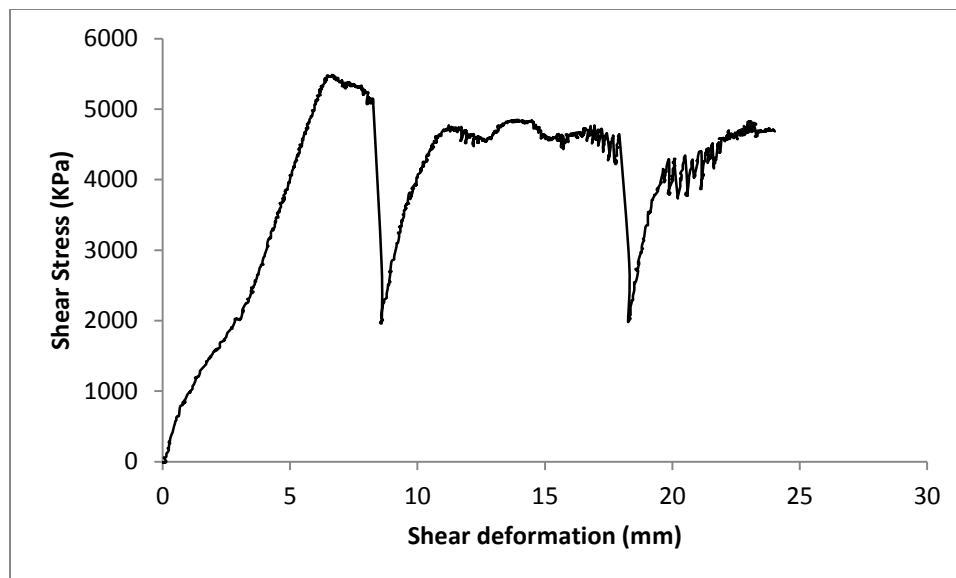
Figure C-5. Shear stress vs shear deformation plot for first sample of davis
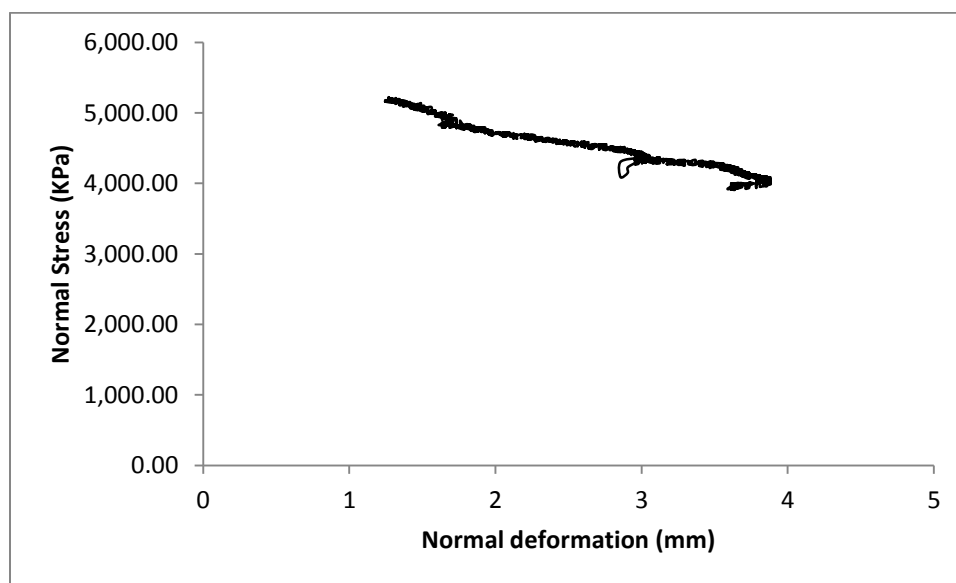
Figure C-6. Normal stress vs Normal deformation plot for first sample of davis
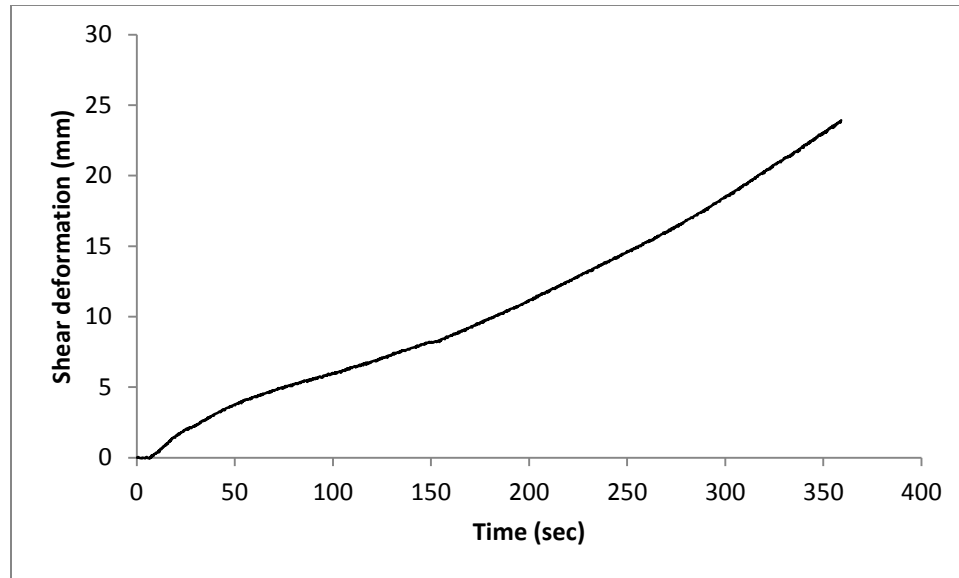
Figure C-7. Shear deformation vs time for second sample of davis
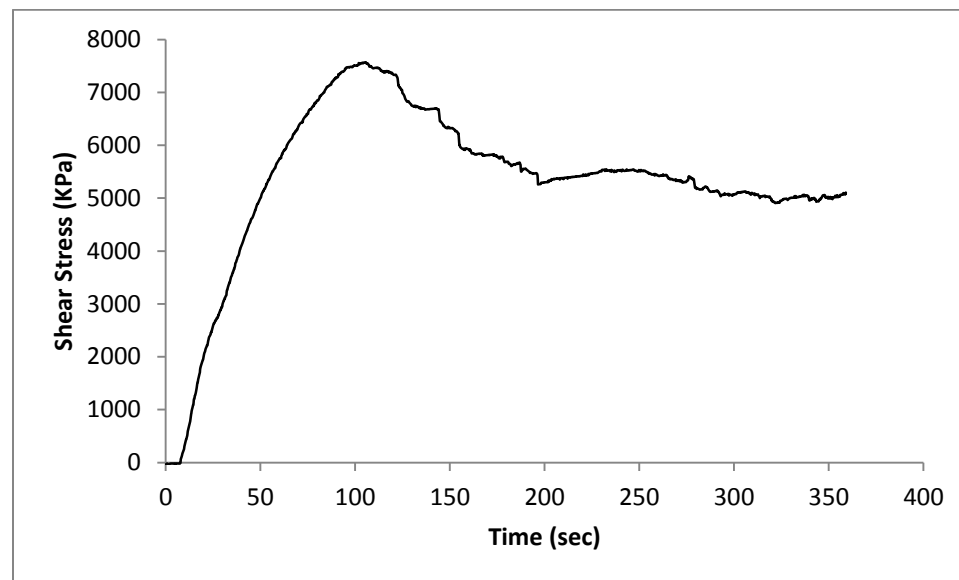
Figure C-8. Shear stress vs time for second sample of davis
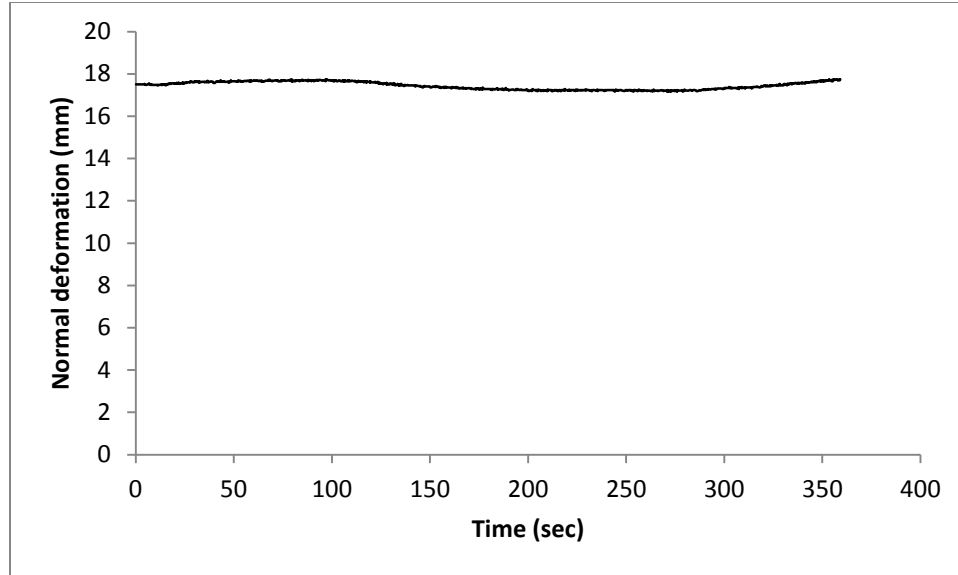
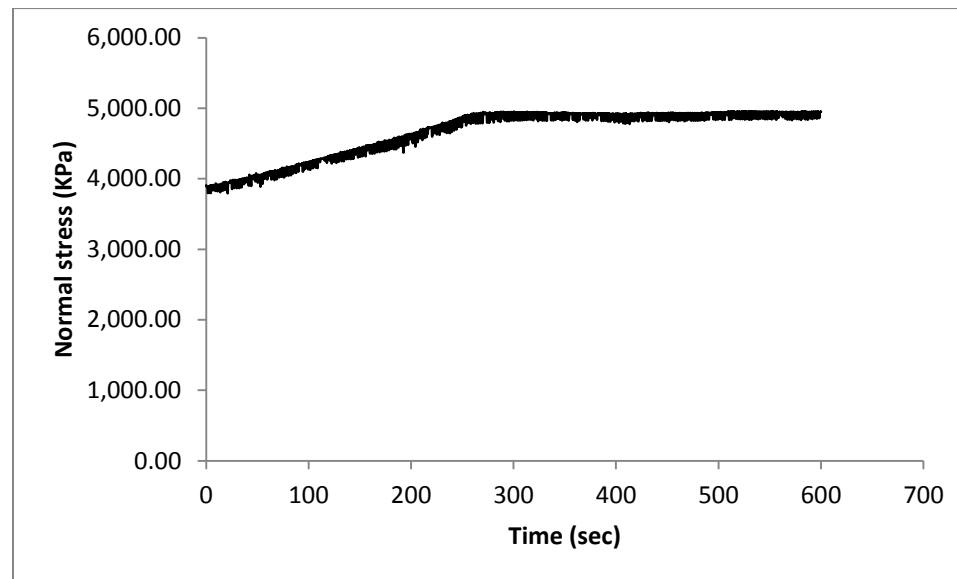Figure C-9. Normal deformation vs time for second sample of davis
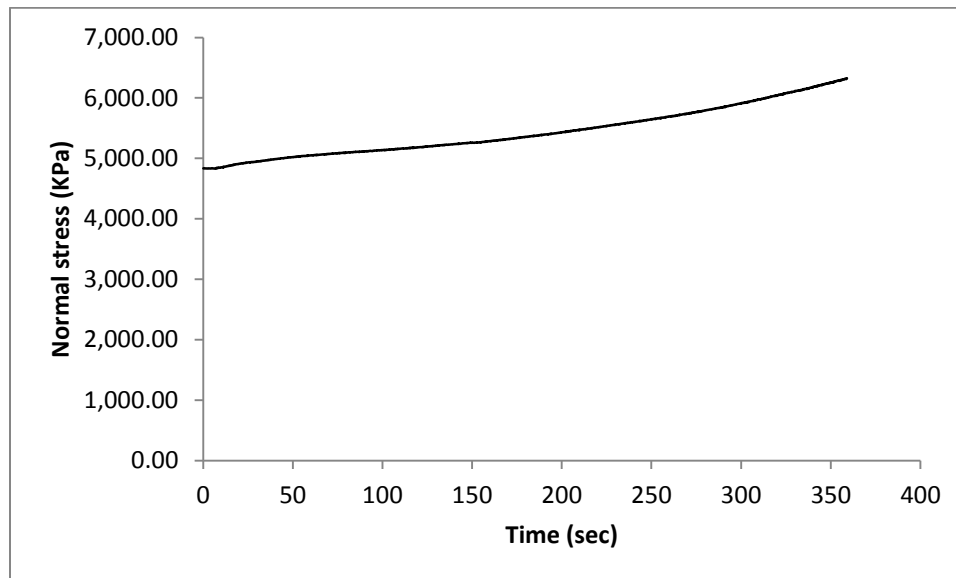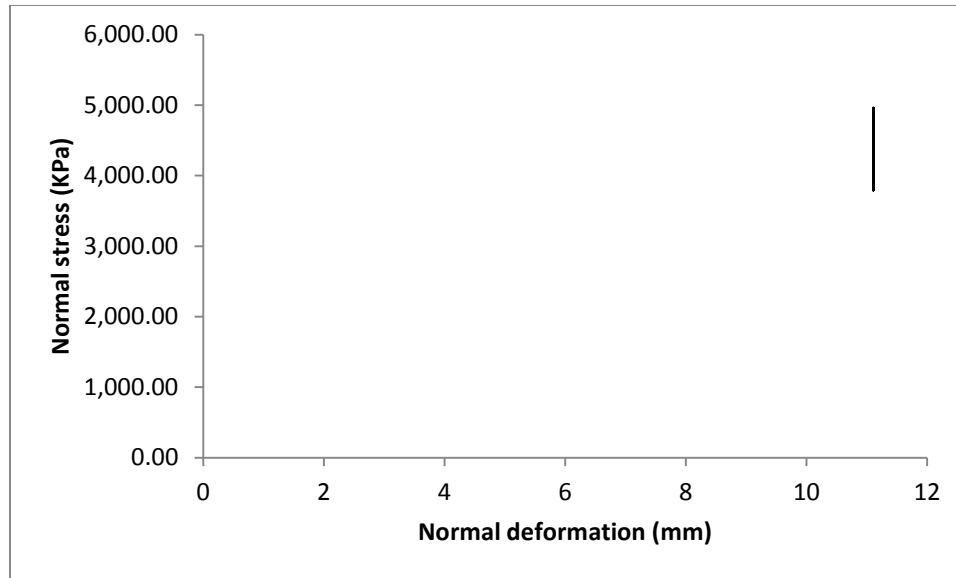

Figure C-10. Normal stress vs time for second sample of davis
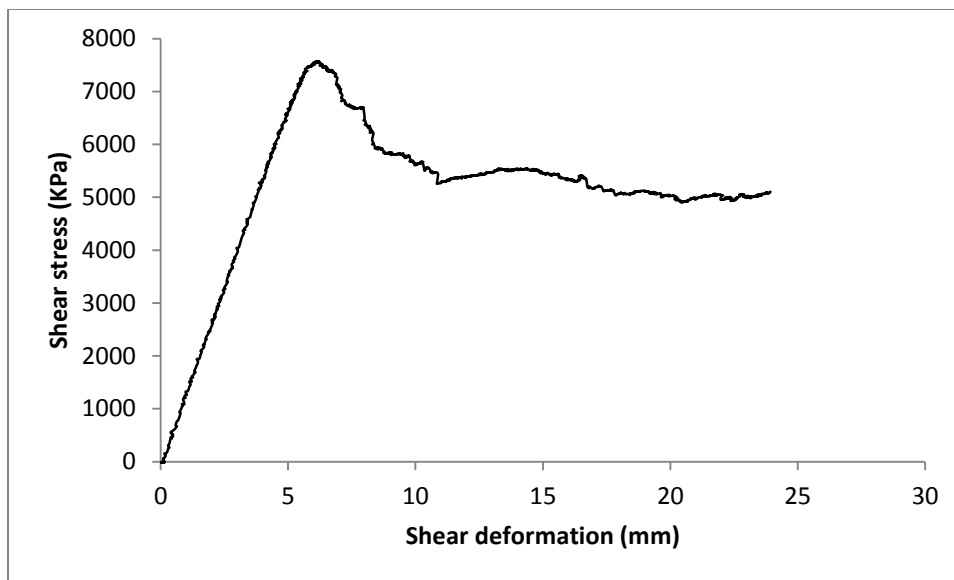
Figure C-11. Shear stress vs shear deformation for second sample of davis
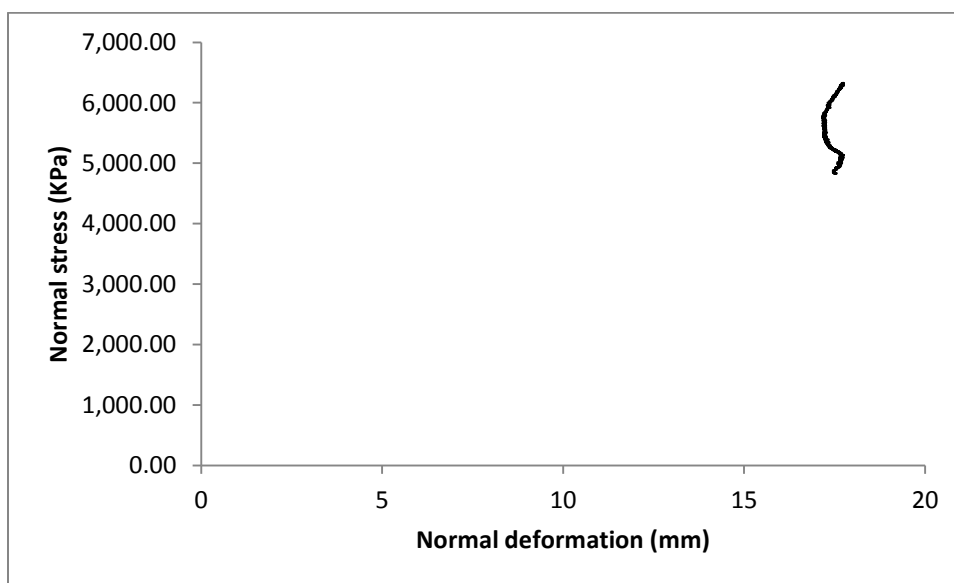
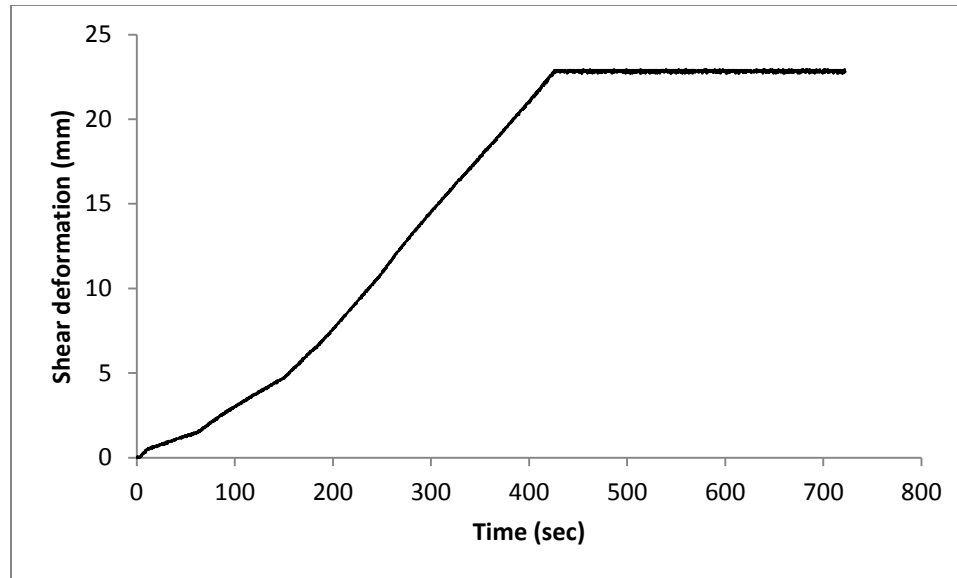Figure C-12. Normal stress vs Normal deformation for second sample of davis
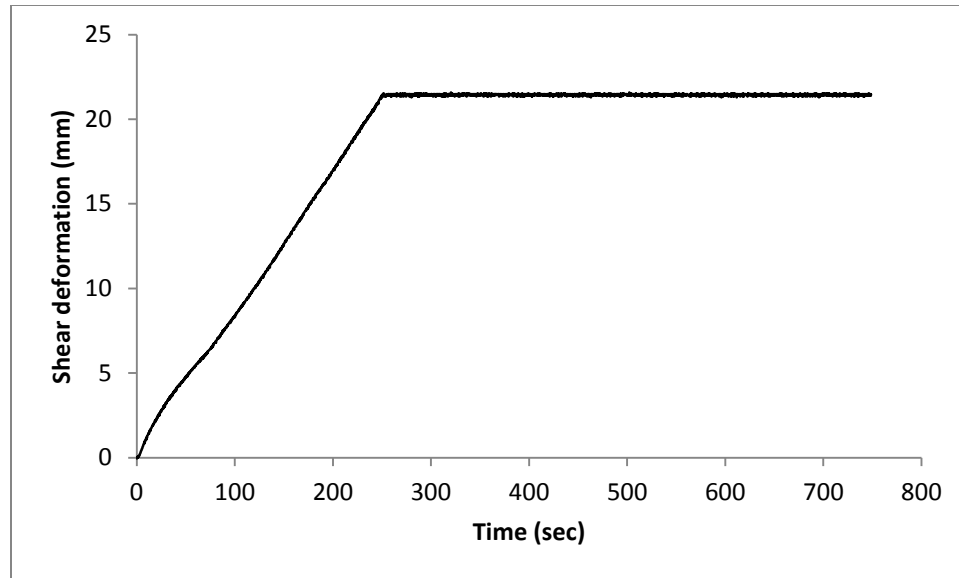
Figure C-13. Shear deformation vs time for third sample of davis
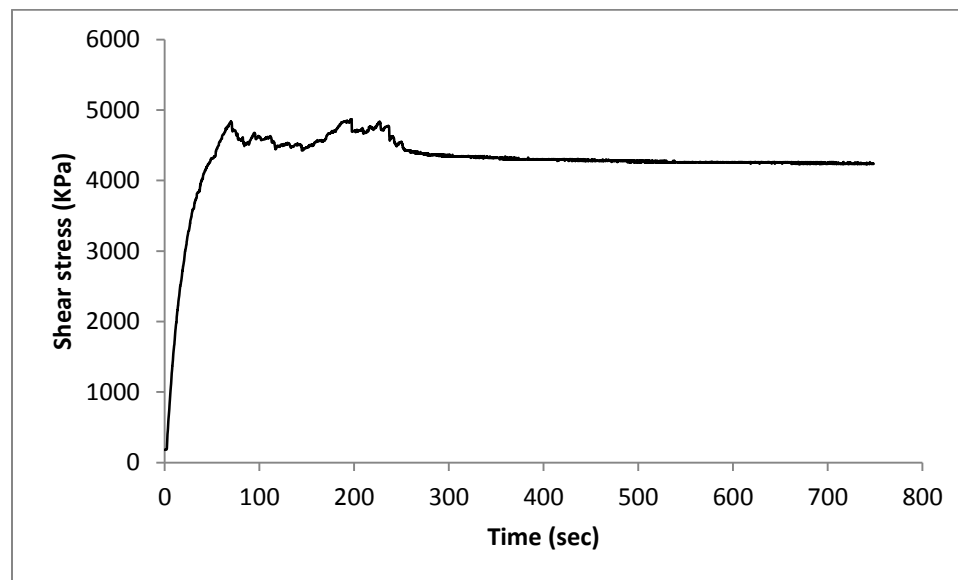
Figure C-14. Shear stress vs time for third sample of davis
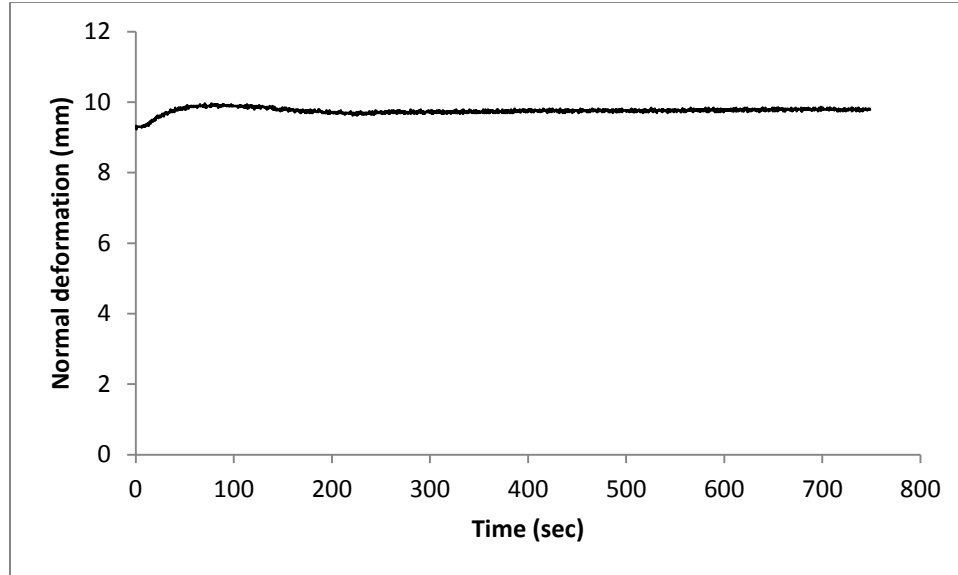
Figure C-15. Normal deformation vs time for third sample of davis
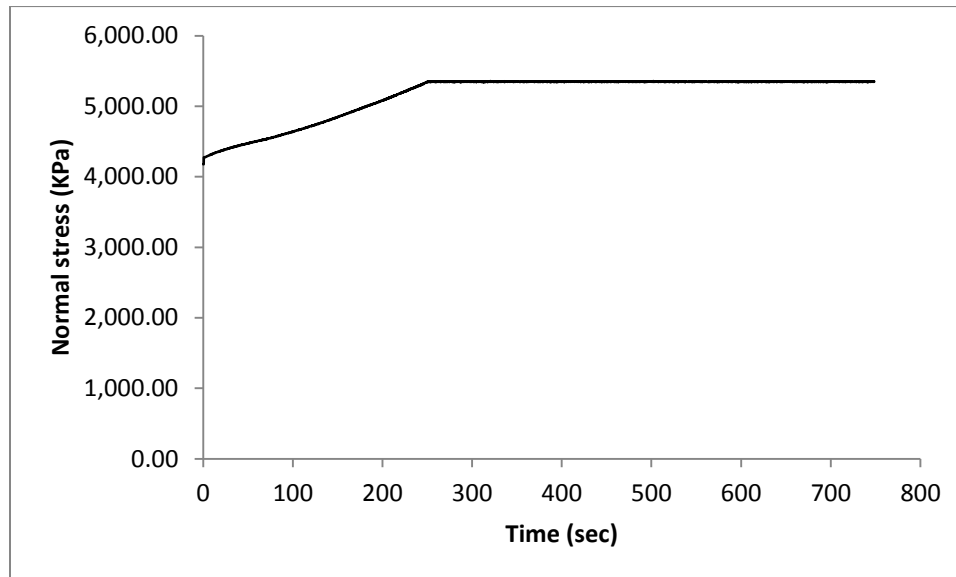
Figure C-16. Shear stress vs time for third sample of davis
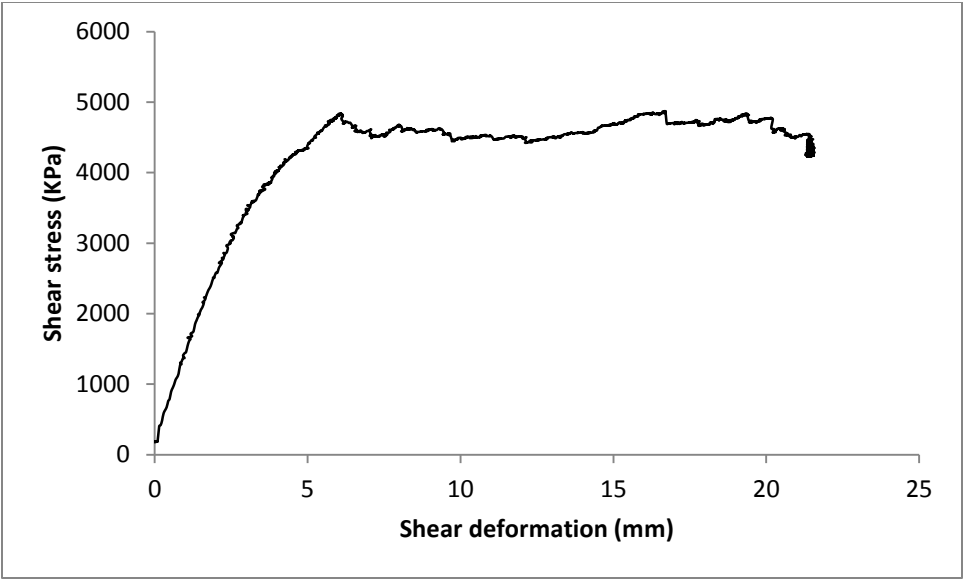
Figure C-17. Shear stress vs shear deformation for third sample of davis
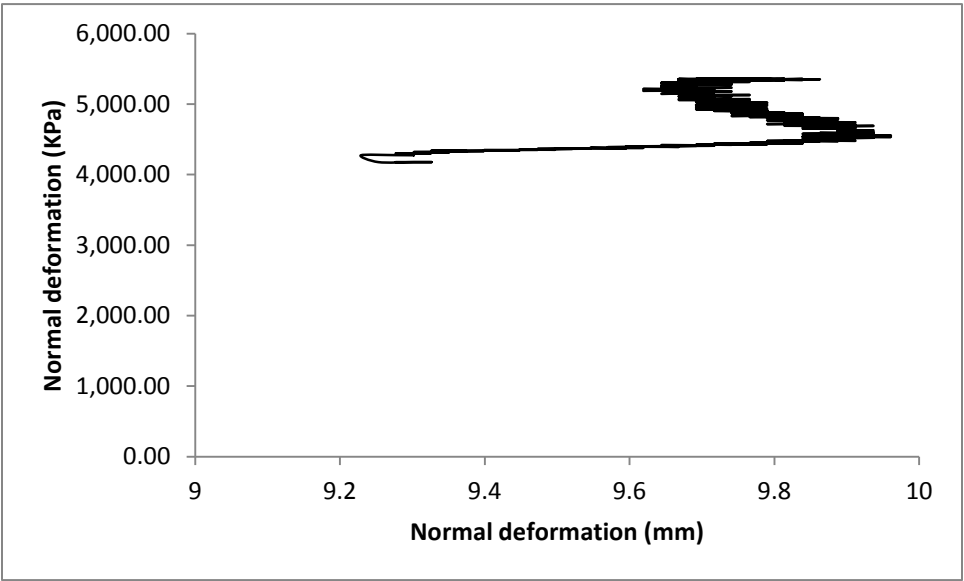
Figure C-18. Normal stress vs Normal deformation for third sample of davis
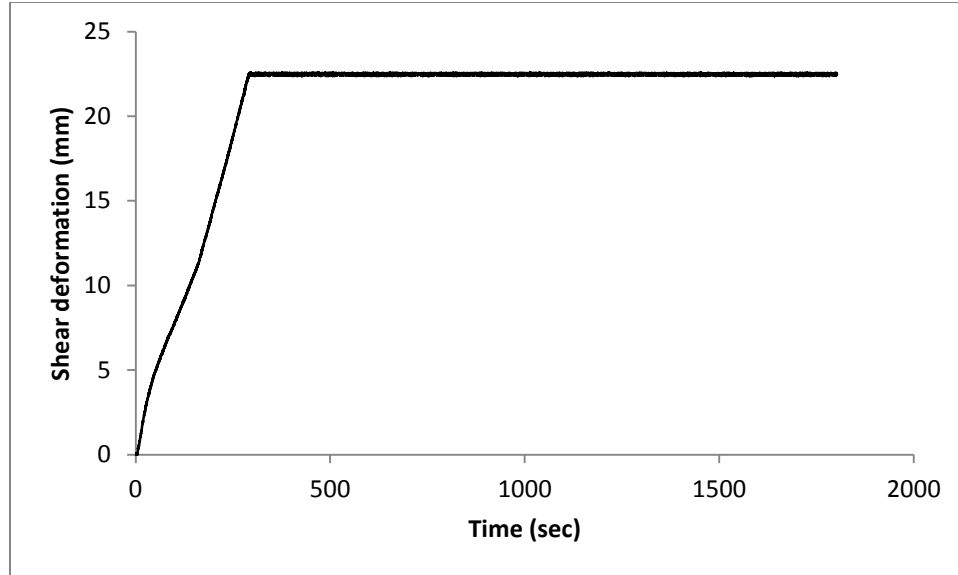
Figure C-19. Shear deformation vs time for fourth sample of davis
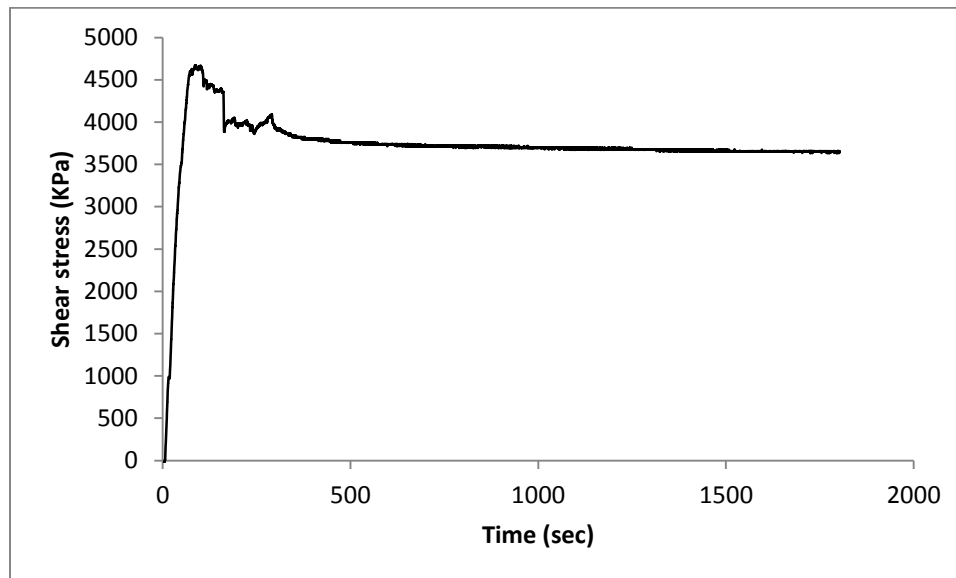
Figure C-20. Shear stress vs time for fourth sample of davis
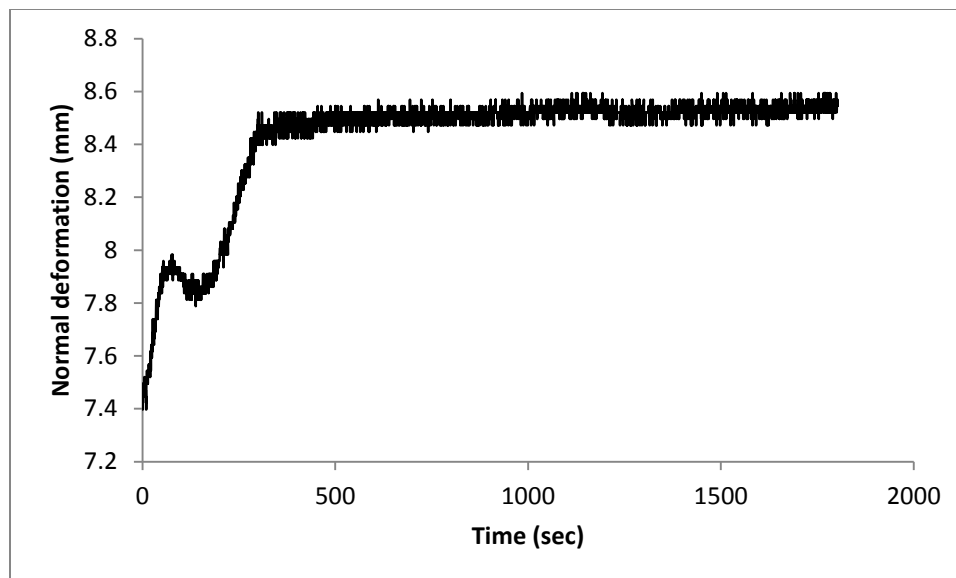
Figure C-21. Normal deformation vs time for fourth sample of davis
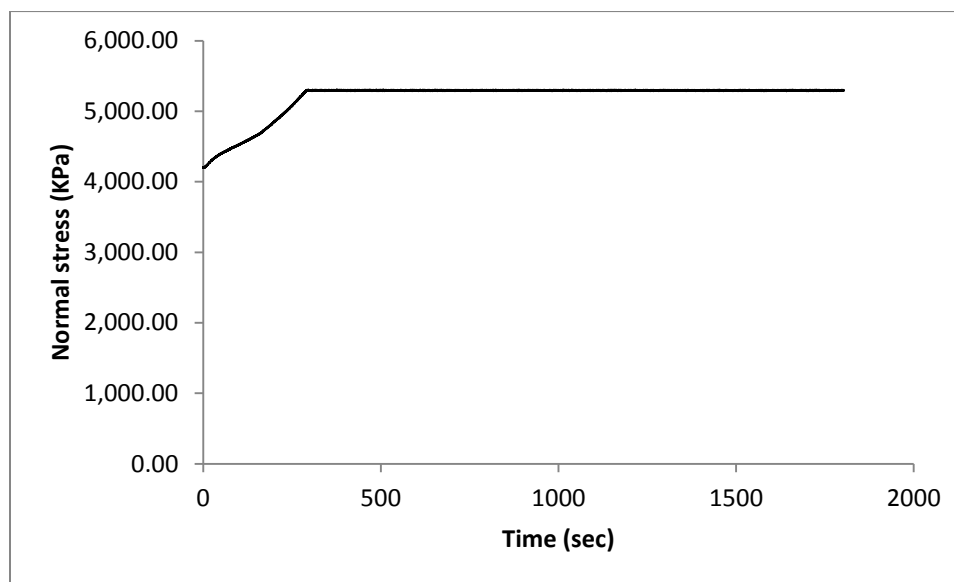
Figure C-22. Normal stress vs time for fourth sample of davis
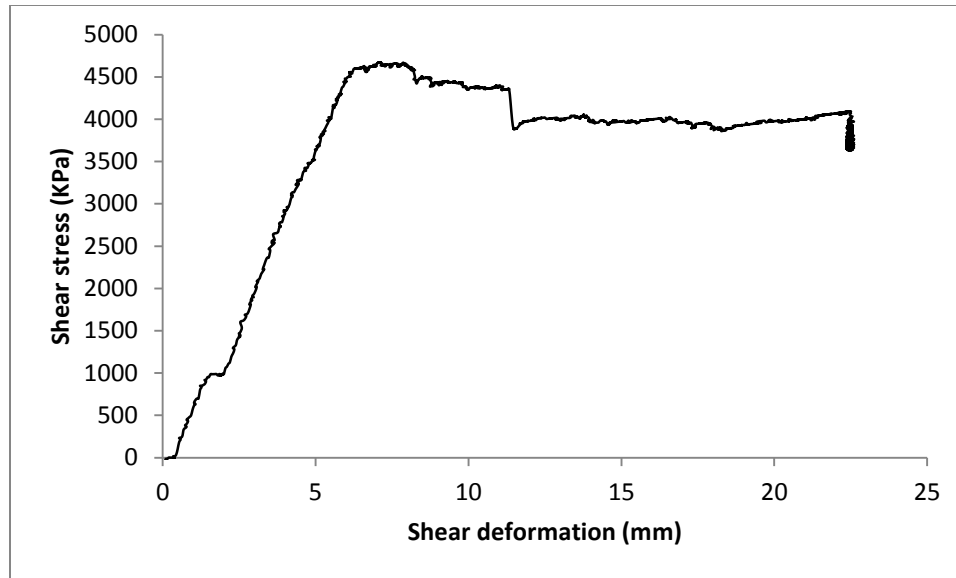
Figure C-13. Shear stress vs Shear deformation for fourth sample of davis
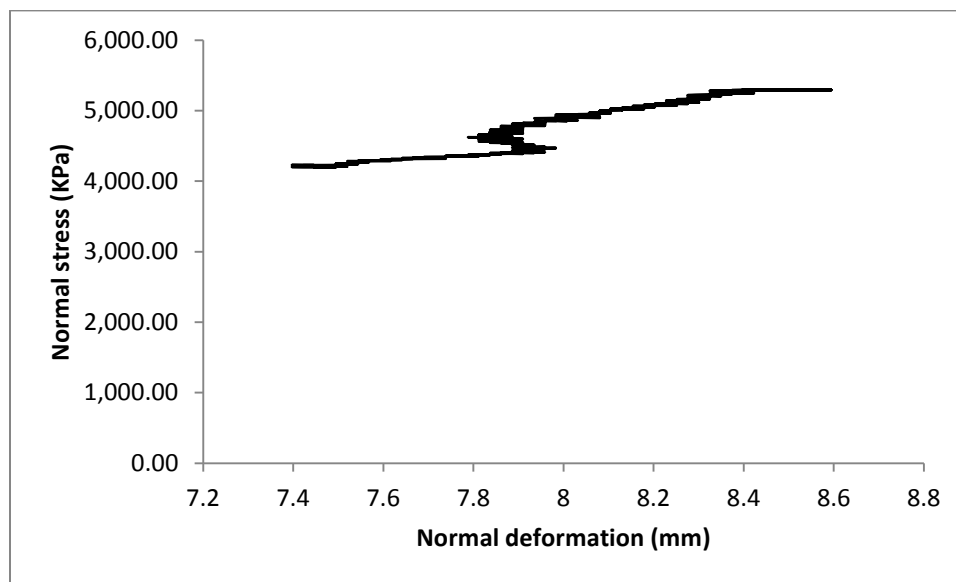
Figure C-24. Normal stress vs Normal deformation for fourth sample of davis
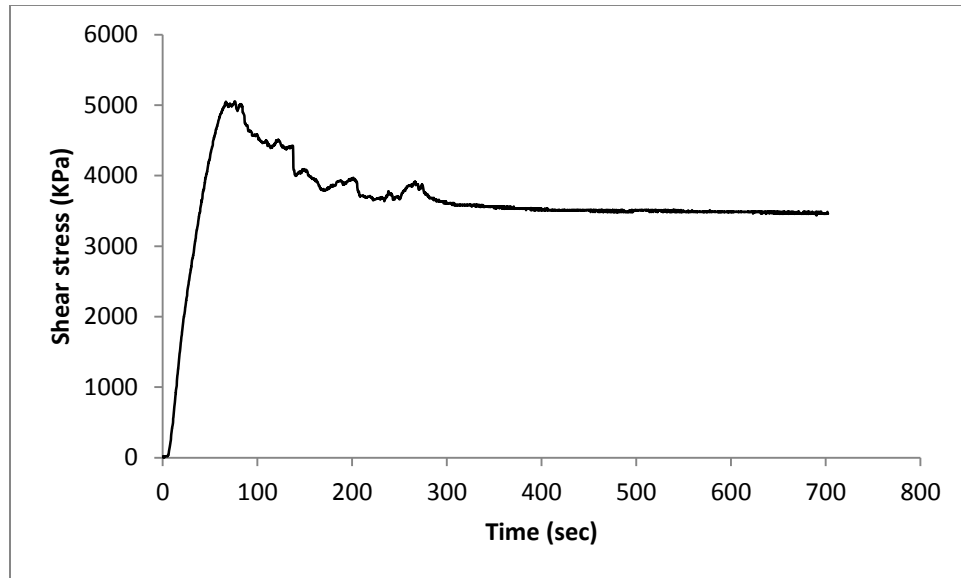
Figure C-25. Shear deformation vs time for first sample of Derby-Doerun
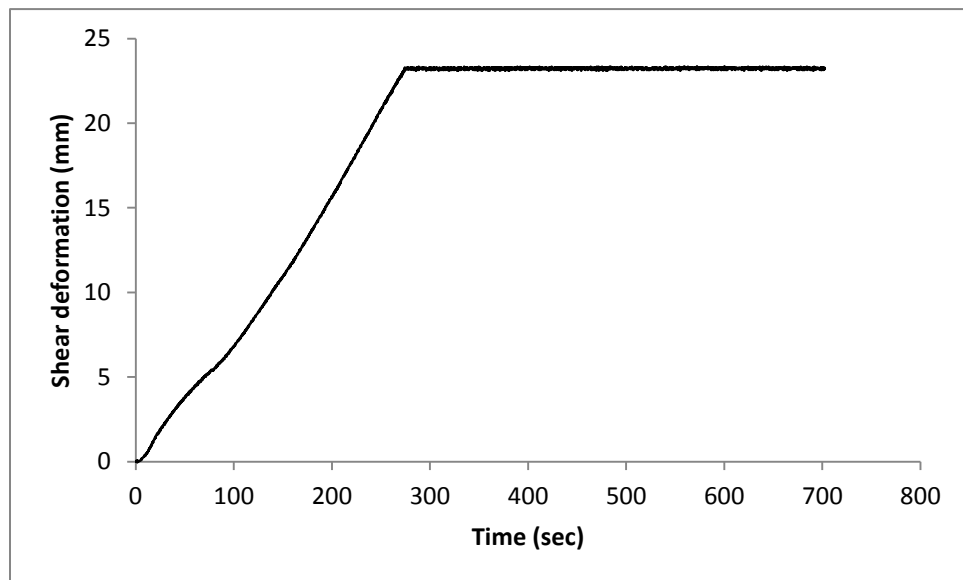
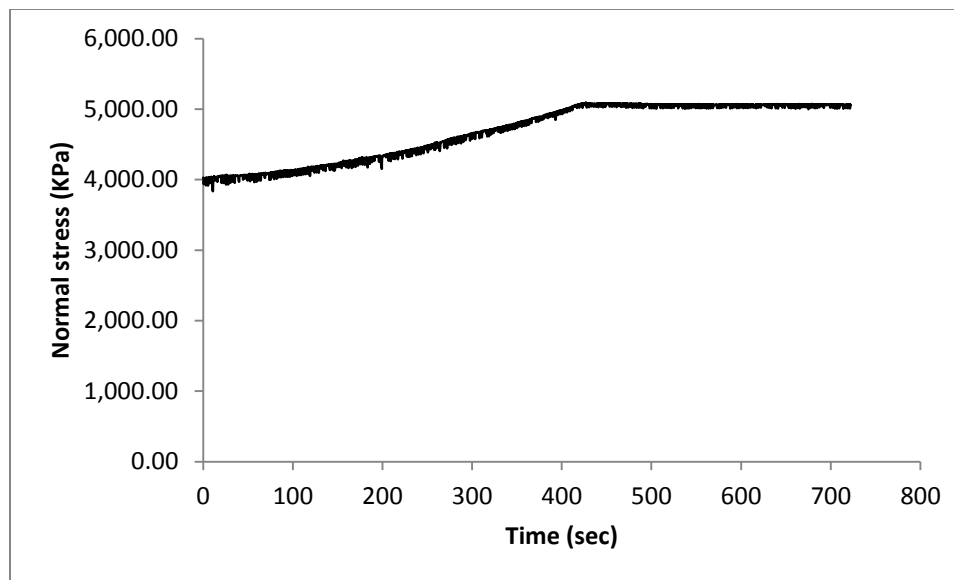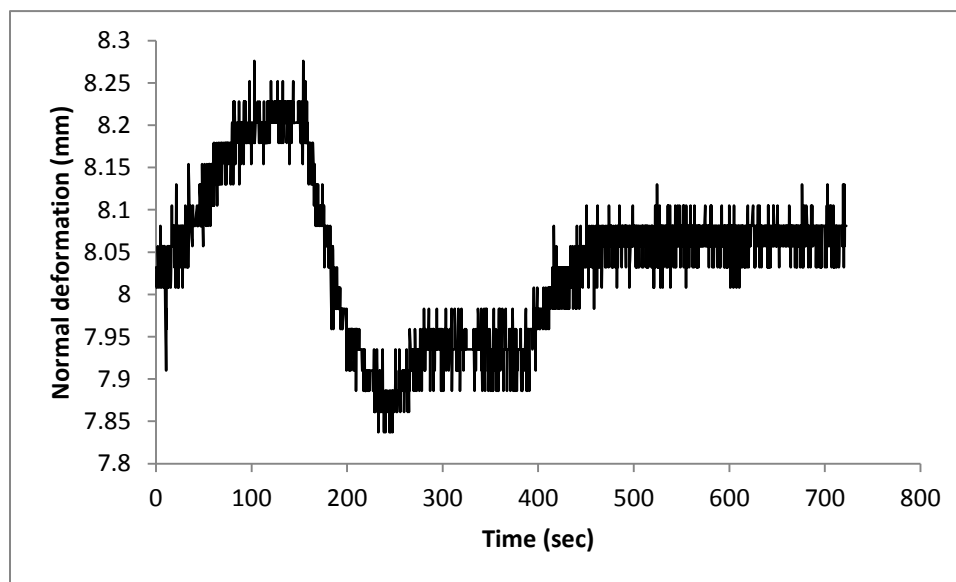Figure C-26. Shear stress vs time for first sample of Derby-Doerun
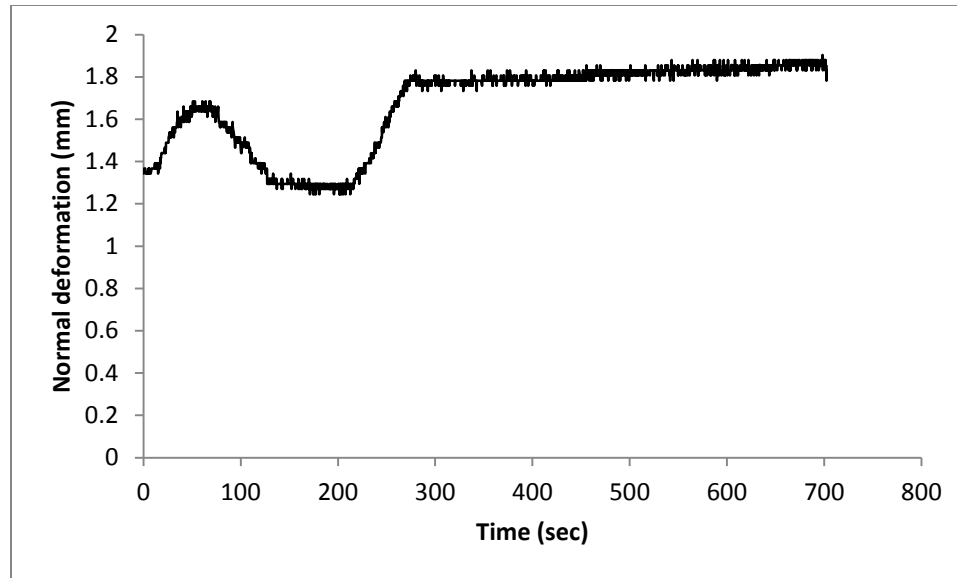
Figure C-27. Normal deformation vs time for first sample of Derby-Doerun
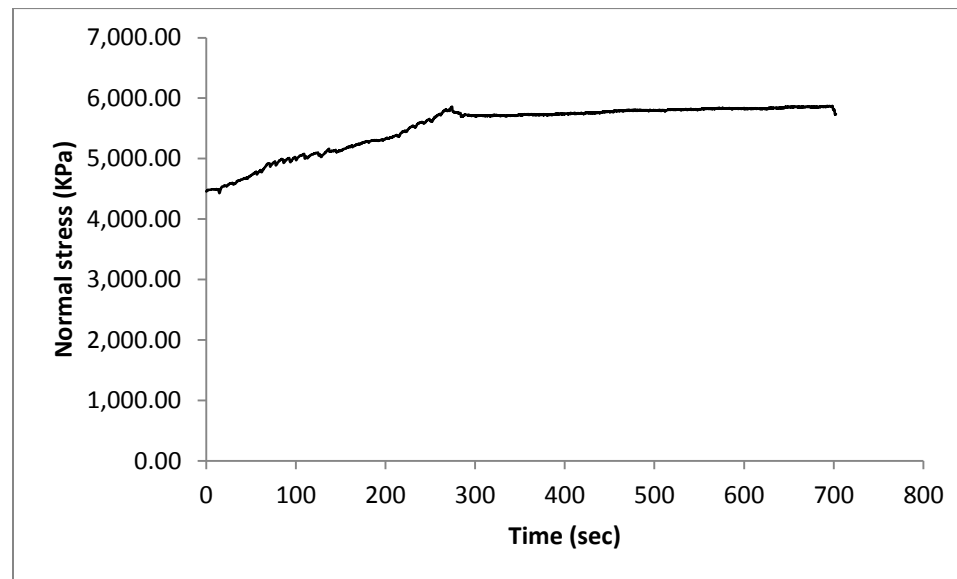
Figure C-28. Normal stress vs time for first sample of Derby-Doerun
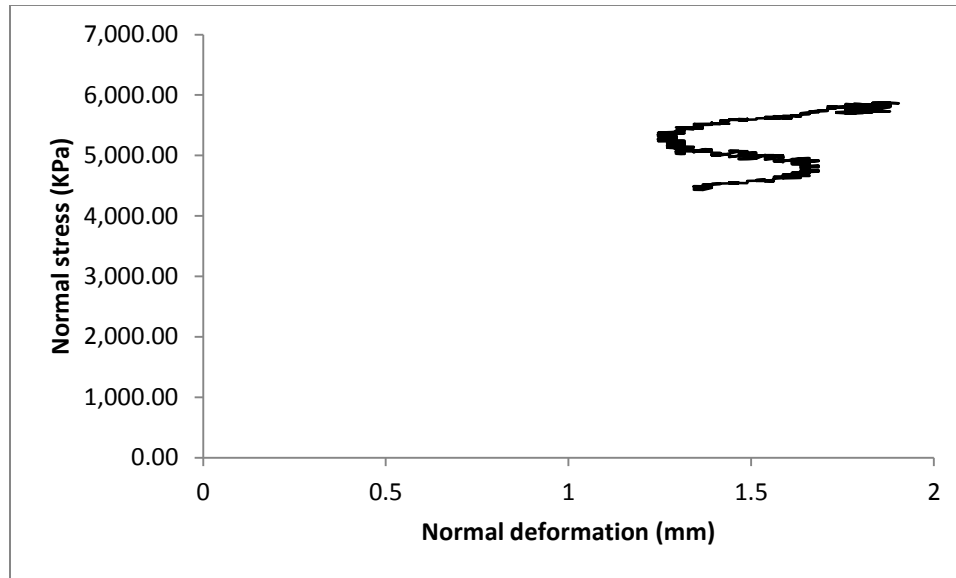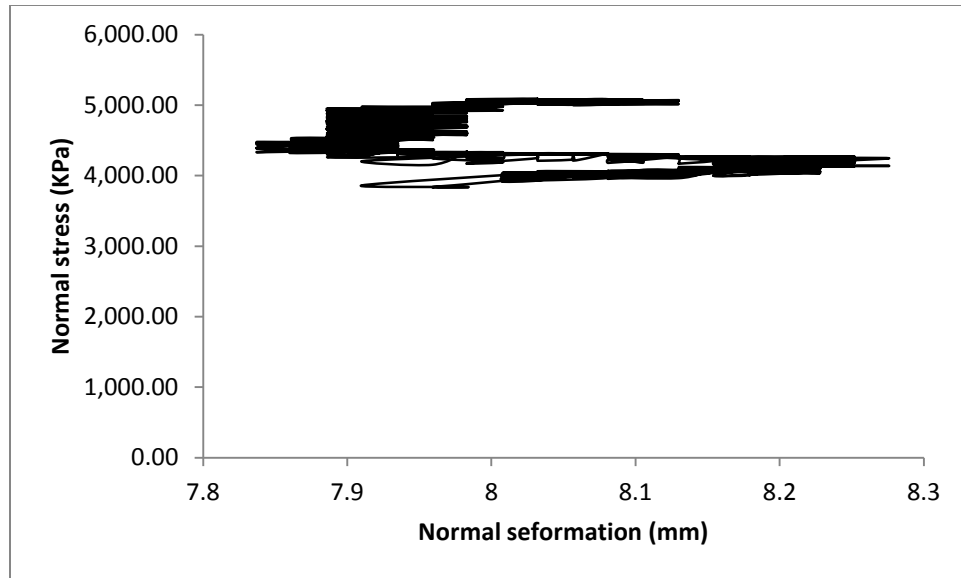
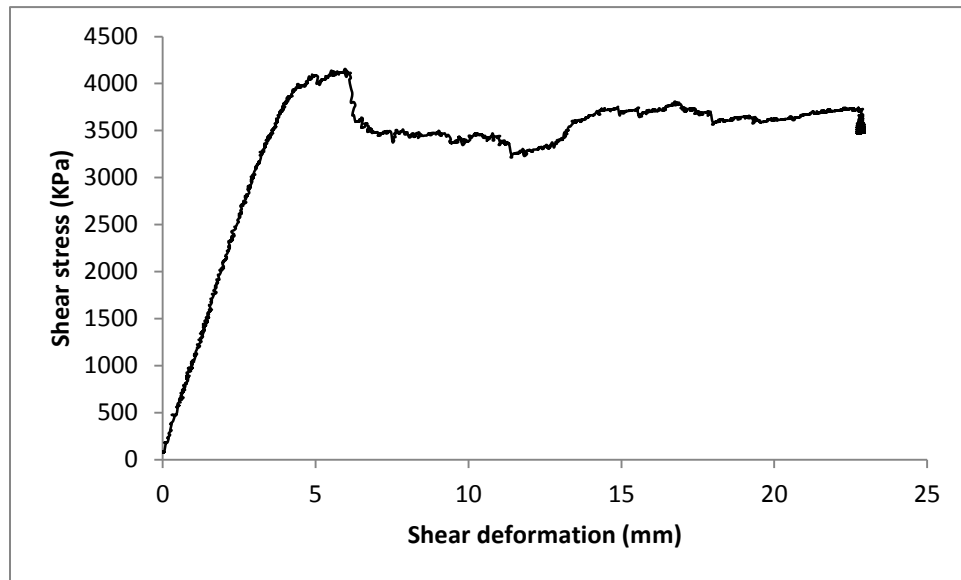Figure C-29. Normal stress vs Normal deformation for first sample of Derby-Doerun
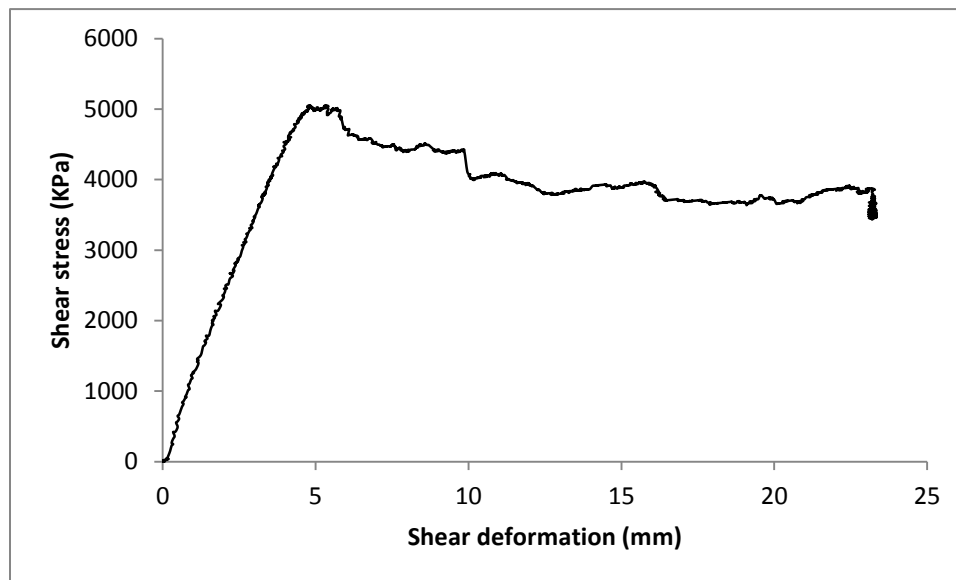
Figure C-30. Shear stress vs Shear deformation for first sample of Derby-Doerun
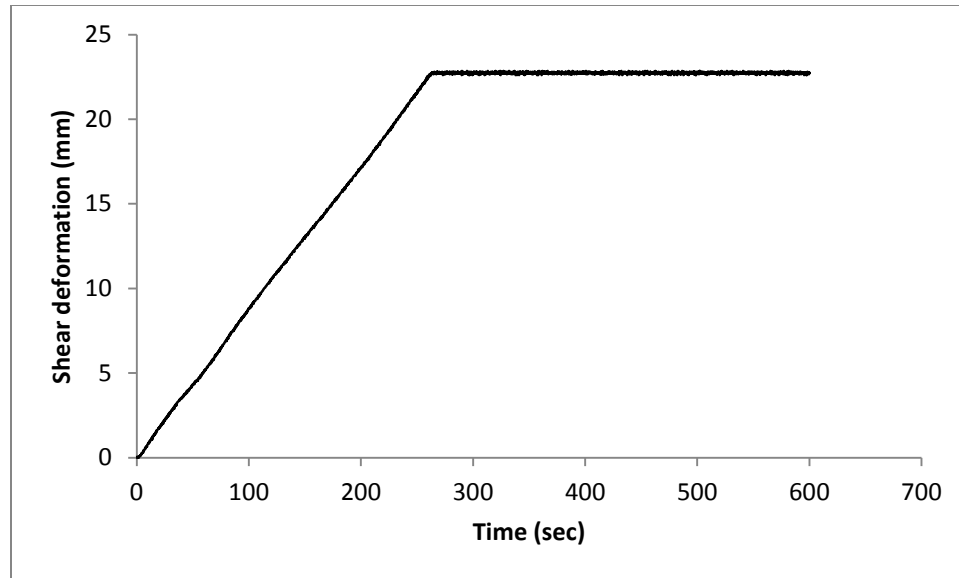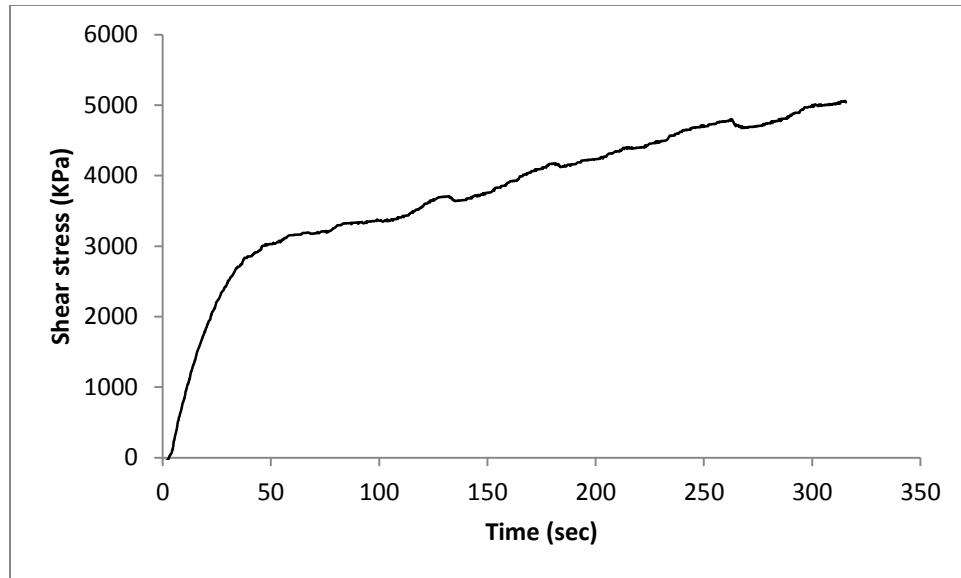
Figure C-31. Shear deformation vs time for second sample of Derby-Doerun
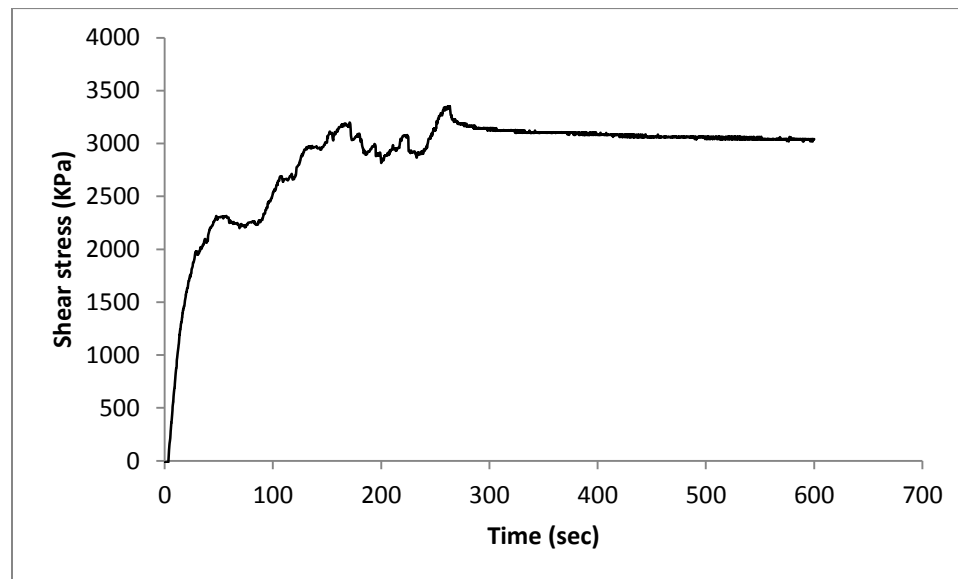
Figure C-32. Shear stress vs time for second sample of Derby-Doerun
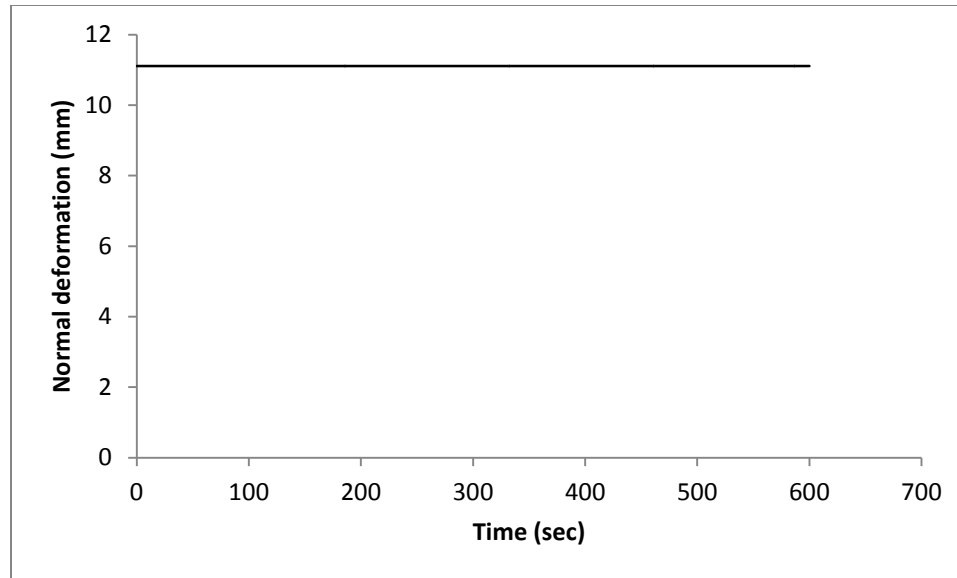
Figure C-33. Normal deformation vs time for second sample of Derby-Doerun

Figure C-34. Shear stress vs time for second sample of Derby-Doerun

Figure C-35. Normal stress vs Normal deformation for second sample of Derby-Doerun
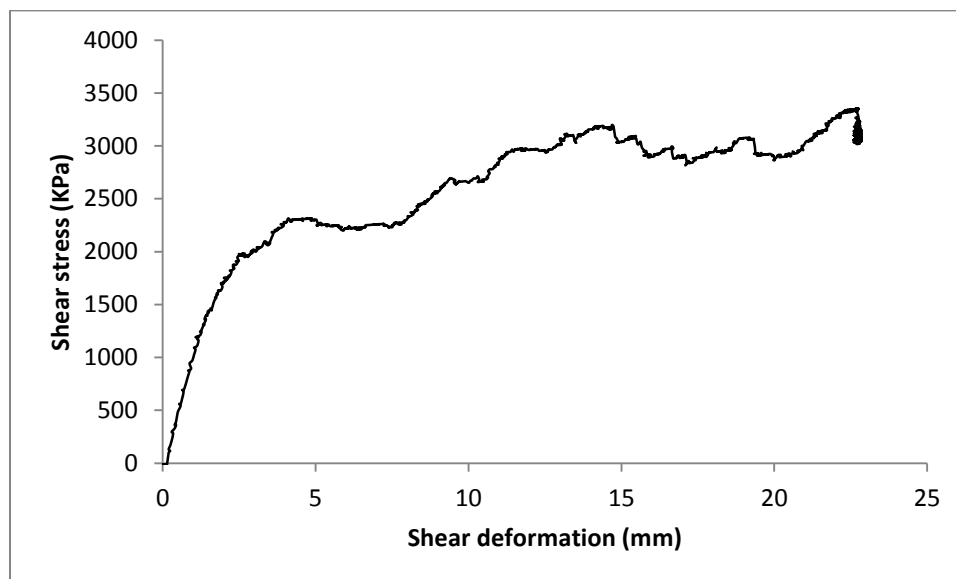
Figure C-36. Shear stress vs Shear deformation for second sample of Derby-Doerun

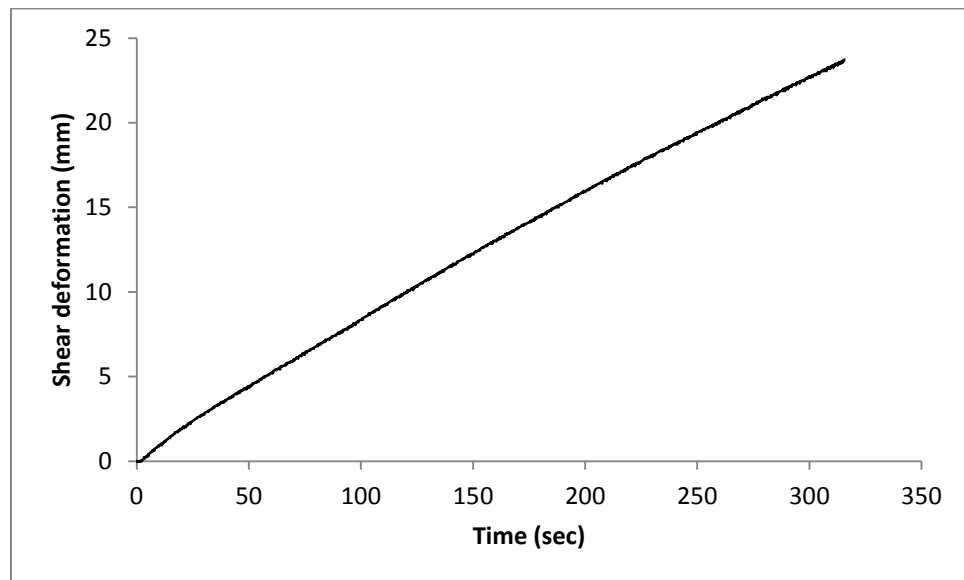Figure C-37. Shear deformation vs time for third sample of Derby-Doerun
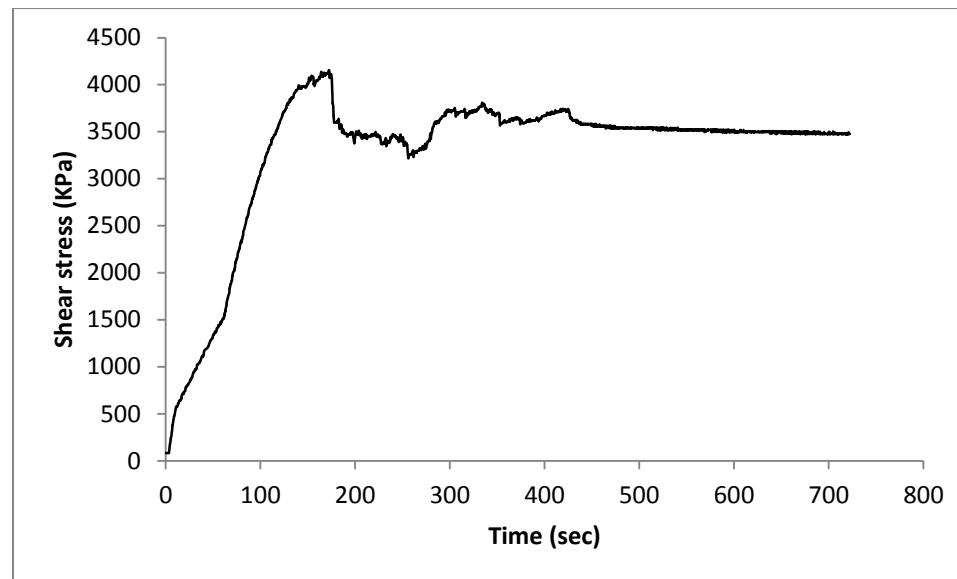
Figure C-38. Shear stress vs time for third sample of Derby-Doerun

Figure C-39. Normal stress vs time for third sample of Derby-Doerun

Figure C-40. Normal deformation vs time for third sample of Derby-Doerun

Figure C-41. Normal stress vs Normal deformation for third sample of Derby-Doerun

Figure C-42. Shear stress vs Shear deformation for third sample of Derby-Doerun

Figure C-43. Shear stress vs time for Lamotte

Figure C-44. Shear deformation vs time for Lamotte
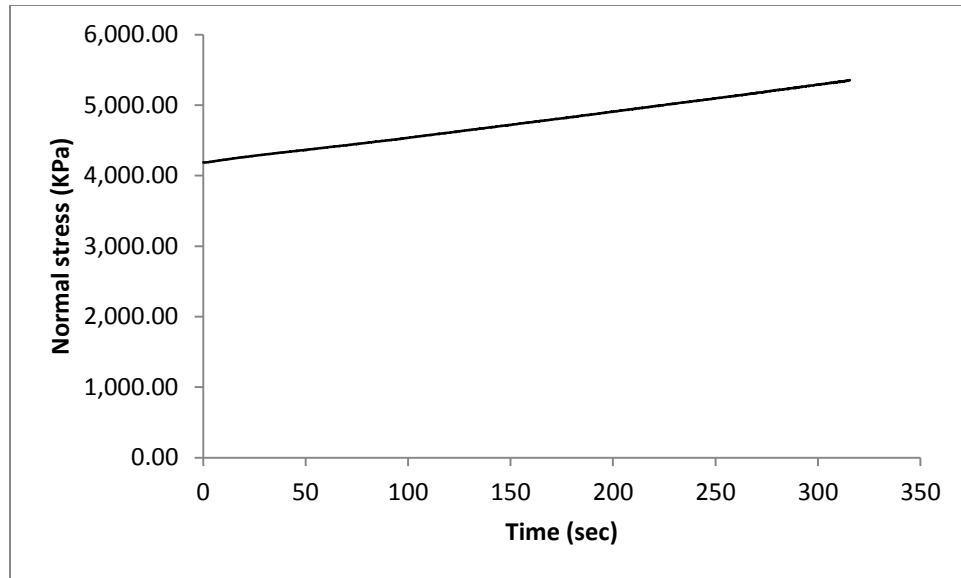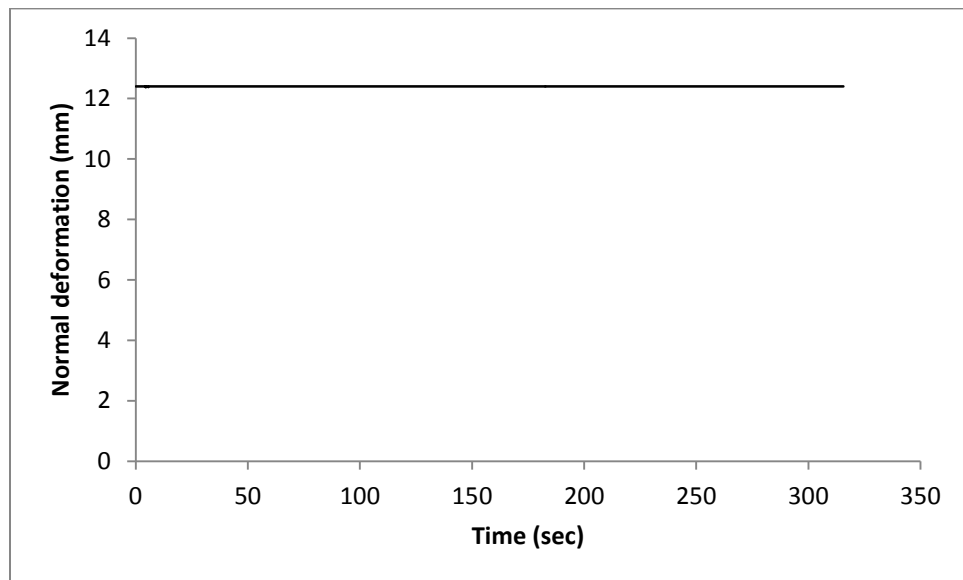
Figure C-45. Normal stress vs time for Lamotte

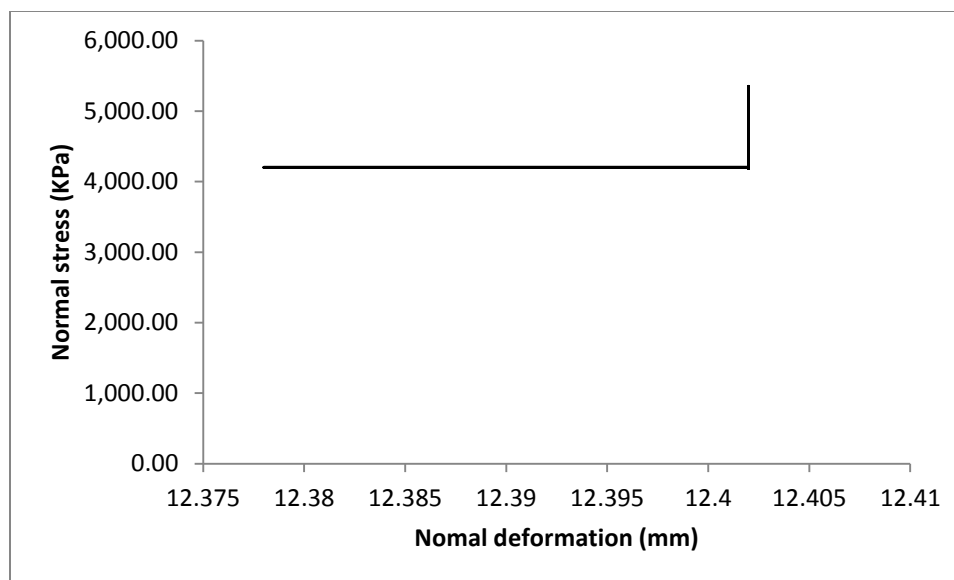Figure C-46. Shear deformation vs time for Lamotte

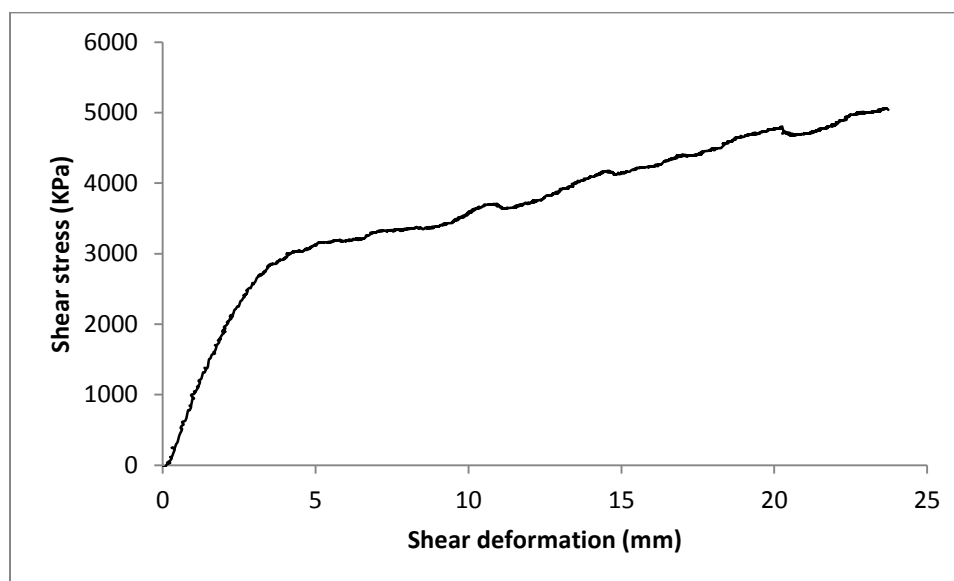Figure C-47. Normal stress vs Normal deformation for Lamotte

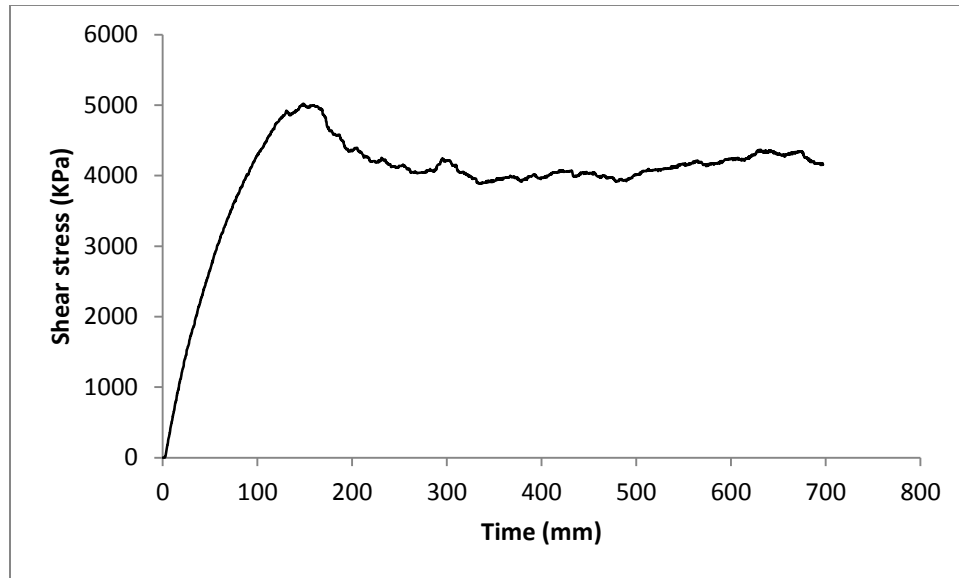Figure C-48. Shear stress vs Shear deformation for Lamotte

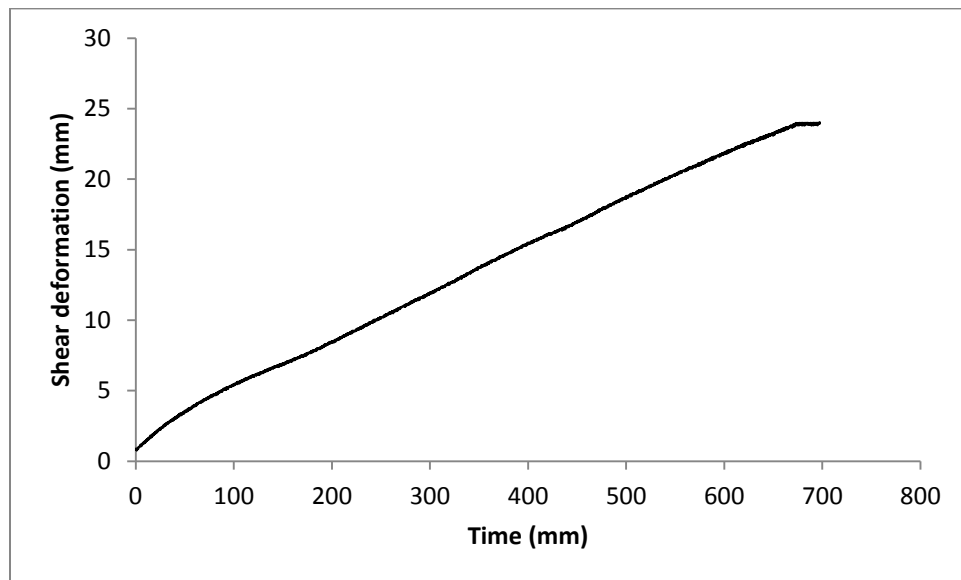Figure C-49. Shear stress vs time for Bonne Terre

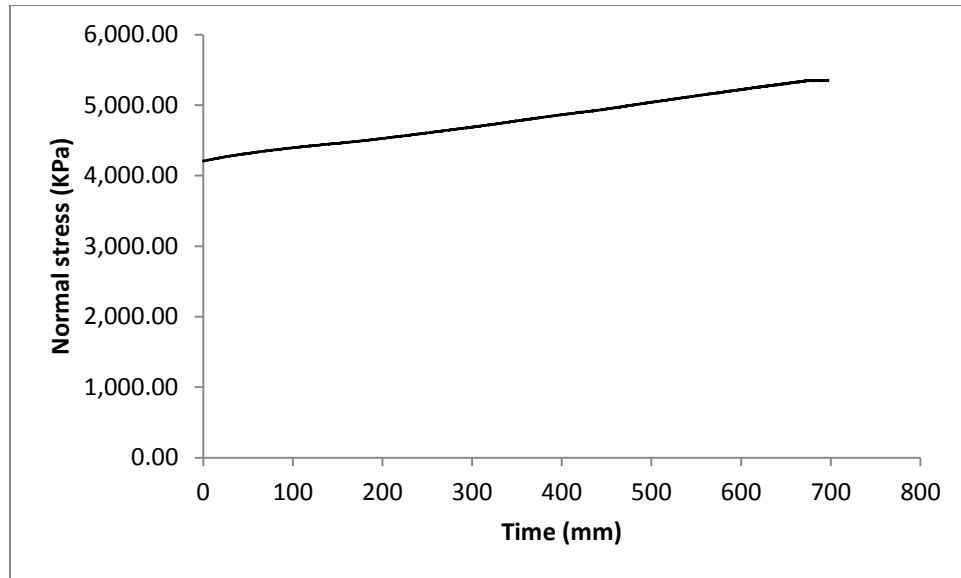Figure C-50. Shear deformation vs time for Bonne Terre

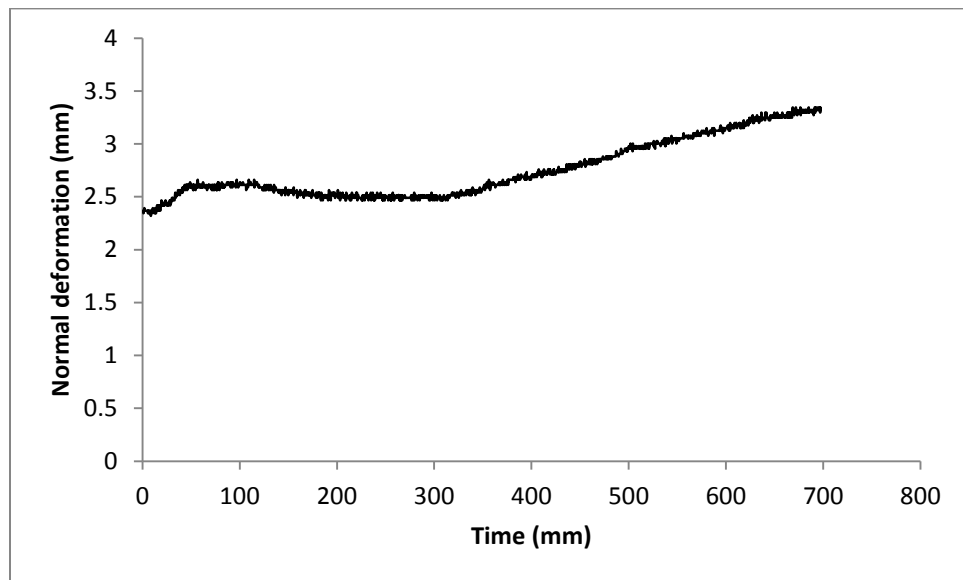Figure C-51. Normal stress vs time for Bonne Terre

Figure C-52. Normal deformation vs time for Bonne Terre

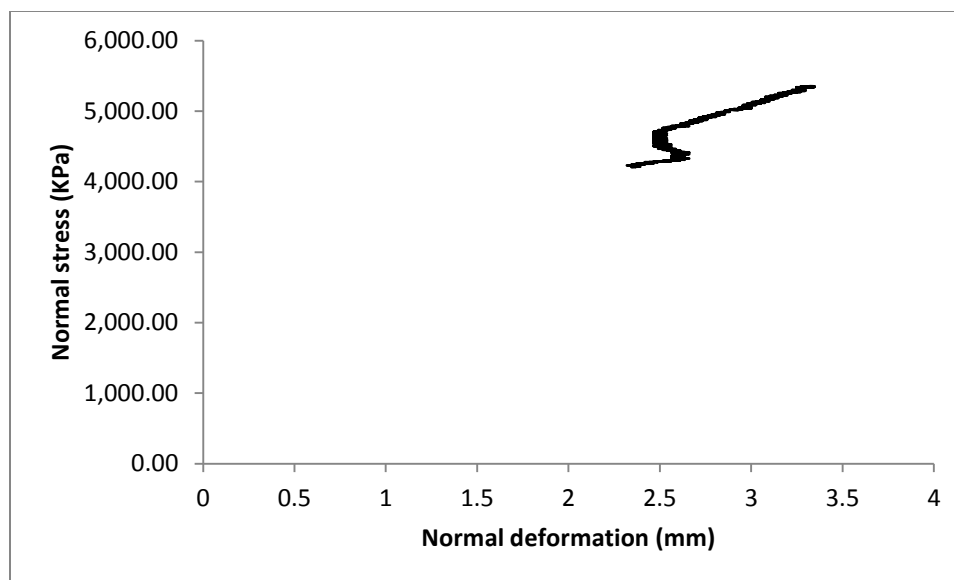Figure C-53. Normal stress vs Normal deformation for Bonne Terre
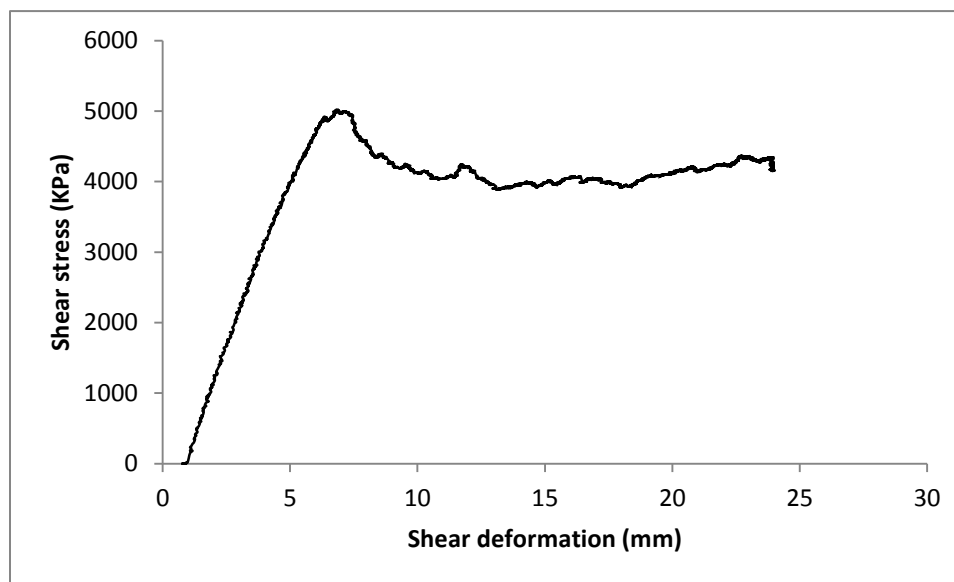
Figure C-54. Shear stress vs Shear deformation for Bonne Terre

APPENDIX D.

SAMPLE PREPARATION IMAGES

(a)

(b)

(c)

(d)

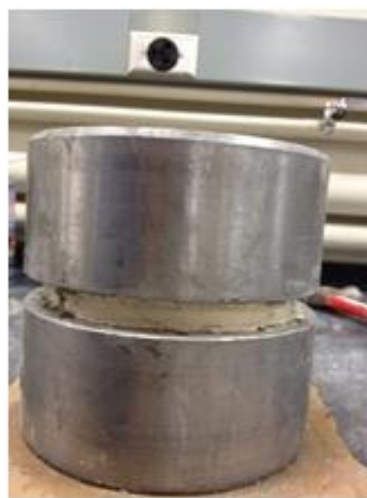Figure D-1. Preparation of rock sample

(a)

(b)

(c)

(d)

Figure D-2. Cementing of rock sample inside the shear ring

(a)

(b)
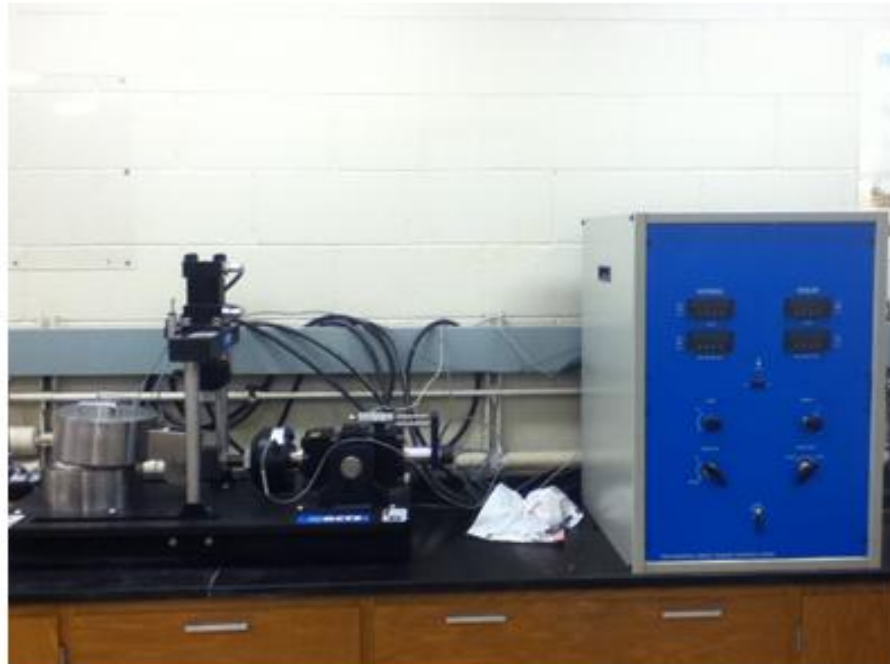
Figure D-3. Mounting of shear ring inside the shear box

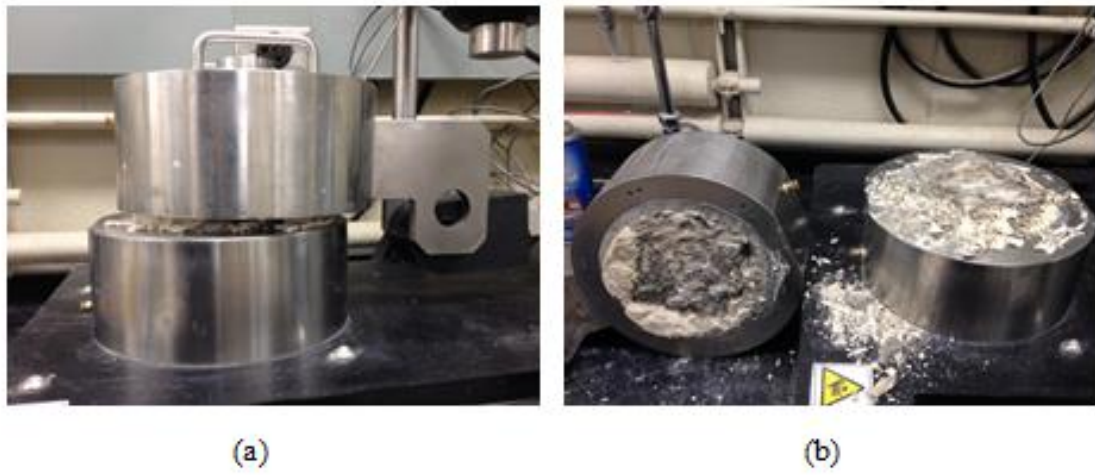

Figure D-4. Direct Shear Apparatus

(a)   (b)

Figure D-5. Rock sample after shearing

Figure D-6. Shear ring stuck inside the shear box

BIBLIOGRAPHY

Aladasani A., Bai B., Wu Y.S., 2012, "Investigating Low-Salinity Water flooding Recovery Mechanisms in Sandstone Reservoirs," Eighteenth SPE Improved Oil Recovery Symposium, Tulsa, Oklahoma, USA, SPE 152997.

Anderson S., Newell R., 2004, "Prospects for Carbon Capture and Storage technologies," Annual Review of the Environmental and Resources, 29: 109-142.

Akpan I.C., 2012, "Development of a Shared Earth Model to Investigate Potential for Carbon Dioxide Sequestration in the Springfield area MO," M.S. Thesis, Missouri University of Science and Technology, Rolla, Missouri.

Bachu S., Bonijoly D., Bradshaw J., Burruss R., Holloway S., Christensen N.P., Maathiassen M.O., 2007, "CO2 Storage Capacity estimation: Methodology and gaps," International Journal of Greenhouse Gas Control, v. 1, no. 4, p. 430-443.

Bachu S., 2003, "Screening and ranking of sedimentary basins for sequestration of CO2 in geological media in response to climate change," Environmental Geology, 44:277-289.

Bachu S., 2000, "Sequestration of CO2 in geological media: criteria and approach for site selection in response to climate change," Energy Conversion and Management, 41-953-970.

Barton N.R., 2008, "Shear strength of Rockfill, Interfaces and Rock Joints, and their Points of Contact in Rock Dump Design," Rock Dumps, Australian centre for Geomechanis, Perth ISBN 978-0-9804185-3-8.

Benson M.S., 2004, "Carbon Dioxide Capture and Storage in Underground Geological Formation," The 10-50 solutions: Technologies and policies for a Low-Carbon Future, The pew center on Global Climate Change and the National Comission on Energy Policy.

Benson M.S., 2006, "Assessment of ricks from Storage of Crbon Dioxide in Deep Underground Geological Formations," Carbon Dioxide Capture and Storage, Lawrence Berkeley National Laboratory, p.4.

Boongird P., Dunn-Norman S., Al-Bazzaz W., Wronkiewicz D., 2006, "Formation Characterization of the Lamotte Sandstone in Southwestern Missouri," Final report to city utilities, Springfield, Missouri (Unpublished)

Davis J., 2004 "Contribution paper: Gasification and Carbon Capture and Storage: The Path Forward,", The 10-50 solution: Technologies and Policies for a Low-Carbon future. The Pew center on Global Climate Change and the National Commision on Energy Policy.

Espie A.A., 2005, "CO2 Capture and Storage: Contributing to Sustainable World Growth," International Petroleum Technology Conference in Doha Qatar, IPTC 10936.

Ferronato M.,Gambolati G., Janna J., Teatini P., 2010 "Geomechanical issues of anthropogenic CO2 sequestration in exploited gas fields," Energy Conversion and Management.

Folger P., 2009 "Carbon Capture and Sequestration (CCS)," Congressional Research Service, RL33801.

Forbes M.S., Verma P., Curry E.T., Friedmann J.S., Wade M.S., 2008, "Guidelines for Carbon Dioxide Capture, transport and Storage," World Resources Institue, Washington, DC.

Govindrajan S., 2012, "Geo-Mechanical Characterization of Reservoir and Caprocks for CO_2 sequestration," M.S. Thesis, Missouri University of Science and Technology, Rolla, Missouri.

Gunter W.D., Bachu S., Benson M.S., 2004 " The role of hydrogeological and geomechanical trapping in sedimentary basins for secure geological storage for carbon dioxide," , Geological Storage of Carbon Dioxide, vol. 233, London, UK, Geological Society Special Publication, p. 129-45.

Hawkes C.D., Bachu S., Mclellan P.J., 2005 "Geomechanical Factors Affecting Geological Storage of CO2 in Depleted Oil and Gas Reservoirs," Journal of Canadian Petroleum Technology.

Lee D., Singh V., Berard T., 2009 "Construction of a Mechanical Earth Model and Wellbore Stability Analysis for a CO_2 Injection Well," International Conference on Co_2 Capture, Storage, and Utilization, San Diego, California, USA, SPE 126624.

Litynski J., Plastnski S., Spangler L., Finley R., Steadman E., Ball D., Nemeth K.J., McPherson B., Myer L., 2009 "U.S. Department of Energy's Regional Carbon Sequestration Partnership Program: Overview," Energy procedia, I, Elsevier ltd.

Metz B., Davidson O., Coninck de H., Loos M., Meyer L., 2005, "IPCC Special Report on Carbon Dioxide Capture and Storage," International Panel on Climate Change, United Nations Framework Convention on Climate Change. ISBN 92-9169-119-4.

Nacht P.K., Oliveira M.F.F.D., Roechl D.M., Costa A.M., 2010 "Investigation of Geological Fault Reactivation and Opening," Association Argentina de Mecanica Computacional, Eduardo Dvorkin, Marcela Goldschmit, Mario Storti (Eds.), Buenos Aires, Aergentina.

Nelson R.C., Evans M.J., Sorenson A.J., Steadman N.E., Harju A.J., 2005, "Factors Affecting The Potential For CO2 Leakage From Geological Sinks," Energy and Environmental Research Center, Plains CO_2 Reduction (PCOR) Partnership, University of North Dakota.

Onishi K., 2002, "The estimation of subsurface carbon stocks for the Kyoto Protocol by ground-penetrating radar," SEG Int'l Exposition and 72nd Annual Meeting, Salt Lake Utah.

Shaw J., Bachu S., 2002, "Screening, Evaluation and Ranking of Oil Reservoirs Suitable for CO2-Flood EOR and Carbon Dioxide Sequestration,"Journal of Canadian Petroleum Tenchnology, v.41, no.9, p. 51-61.

Streit J., Siggins A., Evans B., 2005, "Predicting and monitoring geomechanical effects of CO2 injection, Carbon Dioxide Capture for Storage in Deep Geologic Formations-Results from CO2 Capture project," Geologic Storage of Carbon Dioxide with Monitoring and Verification, London.

Tans. P., 2012, National Oceanic and atmospheric administration (NOAA) USA, Earth System Research laboratory (ESRL).

Vendrig M., Purcell M., Melia K., Archer R., Harris P., Flach T., 2007 "Environmental Assessment for CO2 Capture and Storage," IEA Greenhouse Gas R&D Programme (IEA GHG).

White M.C., Penkala J.S., Gunter D.W., Hidy M.G., Benson M.S., Herzog A., Chow C.C., Watson G.J., 2003, "Separattion and Capture of CO2 from Large Stationary Sources and Sequestration in Geological Formations," Air and Waste Management Association, ISSN 1047-3289.

VITA

Ishan Kumar was born on 9th October 1986. He earned his Bachelor's degree in Mining Engineering from Visvesvaraya National Institute of Technology, Nagpur, India in the spring of 2009 and enrolled in the Master's program in Petroleum Engineering at Missouri University of Science and Technology in the fall of 2010. He earned his Master's degree in Petroleum Engineering in December 2012.